REBUILDING NUCLEAR PORE COMPLEX FUNCTION *IN VITRO*

Inauguraldissertation

zur

Erlangung der Würde eines Doktors der Philosophie

vorgelegt der

Philosophisch-Naturwissenschaftlichen Fakultät

der Universität Basel

von

Suncica Barbato

von

Kroatien

Basel, 2020

Genehmigt von der Philosophisch-Naturwissenschaftlichen Fakultät

auf Antrag von

Prof. Dr. Roderick Y. H. Lim

Prof. Dr. Harald Herrmann-Lerdon

Basel, den 17.09.2019

Prof. Dr. Martin Spiess

Dekan

Suncica Barbato: Rebuilding Nuclear Pore Complex Function *In vitro*. 2020.

ACKNOWLEDGEMENTS

First, I would like to express my sincere gratitude to my advisors, Roderick Y.H. Lim and Larisa E. Kapinos, for their continuous support and patience. I want to thank both of you for the amazing and intense times in the lab and out of it. Without your support, it would not be possible to be where I am now.

I would also like to thank Harald Hermann-Lerdon for taking his time to be my co-examiner and Jan Pieter Abrahams for chairing my defense.

Very warm thanks go to my old and current lab mates et al.: Lajko, Aska, Yusuke, Philipp, Marija, Binlu, Tina, Elena, Toshiya, Irina, Simone, Rafael and Steffie for having a fun time together and for being with me during the less fun times.

I would also like to thank RK for constructive criticism and scientific input on my work.

Many thanks go to Chantal Rencurel for the expression and purification of proteins for my research project.

And finally, I also want to thank to Alessandro for always sticking by my side.

PUBLICATIONS

This thesis includes the following publications in parts or in an extended version:

- "Nucleocytoplasmic Transport: A Paradigm for Molecular Logistics in Artificial Systems."

  Suncica Vujica, Christina Zelmer, Radhakrishnan N. Panatala, and Roderick Y.H. Lim.

  Published in CHIMIA International Journal for Chemistry, 2016;70(6):413-417

- "Nuclear Pore Membrane Proteins Self-Assemble into Nanopores"

  Radhakrishnan N. Panatala, Suncica Barbato, Toshiya Kozai, Jinghui Luo, Larisa E. Kapinos, and Roderick Y.H. Lim

  Published in Biochemistry, 2019;58(6):484-488

- "Karyopherin enrichment at the nuclear pore complex attenuates Ran permeability"

  Suncica Barbato, Larisa E. Kapinos, Chantal Rencurel, and Roderick Y.H. Lim

  Published in Journal of Cell Science, 2020;133(3).

PREFACE

The hallmark of a eukaryotic cell is the segregation of genetic material within the cell's nucleus. The nucleus is separated from the cytoplasm by a double lipid bilayer termed nuclear envelope (NE) that contains a number of proteinaceous channels known as nuclear pore complexes (NPCs).

NPCs enable molecular transport between the nucleus and cytoplasm, termed nucleocytoplasmic transport (NCT), which is bidirectional, fast and selective. Three major groups of proteins are continuously trafficking across the NPC's central channel to orchestrate NCT. These are transport receptors, known as karyopherins (Kaps), signal-specific cargoes and a small GTPase (i.e., Ran) that sustains the process.

Interestingly, NPCs restrict or promote cargo translocation via biochemical selectivity and not size exclusion *per se*. Recent findings suggest that the NPC transport selective barrier is regulated by Kaps. This so-called Kap-centric regulation considers Kaps as integral constituents of the NPC that reinforce its selective barrier against large nonspecific macromolecules while simultaneously promoting the transport of specific cargoes. Nonetheless, an understanding of how Kaps contribute to NPC function remains incomplete.

The aim of this study was to rebuild NPC function *in vitro*.

First, we investigated how Kaps might reinforce the NPC transport barrier to establish a gradient of Ran guanosine triphosphate (RanGTP) and Ran guanosine diphosphate (RanGDP)

in the nucleus and cytoplasm, respectively. Here, we show that the binding of RanGTP to Kaps at the NPC prevents its leakage into the cytosol.

Next, we show that two NPC pore membrane proteins are able to self-assemble into 20 nm-diameter nanopores following their reconstitution into lipid bilayers. This work represents a key step toward using nanopores as a *de novo* platform to construct additional NPC mimics with the aim of promoting NCT-like selective transport.

ACRONYMS

ATP	adenosine tri-phosphate
DC	dendritic cell
DTT	dithiothreitol
EM	electron microscopy
ER	endoplasmatic reticulum
ESCRT	endosomal sorting complex required for the transport
EV	extracellular vesicle
FACS	fluorescence activated cell sorting
FCM	flow cytometry
FG	Phenylalanine-Glycine
FSC	forward scatter light
GDP	guanosine di-phosphate
GTP	guanosine tri-phosphate
GLs	giant liposomes
GPLs	giant proteoliposomes
GFP	green fluorescent protein
HS-AFM	high-speed atomic force microscopy
HRP	horseradish peroxidase
INM	inner nuclear membrane
ITO	indium tin oxide
Kaps	karyopherins
LSM	light scattering microscopy
MST	microscale thermophoresis
MS	mass spectrometry
NCT	nucleocytoplasmic transport
NE	nuclear envelope
NES	nuclear export signal
NLS	nuclear localization signal

NPC	nuclear pore complex
Nups	nucleoporins
NTR	nuclear transport receptor
NTF2	nuclear transport factor 2
ONM	outer nuclear membrane
PLs	proteoliposomes
POMs	pore membrane proteins
RanBP	Ran binding protein
Ran GAP1	GTP-ase activating protein 1
RanGEF	guanine nucleotide exchange factor
RCC1	regulator of chromosome condensation 1
ROS	reactive oxygen species
ROD	reduction of dimensionality
ROI	region of interest
SPR	surface plasmon resonance
SSC	side scatter light
SUV	small unilamellar vesicle
TFA	trifluoroacetic acid
TMB	3,3’,5,5’-tetramethylbenzidine
TM-Nups	transmembrane nucleoporins

TABLE OF CONTENTS

LIST OF FIGURES

LIST OF TABLES

Introduction

Adapted from

Nucleocytoplasmic Transport: A Paradigm for Molecular Logistics in Artificial Systems

Suncica Vujica, Christina Zelmer, Radhakrishnan N. Panatala, and Roderick Y.H. Lim

Published in CHIMIA International Journal for Chemistry, 2016;70(6):413-417

1Introduction

1.1The Nuclear Pore Complex

Sub-cellular compartmentalization is a hallmark of eukaryotic cells. One of the most prominent membrane-enclosed organelles is the nucleus. The nucleus is encapsulated by a double bilayer membrane known as the nuclear envelope (NE) that separates chromatin from the cytoplasm thereby allowing for the regulation of gene expression in space and time (**Figure 1-1**). The nucleus communicates with the cytoplasm through proteinaceous pores named nuclear pore complexes (NPCs) (Kabachinski and Schwartz, 2015), which are assembled in the NE and are the sites where the outer and inner nuclear membranes fuse. A key role of NPCs is to mediate the bidirectional selective transport of diverse macromolecules between the nucleus and cytoplasm (e.g., transcription factors or mRNA) (Fahrenkrog and Aebi, 2003), (Tran and Wente, 2006). Indeed, one of the first observations of NPCs was through the detection of material translocation across nuclear pores using electron microscopy (EM) (Anderson and Beams, 1956).

In yeast, the overall NPC mass is ~60 MDa (Rout and Blobel, 1993), while in metazoans it is ~120 MDa (Reichelt et al., 1990). Large nuclei of *Xenopus laevis* oocytes have an average pore density of ~50 NPCs/μm,^{2} resulting in ~5×10^7 NPCs per oocyte nucleus (Cordes et al., 1995). In contrast, vertebrates have an average pore density of about 10–20 NPCs/μm^2 resulting in 2000–5000 NPCs per nucleus (Maul and Deaven, 1977). Approximately 12 NPCs/μm^2 are found in yeast nuclei, corresponding to ~200 NPCs per nucleus (Winey et al., 1997).

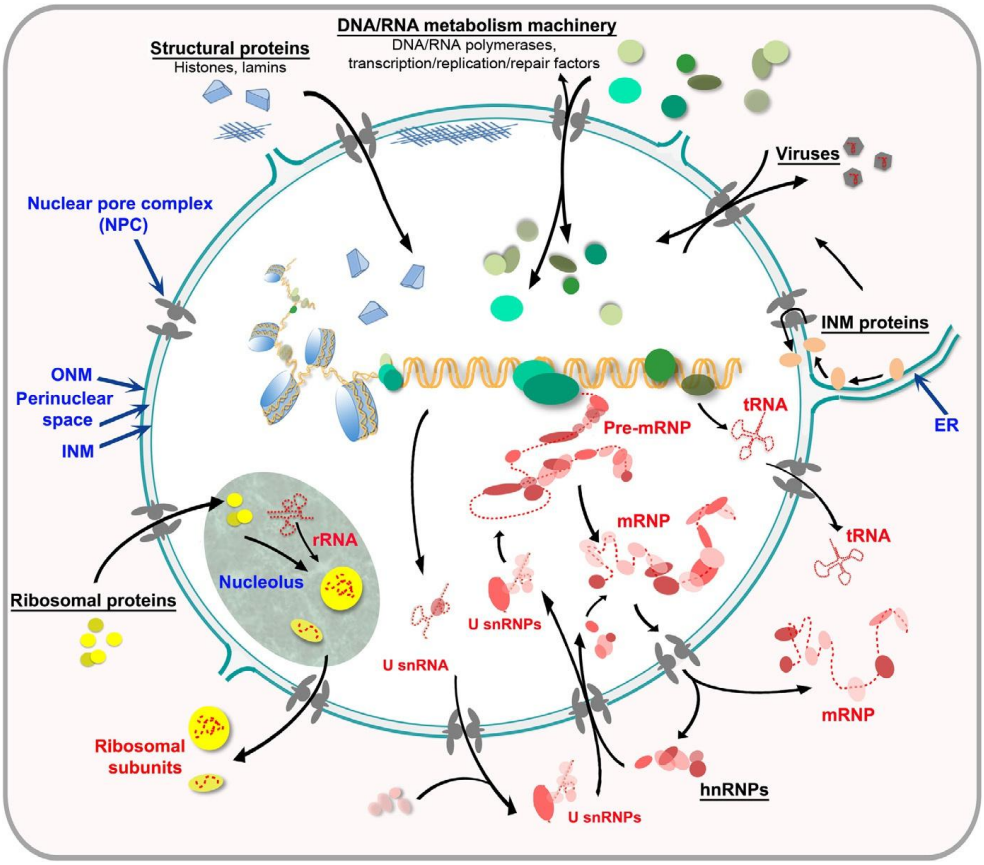

Figure 1-1 An overview of NCT

NPCs are central transport hubs that are involved in several fundamental cellular processes. Reproduced from (Floch et al., 2014).

As shown by cryo-electron microscopy, the *Xenopus* NPC has the following linear dimensions: ~120 nm outer diameter, ~180 nm height and ~50 nm inner channel diameter (Stoffler et al., 2003). These dimensions resemble the NPCs of the human osteosarcoma U2OS cells (Maimon et al., 2012). In comparison, NPCs of *Dictyostelium discoideum* show similar inner and outer diameters of ~50 nm and ~125 nm, respectively, with a smaller height of ~150 nm (Beck et al., 2004), (Beck et al., 2007).

Each NPC is constructed from approximately 30 different proteins known as nucleoporins (Nups), which are present in multiples of eight (**Figure 1-2**), thereby giving rise to its characteristic octagonal symmetry (Cronshaw et al., 2002). Nups are categorized into the following architectural sub-groups (Devos et al., 2006), (Strambio-De-Castillia et al., 2010):

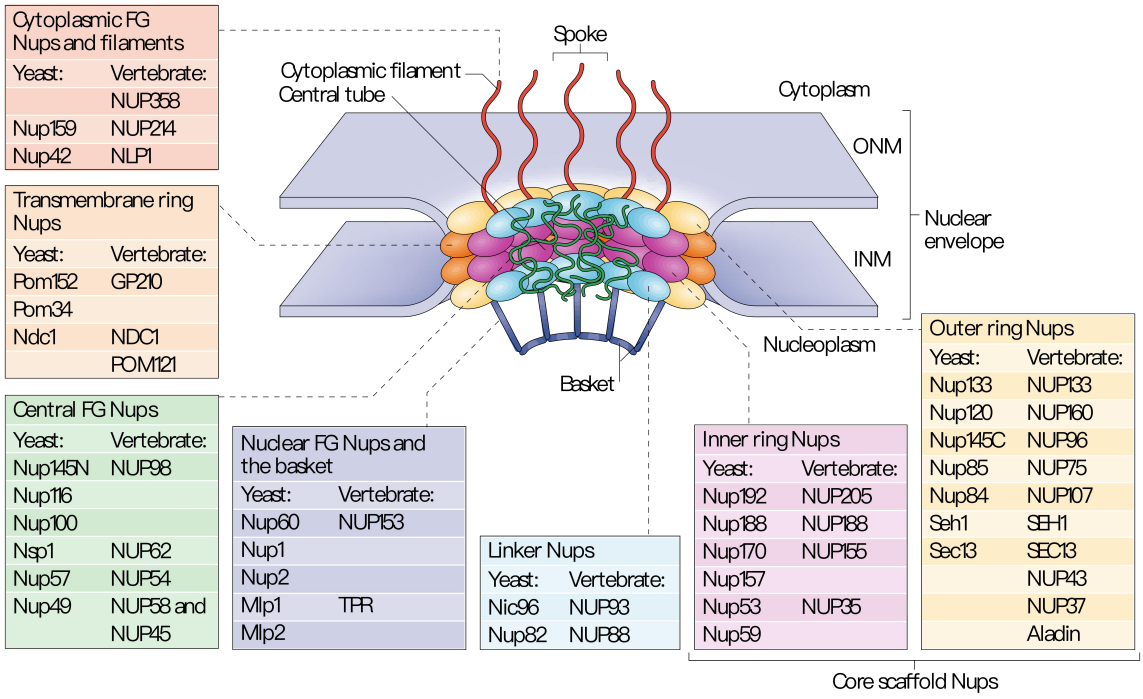

Figure 1-2 Molecular constituents of the NPC

Schematic representation of NPC structure. Each NPC is a cylindrical structure comprised of 30 different Nups categorized in different architectural sub-groups. Reproduced from (Strambio-De-Castillia et al., 2010).

a)Membrane Nups

Pom121 (no homolog in Yeast), Ndc1 (Yeast homolog Ndc1) and gp210 (Yeast homolog Pom152) build the membrane ring of an NPC. They are also termed POMs (TM-Nups) and are the only known transmembrane proteins that anchor the NPC to the NE (Antonin et al., 2008). POMs are arguably the primary candidates for stabilizing NE membrane curvature at the sites of NPCs. They are also considered to play an essential role in NPC biogenesis (Devos et al., 2006), (Strambio-De-Castillia et al., 2010).

b)Structural scaffold Nups

Two essential sub-complexes serve as structural scaffolds for the NPC: Nup93 and Nup107 (the latter is also known as a Y complex because it resembles the letter Y). These Nups have been shown to form a symmetric core that stabilizes the whole NPC (Alber et al., 2007), (Bui et al., 2013), (Sampathkumar et al., 2013), (Kosinski et al., 2016).

c)Cytoplasmic filaments and the nuclear basket

The cytoplasmic filaments extend into the cytosol ∼35–50 nm away from the cytoplasmic ring (Stoffler et al., 2003), (Beck et al., 2004), (Sakiyama et al., 2016). These eight flexible structures can serve as docking sites to transport selective cargoes. Each cytoplasmic filament is decorated with the phenylalanine-glycine-rich nucleoporins (FG-Nups) Nlp1 (Yeast homolog Nup42p) and Nup214 (Yeast homolog Nup159p), together with Nup358. Nup358 is also known as RanBP2 and plays a role in NCT (Walther et al., 2002).

On the nuclear side of NPCs is the nuclear basket, which consists of eight protein filaments (Beck et al., 2007). The filaments protrude ∼50–100 nm into the nucleoplasm where they connect into a distal ring. The nuclear basket is composed of three Nups, Nup153 (an ortholog of Nup1 and Nup60 in yeast), Nup50 (yeast homolog is Nup2) and Tpr (Yeast homolog is Mlp1/2) (Fahrenkrog et al., 2002).

d)Intrinsically disordered FG-Nups

FG-Nups are intrinsically disordered proteins (Eibauer et al., 2015), (Denning et al., 2003), (Lim et al., 2007) that generate a selective permeability barrier within the NPC central channel. Each FG-Nup harbors numerous FG-repeat motifs that serve of binding sites for Kaps (Kapinos et al., 2014), (Wagner et al., 2015). Altogether ∼200 FG-Nups (Cronshaw et

al., 2002) tether to the inner walls of the NPC and are thought to collectively resemble a "supramolecular hydrogel meshwork" (Frey and Gorlich, 2007), (Hulsmann et al., 2012), a "molecular brush" barrier (Lim et al., 2006) or combinations thereof (Yamada et al., 2010).

1.2Nucleocytoplasmic Transport

Although NPCs span species-dependent diameters of between 50 to 100 nm (Elad et al., 2009), (Frenkiel-Krispin et al., 2010), (Stoffler et al., 2003) only small molecules below ~40 kDa (e.g., water and ions) can passively diffuse through the pore, whereas large nonspecific macromolecules are generally withheld (Popken et al., 2015), (Timney et al., 2016). Rapid and exclusive access through the NPC is only permitted to soluble nuclear transport receptors known as karyopherins or Kaps (Chook and Suel, 2011). Interestingly, the mass of Kaps typically exceeds the passive NPC diffusion limit (Bayliss et al., 2000). Thus, NPCs restrict or promote cargo translocation via biochemical selectivity and not size exclusion *per se*. In order to bypass the FG-Nup barrier, Kaps and other transport factors such as nuclear transport factor 2 (NTF2), the RanGDP importer (Bayliss et al., 2000), (Bayliss et al., 2002a), (Bayliss et al., 2002b), (Bayliss et al., 1999) harbor binding sites that exert multivalent interactions with the FG-repeat motifs (i.e., GLFG, FxFG and FG). For example, the classical 97 kDa import receptor Kapβ1, is estimated to engage up to ten FG-repeats (Isgro and Schulten, 2005). This binding is thought to facilitate Kap transport by causing dynamic conformational changes in the FG-Nups to weaken the permeability barrier (Kapinos et al., 2014), (Wagner et al., 2015). On this basis, Kaps orchestrate NCT by authenticating and shuttling specific cargoes destined to the nucleus through the NPCs.

Kaps identify specific cargoes via short peptide sequences known as nuclear localization signals (NLSs) (Boulikas, 1994). Nonspecific macromolecules lacking NLS are rejected by the barrier (Chook and Suel, 2011). On the other hand, by recruiting Kaps, both physiological and artificial cargoes, with sizes that span the inner diameter of the pore, are able to translocate the NPC. These include gold particles decorated with Kap-cargo complexes (39 nm-diameter) (Pante and Kann, 2002), Kap-decorated quantum dot cargoes (30–40 nm-diameter) (Lowe et al., 2010), Hepatitis B virus capsids (34 nm-diameter) (Rabe et al., 2003) and messenger ribonucleoproteins (mRNPs), such as Balbiani Ring particles, which appear to elongate to a 25 nm-diameter during their passage through the central channel (Mehlin et al., 1992). Indeed, viruses are known to hijack the Kap-FG pathway in order to infiltrate the NPC and the nucleus (Whittaker et al., 2000).

1.2.1Ran-dependent regulation of NCT

Kap-cargo translocation is a diffusional process (Kopito and Elbaum, 2007). However, an energy supply is required to regulate the directionality of cargo delivery and release (Schwoebel et al., 1998). Such, a continuous energy cycle is required to sustain bidirectional NCT. This cycle is regulated by the small GTPase Ran, which has GTP- and GDP-bound forms localized in the nucleus and cytoplasm, respectively (Gorlich and Mattaj, 1996) (**Figure 1-3**).

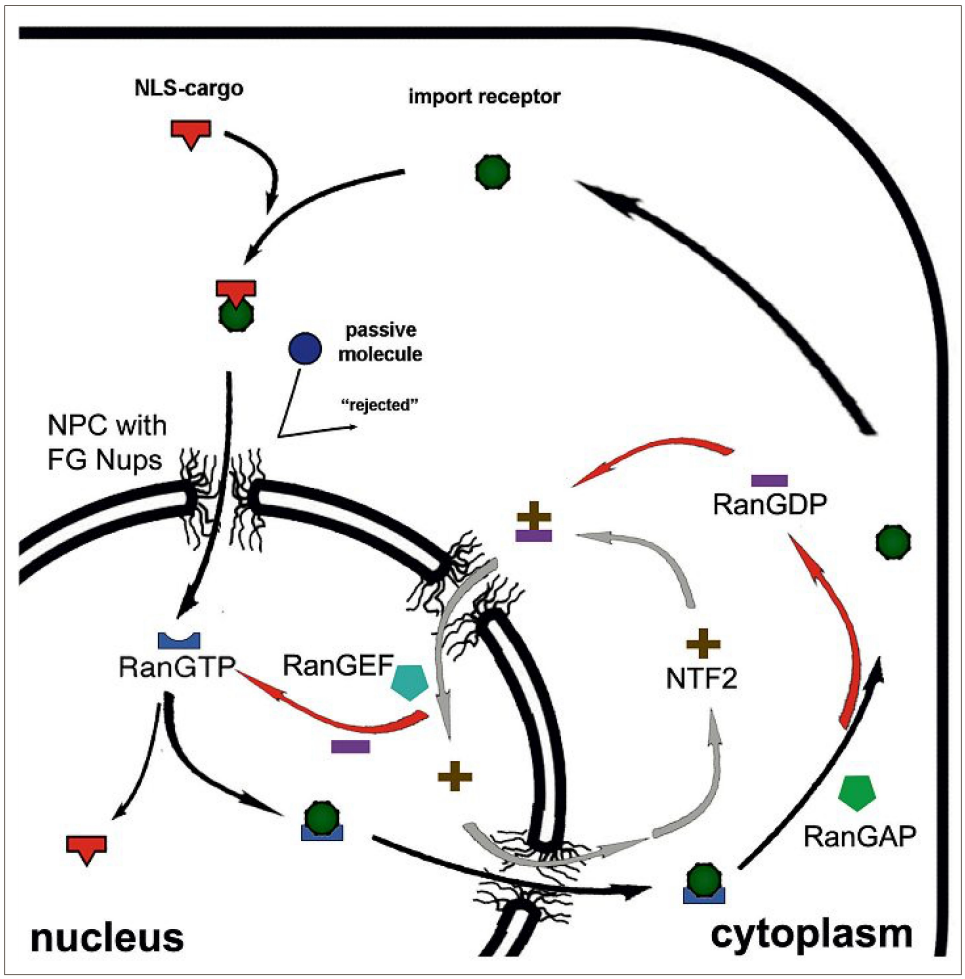

Figure 1-3 Mechanism of nuclear import

Import receptors (Kapβ1) identify and shuttle NLS-cargo from the cytoplasm into the nucleus. The receptor-cargo complex is disassembled in the nucleus by RanGTP, which returns with the import receptor to the cytosol. RanGAP1 triggers the hydrolysis of RanGTP to RanGDP in the cytosol, which frees the receptor for another round of import. RanGDP is imported into the nucleus by NTF2, where it is recharged into RanGTP by RanGEF. In the absence of Kaps, nonspecific cargoes are rejected by the NPC. Reproduced from (Vujica et al., 2016).

Ran has a structure based on a core or G domain (Guanine nucleotide-binding domain), p-loop, Switch I and II, and a 40-amino acid C-terminal extension. The C-terminal region, which is crucial for the binding to Kaps, consists of a linker, an α-helix and an acidic tail (DEDDDL motif). Major conformational changes involving Switch I, Switch II and the C-terminus occurs in Ran as it alternates between its GTP- (Vetter et al., 1999) and GDP-bound forms (Stewart et al., 1998). These conformational changes underlie the different affinities of

RanGTP and RanGDP when binding Kaps (Forwood et al., 2008), (Lonhienne et al., 2009), (Barbato and Kapinos et al., 2020).

RanGTP binding triggers the release of import cargoes from Kapβ1 in the nucleus, whereas in the cytoplasm RanGAP1 (Ran GTPase-activating protein) hydrolyzes RanGTP to RanGDP, which releases Kapβ1 for another cargo-import cycle (Stewart, 2007). RanGDP is then returned to the nucleus by its specific carrier, NTF2 (Ribbeck et al., 1998). In the absence of Kapβ1, even the NLS-cargoes, which are smaller than Kap-cargo complexes are withheld. Accordingly, NLS-cargoes are retained in the nucleus upon dissociation from Kapβ1. The Ran loop is finally closed by regulator of chromosome condensation 1 or RCC1 (also called guanine nucleotide exchange factor or RanGEF), which catalyzes the exchange of RanGDP to RanGTP (Stewart, 2007). Hence, RCC1 and RanGAP1 enable cells to maintain high levels of RanGTP inside the nucleus and high levels of RanGDP within the cytoplasm, respectively (Abu-Arish et al., 2009), (Kalab et al., 2002). This so-called "Ran gradient" drives the transport and accumulation of cargoes against their concentration gradients within the nucleus. Not surprisingly, alterations in the Ran gradient are known to disrupt NCT (Yasuda et al., 2006), (Kelley and Paschal, 2007), (Chatterjee and Paschal, 2015).

1.2.2The role of Ran regulators: RanGEF and RanGAP1

The asymmetric distribution of RanGEF and RanGAP1 is essential for maintaining the Ran gradient (**Figure 1-4**). Moreover, it has been shown that reversing the Ran gradient (i.e., the presence of high concentrations of cytoplasmic Ran-GTP) can invert the direction of transport through the NPC (Nachury and Weis, 1999). RanGEF is imported into the nucleus and is localized at the chromatin (England et al., 2010), (Ohtsubo et al., 1989) where it binds

to nucleosomes and histones H2A and H2B that stimulate RanGEF catalytic activity (Nemergut et al., 2001).

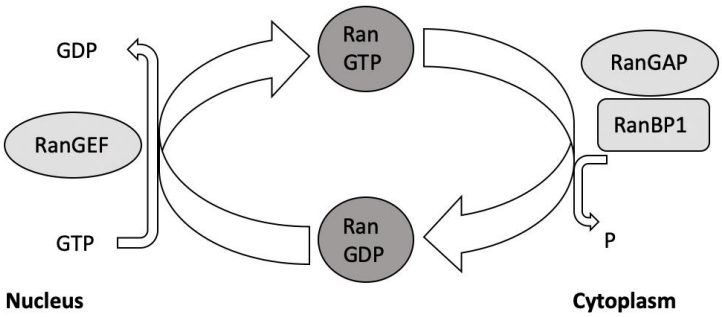

Figure 1-4 Compartmentalization of RanGAP1 and RanGEF
Ran regulators: RanGEF and RanGAP1 ensure asymmetrical distribution of RanGTP and GDP between the cytoplasm and the nucleus. Adapted from (Azuma and Dasso, 2000).

Ran has a seven-fold higher affinity for GDP than GTP (Klebe et al., 1995b). It is noteworthy that RanGEF does not discriminate between GTP and GDP. In fact, the interaction of RanGEF with Ran weakens the affinity of Ran for the nucleotide, resulting in a binary nucleotide-free complex. However, because of the higher cellular concentration of GTP, this complex is not stable and the binding of GTP nucleotide to Ran-RanGEF essentially results in RanGTP formation (Vetter and Wittinghofer, 2001). As a result, RanGEF replaces GDP, and GTP replaces RanGEF.

The GTPase activity of Ran is enhanced by RanGAP1 and by Ran-binding proteins RanBP1 and RanBP2 (Yokoyama et al., 1995). RanGAP1 is bound to the cytoplasmic face of the NPC via the nucleoporin Nup358 upon SUMOylation of its C-terminus (Mahajan et al., 1997), (Matunis et al., 1998). RanGTP has a very slow intrinsic hydrolysis ($k_{cat} = 1.8 \times 10^{-5}$ s^{-1}), and its half-life is of several hours (Bischoff and Ponstingl, 1991), (Bischoff et al., 1994), (Klebe et al., 1995a). RanGAP11 facilitates the hydrolysis of RanGTP up to $k_{cat} = 2.1$ sec^{-1}

(Bischoff et al., 1994), (Klebe et al., 1995a). In this manner, RanGDP is generally concentrated within the cytoplasm.

1.2.3Nuclear Import Regulation

Following GTP hydrolysis, it is necessary for RanGDP to return into the nucleus to be exchanged with GTP by RanGEF. In spite of being smaller than the NPC size exclusion limit, NTF2 is required to facilitate import of RanGDP into the nucleus given that passive diffusion through NPC is not sufficiently rapid (Ribbeck et al., 1998). NTF2 selectively binds to RanGDP with a K_d of around 100 nM (Chaillan-Huntington et al., 2000) because of the specific conformation of Switch II, which enables these interactions (Stewart et al., 1998). Like Kaps, NTF2 passes through the pore upon binding to FG-Nups (Bayliss et al., 1999), (Bayliss et al., 2002a). This binding is promoted in the presence of pre-bound Kapβ1 to FG-Nups (Wagner et al., 2015).

Likewise, NLS-cargoes are imported into the nucleus by Kaps (Chook and Blobel, 2001) (**Figure 1-5**). The best characterized NLS-cargo-import pathway consists of Kapβ1 (Kap95p in Yeast) and the adapter protein Kapα (Kap60p in Yeast). Kapα binds to Kapβ1 through its IBB domain (importin-β binding domain), followed by the NLS cargo binding to Kapα (Cingolani et al., 1999). The tripartite import complex NLS-cargo•Kapα•Kapβ1 then exerts multivalent interactions with the FG-repeats to traverse the NPC (Bayliss et al., 2000). Upon reaching the nucleus, RanGTP disassociates NLS-cargo•Kapα•Kapβ1 by binding to Kapβ1. As Kapβ1-RanGTP shuttles back to the cytoplasm, it encounters RanGAP1, which catalyzes GTP hydrolysis to free Kapβ1 for another cargo-import cycle. Simultaneously, in the nucleus,

Kapα frees the NLS-cargo due to the action of its auto-inhibitory IBB domain (Harreman et al., 2003), (Kobe, 1999).

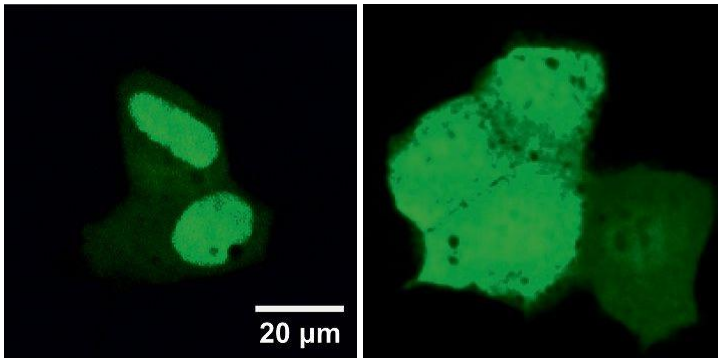

Figure 1-5 NLS-GFP vs. GFP import in HeLa cells
NLS-modified green fluorescent proteins (GFPs) are selectively trafficked by transport receptors across NPCs and accumulate against concentration gradients within the nuclei of living cells (left). In contrast, GFP molecules lacking the NLS are homogenously distributed throughout entire cells (right). Scale bar = 20 µm. Reproduced from (Vujica et al., 2016). Courtesy of Kai Schleicher.

1.2.4Nuclear Export Regulation

The nuclear export of proteins and RNAs is mediated by Kap-based export factors termed exportins. Exportins recognize their cargoes via a short peptide sequences known as nuclear export signals (NESs) (Wen et al., 1995). Some well-studied exportins include CRM1 (chromosomal maintenance 1), also known as exportin 1 (XPO1), and CAS (cellular apoptosis susceptibility gene, Cse1p in Yeast). CRM1 has a role in the export of mRNA, snRNA and rRNA as well as some proteins (Fornerod et al., 1997), while CAS is a specific exportin for Kapα (Kutay et al., 1997).

In contrast to nuclear import, where RanGTP-Kap binding results in cargo-complex disassembly, NES-cargo-exportin complex formation in the nucleus requires RanGTP binding. Upon traversing the pore, the NES-cargo-exportin-RanGTP complex is

disassembled following the hydrolysis of RanGTP by RanGAP1, resulting in the release of NES-cargo into the cytoplasm.

1.2.5Ran mobility and nuclear accumulation

Fluorescence-intensity measurements typically report a high abundance of Ran within the nucleus. The detection of endogenous Ran by monoclonal antibodies in fixed HeLa cells gave a nuclear-to-cytoplasmic ratio of 3.1 ± 0.5 (Abu-Arish et al., 2009), which is slightly higher than the 2.36 obtained before exposure to hyperosmotic stress (Kelley and Paschal, 2007). Interestingly, the nuclear accumulation of Ran in living cells appears higher. To support this finding, fluorescent-labeled exogenous Ran was injected into the cytosol of BHK-21 cells and imaged until nuclear accumulation reached a steady state. The results show a nuclear-to-cytoplasmic ratio of ~4 (Smith et al., 2002). Moreover, this ratio was increased to ~6 after addition of exogenous NTF2. Similar values were obtained for EYFP-Ran in live interphase HeLa cells i.e., 3.9 ± 0.4 (Abu-Arish et al., 2009).

Fluorescence recovery after photobleaching (FRAP) was used to investigate the intracellular mobility of Ran in U2OS cells (Hutchins et al., 2009). This study revealed an exceptional mobility of GFP-Ran, with recovery half-times of $\tau_{1/2} = 0.13$ sec in the nucleus and $\tau_{1/2} = 0.19$ sec in the cytoplasm. More recently, FRAP and FCS analysis confirmed that there is no significant immobile population of Ran; instead, 30% of Ran in the nucleus and 10% of Ran in the cytoplasm are engaged in molecular interactions at any time (Abu-Arish et al., 2009).

1.2.6NPC Permeability Barrier Models

Approximately 1000 translocation events happen per NPC per second (Ribbeck and Gorlich, 2001) at a rate of ~5 ms per cargo (Dange et al., 2008). At the present time, it is still not fully understood how such high transport rates are achieved. Several models describing nuclear transport exist, and even though they are different, the consensus is that the dynamic FG-Nups (Sakiyama et al., 2016) form a collective barrier that rejects inert molecules but can be bypassed by Kaps, such as Kapβ1 (Grunwald et al., 2011).

1.2.6.1The Selective Phase Model

The selective phase model was first proposed by Ribbeck et al. (Ribbeck and Gorlich, 2001) (**Figure 1-6**). This model assumes that: a) a sieve-like barrier is formed based on hydrophobic interactions between neighboring FG-Nups; b) the barrier prevents the passage of inert macromolecules; and c) the binding of Kaps to FG-Nups weakens inter-FG interactions to cause local disruptions in the barrier. Subsequent work by Ribbeck et al. further supported the proposed model by showing a reversible collapse of the barrier in cells caused by interfering with the hydrophobic interactions of FG-Nups using mild apolar solvents (e.g., cyclohexane-1,3-diol) (Ribbeck and Gorlich, 2002). In work that followed, it was demonstrated that lyophilized FG-Nups can indeed form hydrogels up to a few mm in size when dissolved (~200 mg/ml) in a highly hydrophobic solvent (0.2% TFA) (Frey et al., 2006), (Frey and Gorlich, 2009). These macroscopic hydrogels exhibit the permeability barrier of a fully saturated NPC (i.e., when every FG-Nup is crosslinked) (Frey and Gorlich, 2007), suggesting that each mesh in the gel defines the size of molecules that can freely pass through the meshwork.

Subsequent work further showed that central FG-Nups were more cohesive than peripheral FG-Nups (Patel et al., 2007). Likewise, the Nup153 FG domains could not form hydrogels in the presence of Kaps, as shown in one study (Milles et al., 2013).

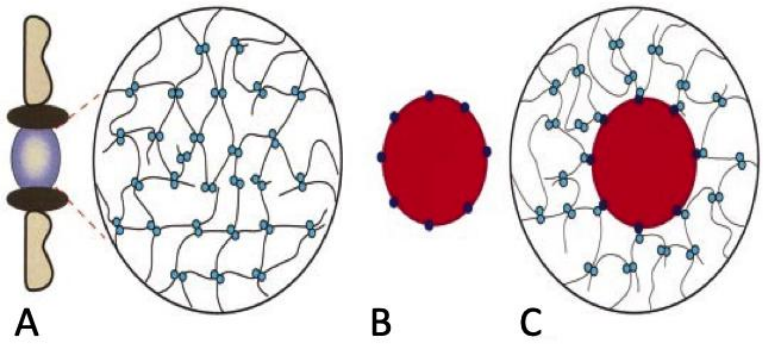

Figure 1-6 Selective phase model

The permeability barrier of the central plug filled with FG-Nups (light blue circles) that forms a meshwork restricting transport of inert objects is shown in (A). (B) An object (red) that has FG binding sites (dark blue circles) can translocate by binding to the meshwork (C), where it dissolves in the central plug and crosses the permeability barrier. Reproduced from (Ribbeck and Gorlich, 2001).

1.2.6.2The Virtual Gating Model

The virtual gating model (Rout et al., 2003) proposes that the NPC acts as a catalyst that can lower the activation energy necessary for the translocation process. Here, the FG-Nups are envisaged as "entropic bristles," moving around their anchoring points to explore a large volume around their tether site. Their motion also causes the molecules that move with the same speed to be "pushed away." Thus, the entropic barrier can be overcome solely by the binding of transport receptors to the FG-Nups.

1.2.6.3The Polymer Brush Model

At high surface densities, surface-tethered FG-Nups can extend away from their anchoring points in a manner that resembles a polymer brush. Indeed, Lim et al. found that surface-

grafted Nup153 FG domains exhibited a pronounced steric repulsive force being characteristic of molecular brush formation (**Figure 1-7**) (Lim et al., 2007). Treatment with hexanediol led to the collapse of the FG domain brushes, which could fully recover by switching buffer conditions (Lim et al., 2006). Likewise, extended Nup153 was observed to collapse after Kapβ1 binding, whereas the collapse was reversed upon removal of bound Kapβ1 (Lim et al., 2007). These findings suggest that an entropic barrier composed of highly dynamic FG-Nups guards the NPC against nonspecific molecules and the barrier can only be overcome by Kaps that bind to FG-Nups, resulting in their collapse. The Kaps move from one FG-Nup to the next by generating the local collapse within the pore. In contrast, each unbinding leads to a re-extension of the FG domains, thus restoring the barrier function. Hence, rapid translocation of Kaps occurs while barrier integrity is retained at the same time.

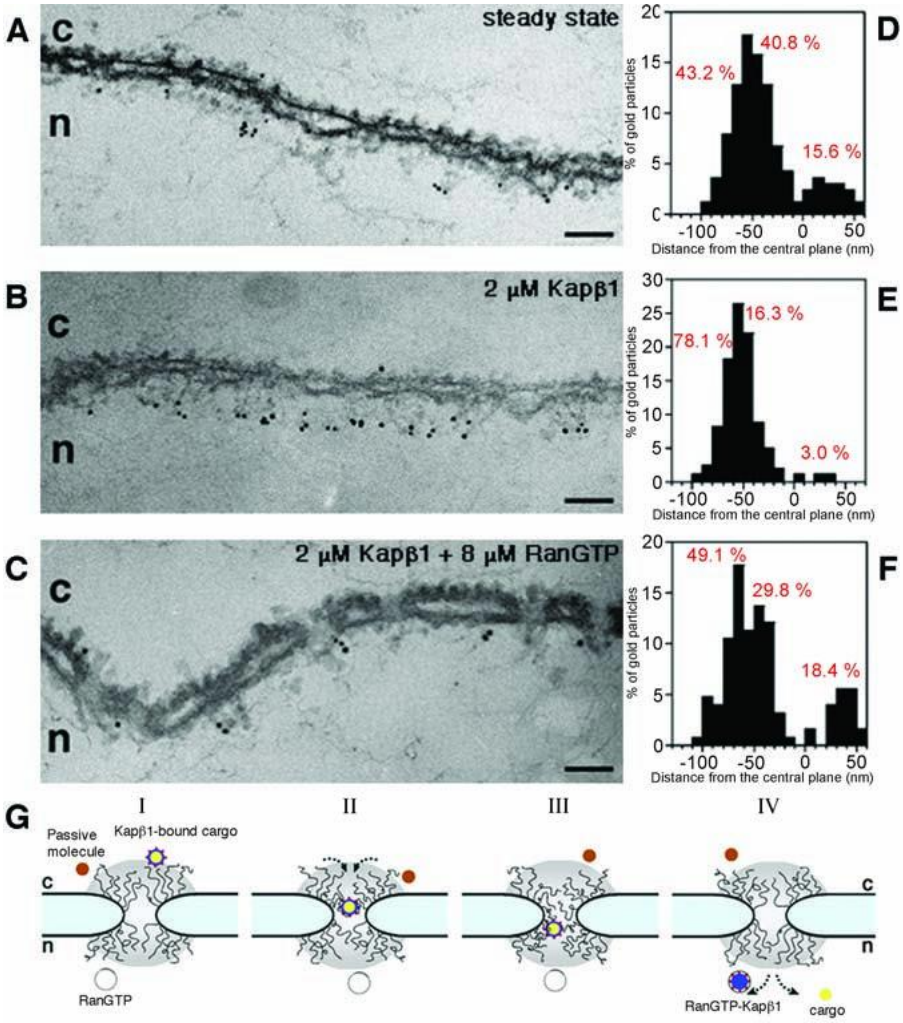

Figure 1-7 The polymer brush model

Immunogold electron microscopy reveals the reversible collapse of Nup153 in the NPC. At the steady state, Nup153 diffuses within the nuclear periphery (A). Upon Kapβ1 injection into the cytoplasm, Nup153 localizes at the distal ring of the NPC, resulting in a collapse of Nup153 to its anchoring site (B). Further addition of RanGTP reverses the Kapβ1-induced collapse that results with Nup153 back in the steady state (C). (A – C) The scale bars are 100 nm, c – cytoplasm, n – nucleus. The histograms (D–F) summarize all the observations. The 0 nm value in the x axis corresponds to the central plane of the NPC, while the distal ring, nuclear ring and cytoplasmic ring moieties are located at -100–50 nm, -50–0 nm and 0–60 nm. The selective gating-based model that takes into consideration the reversible collapse of the FG domains is shown in (G). (I) The FG domains surround the NPC when there is no Kapβ1-FG-Nups binding. The grey area points out the range of the entropic barrier and the fluctuations of the FG domains. (II) Kapβ1-FG-Nups binding causes the local collapse of the FG-Nups toward their anchoring sites. (III) Kapβ1 transport cargo through the NPC via continuous binding and unbinding to FG domains. (IV) In the nucleus, RanGTP binding to Kapβ1 triggers the cargo release and prevents further Kapβ1-FG-Nups interactions. Meanwhile, FG domains extend and re-create the entropic barrier (I) that will prevent passive entry of nonspecific cargoes. Reproduced from (Lim et al., 2007).

1.2.6.4Reduction of Dimensionality

Peters et al. proposed a model of NCT based on "reduction of dimensionality" (ROD) (Peters, 2005), (Peters, 2009a), (Peters, 2009b). The ROD model suggests that most FG-Nups are collapsed *in vivo*, resembling a "hydrophobic surface" (Berg and von Hippel, 1985). This collapse is caused by Kaps that bind to the FG layer. However, because of their multivalent binding within the FG layer, Kaps have a substantial degree of lateral mobility. Thus, Kaps ferry cargoes along NPC walls by diffusion in two dimensions, making the path through NPC much shorter than in three dimensions. In agreement with the ROD model, the nuclear accumulation of Kaps is 10–100 times faster in comparison to the passive diffusion of nonspecific molecules of a similar size (Ribbeck and Gorlich, 2001), (Siebrasse and Peters, 2002). Similarly, single-molecule-tracking experiments show that Kap-based transport occurs along the NPC wall while nonspecific molecules are simultaneously transported through the center of the pore (Ma et al., 2012).

1.2.6.5The Forest and Trees Model

FG-Nups can be classified into two categories based on their chemical and structural differences (Yamada et al., 2010), (Patel et al., 2007). One category includes low-charge FG-Nups, which have globular, collapsed coil configurations. The other category comprises high-charge FG-Nups, which adopt dynamic "extended coil" conformations. A third group of FG-Nups are thought to comprise of both compact and extended structures named "trees." Therefore, the "forest" model proposes that the FG-Nups are organized based on the above-mentioned conformational groups, which might carve out separate transport zones within the NPC channel (Yamada et al., 2010). FG-Nups form a hydrophobic cohesive meshwork, with their free ends sticky and with the globular conformations filling the central channel (or zone

1). These FG-Nups are linked to the NPC scaffold by non-cohesive relaxed or extended domains resembling the aforementioned molecular brush (zone 2). It therefore follows that the small cargoes with Kaps are limited to zone 2, while larger Kap-specific cargoes are transported through zone 1. In contrast, small molecules can passively diffuse in both zones. Experimental evidence for this model was provided by immunogold electron microscopy using instant cargoes trapped at the NPCs within a cell. Small cargoes were predominantly found at the periphery of the channel, while bigger cargoes were mostly located in the central channel (Fiserova et al., 2010).

1.2.6.6The Kap-Centric Model

A shift from the abovementioned "FG-centric" barrier models to a more Kap-centric description (Lim et al., 2015) was based on the observation that at steady state the FG-Nups were occupied by Kaps at physiological concentrations. Therefore, this suggested that the selective transport barrier is not composed of FG-Nups alone. This model might also explain how Kap transport can be both selective and fast. Such a view is consistent with single-molecule studies, which showed that an increase in Kapβ1 concentration leads to higher nuclear import efficiency in permeabilized cells (Yang and Musser, 2006).

A surface plasmon resonance (SPR)-based study subsequently showed that low concentrations of Kapβ1 cause collapse in FG domains and that an increase of Kapβ1 concentrations results in re-extension of FG domains (Schoch et al., 2012). Moreover, physiological concentrations of Kapβ1 can lead to maximal saturation and "pile up" whereby Kapβ1 molecules can still bind albeit weakly to unoccupied FG repeats at the top of the layer. Hence, at least two Kapβ1 binding phases may exist at physiological concentrations: strongly bound at the pore walls and weakly bound near the pore center. This so called "highway

effect" implies slow transport at the pore walls and fast transport near the pore center. Later, it was further suggested that Kapβ1 acts as an integral constituent within the FG-Nups given that a slow exchanging Kapβ1 phase co-exists with a fast phase (Kapinos et al., 2014). Subsequently, the use of digitonin permeabilized cells showed that exogenous Kapβ1 co-existed in at least two kinetically distinct pools (Lowe et al., 2015). Kap-preloading may also influence the binding of different nuclear transport receptors, such as NTF2 to FG-Nup layers (Wagner et al., 2015). Here, the promiscuous binding of Kapβ1 reduces the number of FGs available for NTF2, which translates into predominantly weak, short-lived interactions of NTF2 with FG-Nups, promoting faster NTF2 kinetics. Remarkably, depleting the highly enriched pool of Kapβ1 from the NPC abolished NPC barrier function against large nonspecific cargos (Kapinos et al., 2017). (**Figure 1-8**).

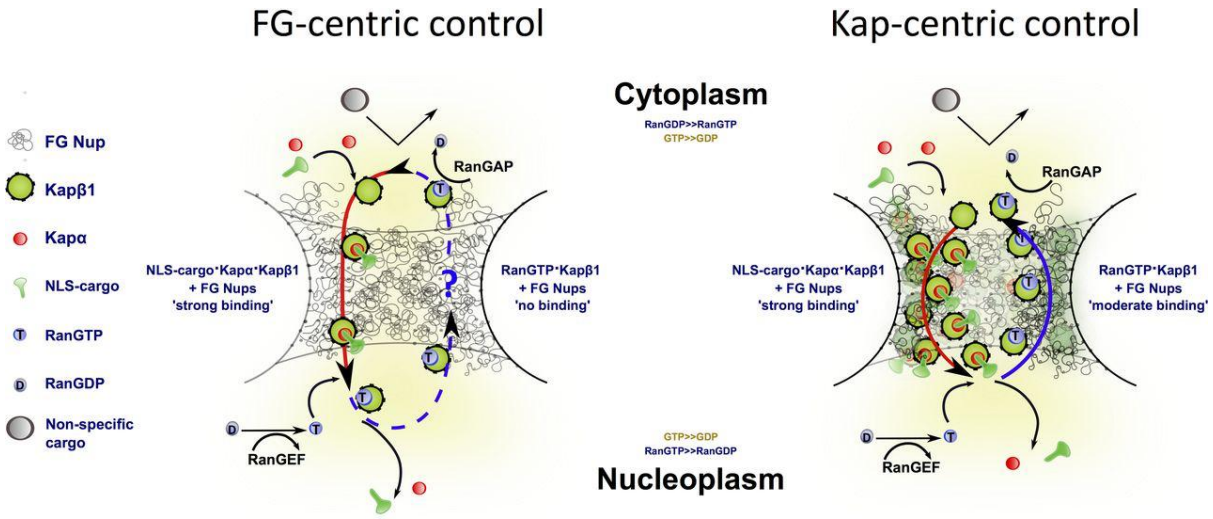

Figure 1-8 FG-centric versus Kap-centric NPC models

The FG-centric model focuses on the FG-Nups as the main components in the formation of NPC transport barriers, while the Kap-centric model emphasizes the role of transport receptors in the barrier formation and argues that, together with FG-Nups, the transport receptors are reinforcing the NPC barrier. Reproduced from (Kapinos et al., 2017).

1.3NPC assembly

There are two fundamentally different mechanisms of the NPC assembly that occur at distinct phases of the cell cycle: postmitotic and interphasic (Otsuka and Ellenberg, 2018). The series of events during postmitotic NPC assembly is as follows: At the onset of the mitosis, the NPC disassembles, whereas at the end of the mitosis, the NPC and NE reassemble. The reassembly of all the NPCs during the telophase lasts less than 10 minutes, as shown in mammalian tissue culture cells (Dultz et al., 2008). In contrast, in the interphase assembly, the NE stays intact while the number of NPCs in a given nucleus doubles. The interphase assembly of individual NPCs can last several hours (Dultz and Ellenberg, 2010).

1.3.1Mitotic NPC assembly

At the beginning of mitosis, the NE is absorbed into the mitotic endoplasmatic reticulum (ER) membrane network while the NPCs undergo disassembly (Ellenberg et al., 1997). The mitotic ER membranes are reorganized, and the NE re-forms towards the end of mitosis in late anaphase and telophase. The formation of the NE requires membrane fusion; this process is enabled by the SNARE machinery (Baur et al., 2007). It has also been reported that the endosomal sorting complex required for transport (ESCRT)-III components has a crucial role for NE closure (Vietri et al., 2015). The ESCRT-III complex localizes into the NE adjacent to its gaps and further co-localizes with the microtubule-degrading enzyme at the points where the microtubules and the reforming NE intersect in order to coordinate spindle disassembly and NE sealing (Vietri et al., 2015).

So far, two models have been proposed based on insertion and enclosure. The insertion model theorizes that NPCs are reassembled into an intact NE at the fusion spot of the inner

and outer nuclear membrane in order to allow NPC insertion (Macaulay and Forbes, 1996), (Fichtman et al., 2010). The fusion machinery is yet to be identified. In comparison, according to the enclosure model, the NPC assembly happens prior to the chromatin surrounding made by the NE (Burke and Ellenberg, 2002), (Antonin et al., 2008), (Dultz et al., 2008). Consequently, the NPCs are surrounded by expanding NE membranes, and no fusion between the ONM and INM is necessary.

The agreement between the two models is that the mitotic NPC assembly is initiated by the association of the nucleoporins MEL28 (also known as ELYS) and that the chromatin decondensation happens before the reformation of the NE. As shown by one study (Rasala et al., 2008), MEL28 can bind *in vitro* to the DNA through its AT-hooks. In addition, MEL28 recruits the Y-complex to the NPC assembly sites (von Appen et al., 2015). Subsequently, the transmembrane nucleoporins POM121 and NDC1 follow the assembling complex to initiate association with the membrane (Rasala et al., 2008) (**Figure 1-9**). The NDC1-binding nucleoporin Nup53 then recruits Nup155 and Nup93, which are in a complex with Nup188 or Nup205 (Eisenhardt et al., 2014). Next, Nup93 recruits the Nup62 complex, which consists of FG-Nups Nup62, Nup58 and Nup54, forming a large part of the hydrophobic meshwork within the central NPC (Sachdev et al., 2012), (Chug et al., 2015). Meanwhile, Nup98 recruits Nup155 and Nup205, as shown in yeast (Fischer et al., 2015), and similar interactions likely play a role in vertebrates NE assembly.

Even though the early events of the mitotic NPC assembly are rather well understood, the full assembly choreography of the NPC is still lacking.

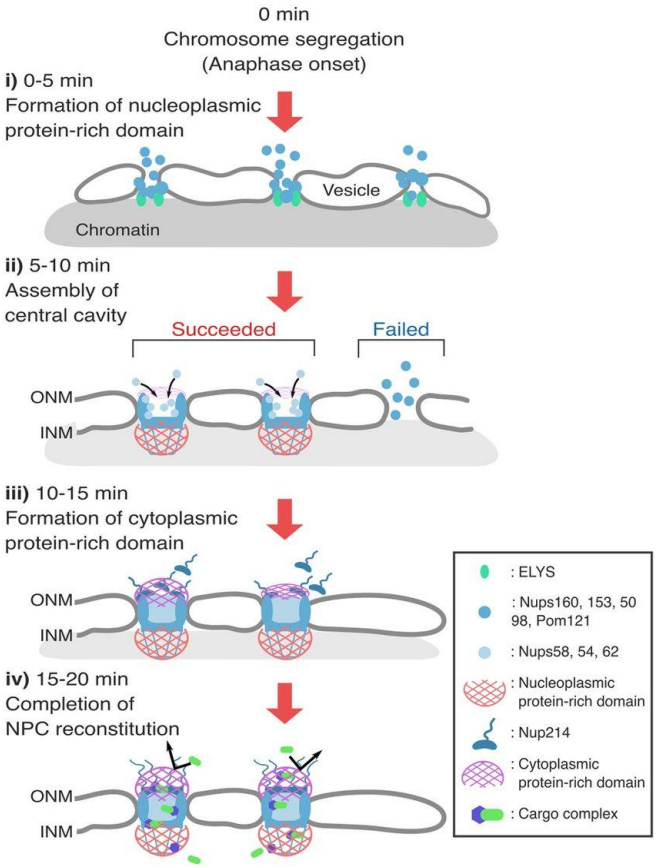

Figure 1-9 Schematic illustration of the NPC postmitotic assembly process

(i) The reconstitution of the NPC starts 5 min after the onset of anaphase. ELYS complex binds to the chromosome, while scaffold and FG-Nups start to assemble, forming protein-rich domains. Among these is also a membrane, nucleoporin Pom121. (ii) The next step is the recruitment of the central channel Nups toward the properly preassembled structures. (iii) The cytoplasmic Nups then bind to the entire complex, resulting in formation of the cytoplasmic protein-rich phase. (iv) In just 15–20 min, the reconstruction of the NPC is completed. Reproduced from (Konishi et al., 2017).

1.3.2Interphase NPC assembly

The interphase NPC assembly is the only mode of NPC assembly for organisms with a closed mitosis, such as the yeast *Saccharomyces cerevisiae* (Winey et al., 1997). However, higher organisms use interphase assembly to double the NPC number in response to changes during cell differentiation (Doucet et al., 2010), (Dultz and Ellenberg, 2010).

In order to integrate the NPCs into the NE, extensive membrane deformation is a prerequisite. That said, it is important to highlight that various mechanisms make this process possible, such as e.g. curved membrane-binding proteins and the insertion of amphipathic helices or wedge-shaped membrane domains into the lipid leaflet (Antonin et al., 2008), (Rothballer and Kutay, 2013). A recent study in living cells revealed the fusion of dome-shaped invaginations in the INM that grow in diameter and depth with the ONM (Otsuka et al., 2016). Such a membrane deformation can come from multiple mechanisms (e.g., insertion of amphipathic helices into the lipid leaflet (Antonin et al., 2008). Interestingly, some nucleoporins possess amphipathic helices, through which they can bind and deform the membranes (Drin et al., 2007), (von Appen et al., 2015). It has been shown that the mutation of the membrane-binding region in Nup153 prevents membrane association, resulting in the inhibition of the interphase assembly without affecting the mitotic NPC assembly (Vollmer et al., 2015). However, membrane binding is not the main function of the Nup153 amphipathic helix. This motif can be replaced by a transmembrane region that does not deform the membrane. Nup153 interacts instead with the Y-complex and directs it toward the NPC assembly sites in the inner nuclear membrane. Similarly, it has been shown that Nup133, with its amphipathic helices, is also only essential for the interphase NPC assembly (Doucet et al., 2010).

Even though Nup53 lacks its amphipathic helix, it is still considered to be essential for the interphase assembly process (Vollmer et al., 2012). A study involving RNA interference and biochemical depletion suggested that the membrane nucleoporin NDC1 plays a crucial role in the formation of a link between the NE membrane and soluble nucleoporins, such as Nup53, resulting in NPC anchoring to the membrane (Mansfeld et al., 2006).

The order of events for the interphase assembly is less known than that of mitotic NPC assembly. It is a matter of speculation that the recruitment of the Y-complex by the Nup153 binding to the inner nuclear membrane is a trigger event. However, it is highly possible that Nup153 does not deform the membrane but instead acts as a sensor of membrane bending by preferentially binding to positively curved membranes. Those deformed sites could be generated by Nup53 and Nup122, reticulons that act as membrane-deforming proteins, SUN proteins and LINC complex (Dawson et al., 2009), (Talamas and Hetzer, 2011). Additionally, the transmembrane nucleoporin POM121, crucial for the interphase NPC assembly, localizes to the NPC assembly sites prior to Y-complex (Doucet et al., 2010), (Funakoshi et al., 2011). (**Figure 1-10**). This analysis of the dynamics of individual NPCs in living mammalian cells during the interphase was made using high resolution live cell microscopy. It shows that NPC assembly is initiated by a slow accumulation of the membrane nucleoporin Pom121, followed by the more rapid association of the soluble NPC sub-complex Nup107–160 (Dultz and Ellenberg, 2010).

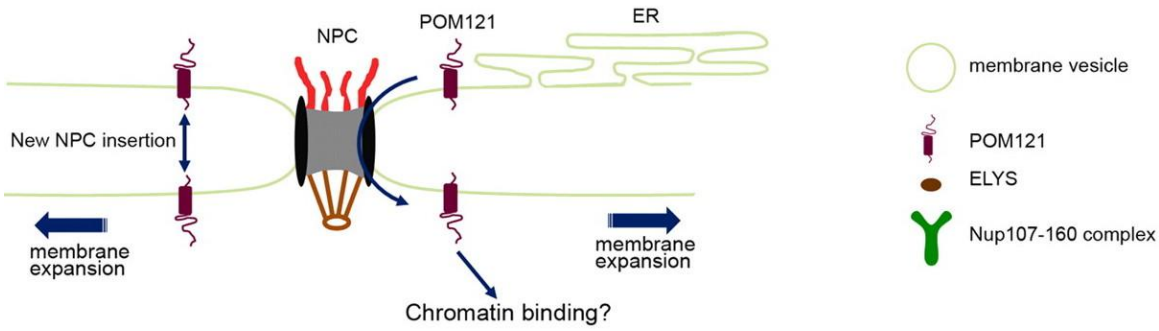

Figure 1-10 Schematic illustration of the NPC interphase assembly

Pom121 accumulates at the inner nuclear membrane. Thereafter, de novo NPC assembly occurs through interactions between the inner and outer nuclear membrane, followed by continued membrane expansion. Meanwhile, Pom121 recruits soluble Nups to the NPC assembly sites. In addition, Pom121 has chromatin-binding sites that might also be involved in the process. Reproduced from (Shaulov et al., 2011).

1.4Aim of the thesis

So far, the Kap-centric model (Kapinos et al., 2017) suggests that Kaps enrich at NPCs and serve to reinforcement the permeability barrier. However, it remains unknown how Kap enrichment might impact on other aspects of NCT.

The objective of this work was as follows:

1. To understand how Kap enrichment at the NPC might influence the movement of Ran across the pore to regulate the RanGTP gradient.
2. To test for pore formation by reconstituting TM-Nups in lipid membranes.

1.5Thesis Layout

Following the introduction to NCT and NPCs in Chapter 1, the role of Kaps in maintaining the steep Ran gradient at the NPCs is treated in Chapter 2. Chapter 3 summarizes our efforts to construct nanopores using TM-Nups. Finally, the thesis is concluded in Chapter 4.

1.6References

Abu-Arish, A., P. Kalab, J. Ng-Kamstra, K. Weis, and C. Fradin. 2009. Spatial distribution and mobility of the Ran GTPase in live interphase cells. *Biophys J*. 97:2164-2178.

Alber, F., S. Dokudovskaya, L.M. Veenhoff, W. Zhang, J. Kipper, D. Devos, A. Suprapto, O. Karni-Schmidt, R. Williams, B.T. Chait, A. Sali, and M.P. Rout. 2007. The molecular architecture of the nuclear pore complex. *Nature*. 450:695-701.

Anderson, E., and H.W. Beams. 1956. Evidence from electron micrographs for the passage of material through pores of the nuclear membrane. *J Biophys Biochem Cytol*. 2:439-444.

Antonin, W., J. Ellenberg, and E. Dultz. 2008. Nuclear pore complex assembly through the cell cycle: regulation and membrane organization. *FEBS Lett*. 582:2004-2016.

Azuma, Y., and M. Dasso. 2000. The role of Ran in nuclear function. *Curr Opin Cell Biol*. 12:302-307.

Barbato, S., L.E. Kapinos, C. Rencurel, and R.Y.H. Lim. 2020. Karyopherin enrichment at the nuclear pore complex attenuates Ran permeability. *J. Cell Science* 133(3).

Baur, T., K. Ramadan, A. Schlundt, J. Kartenbeck, and H.H. Meyer. 2007. NSF- and SNARE-mediated membrane fusion is required for nuclear envelope formation and completion of nuclear pore complex assembly in Xenopus laevis egg extracts. *J Cell Sci*. 120:2895-2903.

Bayliss, R., S.W. Leung, R.P. Baker, B.B. Quimby, A.H. Corbett, and M. Stewart. 2002a. Structural basis for the interaction between NTF2 and nucleoporin FxFG repeats. *EMBO J*. 21:2843-2853.

Bayliss, R., T. Littlewood, and M. Stewart. 2000. Structural basis for the interaction between FxFG nucleoporin repeats and importin-beta in nuclear trafficking. *Cell*. 102:99-108.

Bayliss, R., T. Littlewood, L.A. Strawn, S.R. Wente, and M. Stewart. 2002b. GLFG and FxFG nucleoporins bind to overlapping sites on importin-beta. *J Biol Chem*. 277:50597-50606.

Bayliss, R., K. Ribbeck, D. Akin, H.M. Kent, C.M. Feldherr, D. Gorlich, and M. Stewart. 1999. Interaction between NTF2 and xFxFG-containing nucleoporins is required to mediate nuclear import of RanGDP. *J Mol Biol*. 293:579-593.

Beck, M., F. Forster, M. Ecke, J.M. Plitzko, F. Melchior, G. Gerisch, W. Baumeister, and O. Medalia. 2004. Nuclear pore complex structure and dynamics revealed by cryoelectron tomography. *Science*. 306:1387-1390.

Beck, M., V. Lucic, F. Forster, W. Baumeister, and O. Medalia. 2007. Snapshots of nuclear pore complexes in action captured by cryo-electron tomography. *Nature*. 449:611-615.

Berg, O.G., and P.H. von Hippel. 1985. Diffusion-controlled macromolecular interactions. *Annu Rev Biophys Biophys Chem*. 14:131-160.

Bischoff, F.R., C. Klebe, J. Kretschmer, A. Wittinghofer, and H. Ponstingl. 1994. RanGAP11 induces GTPase activity of nuclear Ras-related Ran. *Proc Natl Acad Sci U S A*. 91:2587-2591.

Bischoff, F.R., and H. Ponstingl. 1991. Catalysis of guanine nucleotide exchange on Ran by the mitotic regulator RCC1. *Nature*. 354:80-82.

Boulikas, T. 1994. Putative nuclear localization signals (NLS) in protein transcription factors. *J Cell Biochem*. 55:32-58.

Bui, K.H., A. von Appen, A.L. DiGuilio, A. Ori, L. Sparks, M.T. Mackmull, T. Bock, W. Hagen, A. Andres-Pons, J.S. Glavy, and M. Beck. 2013. Integrated structural analysis of the human nuclear pore complex scaffold. *Cell*. 155:1233-1243.

Burke, B., and J. Ellenberg. 2002. Remodelling the walls of the nucleus. *Nat Rev Mol Cell Biol*. 3:487-497.

Chaillan-Huntington, C., C.V. Braslavsky, J. Kuhlmann, and M. Stewart. 2000. Dissecting the interactions between NTF2, RanGDP, and the nucleoporin XFXFG repeats. *J Biol Chem*. 275:5874-5879.

Chatterjee, M., and B.M. Paschal. 2015. Disruption of the ran system by cysteine oxidation of the nucleotide exchange factor RCC1. *Mol Cell Biol*. 35:566-581.

Chook, Y.M., and G. Blobel. 2001. Karyopherins and nuclear import. *Curr Opin Struct Biol*. 11:703-715.

Chook, Y.M., and K.E. Suel. 2011. Nuclear import by karyopherin-betas: recognition and inhibition. *Biochim Biophys Acta*. 1813:1593-1606.

Chug, H., S. Trakhanov, B.B. Hulsmann, T. Pleiner, and D. Gorlich. 2015. Crystal structure of the metazoan Nup62*Nup58*Nup54 nucleoporin complex. *Science*. 350:106-110.

Cingolani, G., C. Petosa, K. Weis, and C.W. Muller. 1999. Structure of importin-beta bound to the IBB domain of importin-alpha. *Nature*. 399:221-229.

Cordes, V.C., S. Reidenbach, and W.W. Franke. 1995. High content of a nuclear pore complex protein in cytoplasmic annulate lamellae of Xenopus oocytes. *Eur J Cell Biol*. 68:240-255.

Cronshaw, J.M., A.N. Krutchinsky, W. Zhang, B.T. Chait, and M.J. Matunis. 2002. Proteomic analysis of the mammalian nuclear pore complex. *J Cell Biol*. 158:915-927.

Dange, T., D. Grunwald, A. Grunwald, R. Peters, and U. Kubitscheck. 2008. Autonomy and robustness of translocation through the nuclear pore complex: a single-molecule study. *J Cell Biol*. 183:77-86.

Dawson, T.R., M.D. Lazarus, M.W. Hetzer, and S.R. Wente. 2009. ER membrane-bending proteins are necessary for de novo nuclear pore formation. *J Cell Biol*. 184:659-675.

Denning, D.P., S.S. Patel, V. Uversky, A.L. Fink, and M. Rexach. 2003. Disorder in the nuclear pore complex: the FG repeat regions of nucleoporins are natively unfolded. *Proc Natl Acad Sci U S A*. 100:2450-2455.

Devos, D., S. Dokudovskaya, R. Williams, F. Alber, N. Eswar, B.T. Chait, M.P. Rout, and A. Sali. 2006. Simple fold composition and modular architecture of the nuclear pore complex. *Proc Natl Acad Sci U S A*. 103:2172-2177.

Doucet, C.M., J.A. Talamas, and M.W. Hetzer. 2010. Cell cycle-dependent differences in nuclear pore complex assembly in metazoa. *Cell*. 141:1030-1041.

Drin, G., J.F. Casella, R. Gautier, T. Boehmer, T.U. Schwartz, and B. Antonny. 2007. A general amphipathic alpha-helical motif for sensing membrane curvature. *Nat Struct Mol Biol*. 14:138-146.

Dultz, E., and J. Ellenberg. 2010. Live imaging of single nuclear pores reveals unique assembly kinetics and mechanism in interphase. *J Cell Biol*. 191:15-22.

Dultz, E., E. Zanin, C. Wurzenberger, M. Braun, G. Rabut, L. Sironi, and J. Ellenberg. 2008. Systematic kinetic analysis of mitotic dis- and reassembly of the nuclear pore in living cells. *J Cell Biol*. 180:857-865.

Eibauer, M., M. Pellanda, Y. Turgay, A. Dubrovsky, A. Wild, and O. Medalia. 2015. Structure and gating of the nuclear pore complex. *Nat Commun*. 6:7532.

Eisenhardt, N., J. Redolfi, and W. Antonin. 2014. Interaction of Nup53 with Ndc1 and Nup155 is required for nuclear pore complex assembly. *J Cell Sci*. 127:908-921.

Ellenberg, J., E.D. Siggia, J.E. Moreira, C.L. Smith, J.F. Presley, H.J. Worman, and J. Lippincott-Schwartz. 1997. Nuclear membrane dynamics and reassembly in living cells: targeting of an inner nuclear membrane protein in interphase and mitosis. *J Cell Biol*. 138:1193-1206.

England, J.R., J. Huang, M.J. Jennings, R.D. Makde, and S. Tan. 2010. RCC1 uses a conformationally diverse loop region to interact with the nucleosome: a model for the RCC1-nucleosome complex. *J Mol Biol*. 398:518-529.

Fahrenkrog, B., and U. Aebi. 2003. The nuclear pore complex: nucleocytoplasmic transport and beyond. *Nat Rev Mol Cell Biol*. 4:757-766.

Fahrenkrog, B., B. Maco, A.M. Fager, J. Koser, U. Sauder, K.S. Ullman, and U. Aebi. 2002. Domain-specific antibodies reveal multiple-site topology of Nup153 within the nuclear pore complex. *J Struct Biol*. 140:254-267.

Fichtman, B., C. Ramos, B. Rasala, A. Harel, and D.J. Forbes. 2010. Inner/Outer nuclear membrane fusion in nuclear pore assembly: biochemical demonstration and molecular analysis. *Mol Biol Cell*. 21:4197-4211.

Fischer, J., R. Teimer, S. Amlacher, R. Kunze, and E. Hurt. 2015. Linker Nups connect the nuclear pore complex inner ring with the outer ring and transport channel. *Nat Struct Mol Biol*. 22:774-781.

Fiserova, J., S.A. Richards, S.R. Wente, and M.W. Goldberg. 2010. Facilitated transport and diffusion take distinct spatial routes through the nuclear pore complex. *J Cell Sci*. 123:2773-2780.

Fornerod, M., M. Ohno, M. Yoshida, and I.W. Mattaj. 1997. CRM1 is an export receptor for leucine-rich nuclear export signals. *Cell*. 90:1051-1060.

Frey, S., and D. Gorlich. 2007. A saturated FG-repeat hydrogel can reproduce the permeability properties of nuclear pore complexes. *Cell*. 130:512-523.

Frey, S., and D. Gorlich. 2009. FG/FxFG as well as GLFG repeats form a selective permeability barrier with self-healing properties. *EMBO J*. 28:2554-2567.

Frey, S., R.P. Richter, and D. Gorlich. 2006. FG-rich repeats of nuclear pore proteins form a three-dimensional meshwork with hydrogel-like properties. *Science*. 314:815-817.

Funakoshi, T., M. Clever, A. Watanabe, and N. Imamoto. 2011. Localization of Pom121 to the inner nuclear membrane is required for an early step of interphase nuclear pore complex assembly. *Mol Biol Cell*. 22:1058-1069.

Gorlich, D., and I.W. Mattaj. 1996. Nucleocytoplasmic transport. *Science*. 271:1513-1518.

Grunwald, D., R.H. Singer, and M. Rout. 2011. Nuclear export dynamics of RNA-protein complexes. *Nature*. 475:333-341.

Harreman, M.T., P.E. Cohen, M.R. Hodel, G.J. Truscott, A.H. Corbett, and A.E. Hodel. 2003. Characterization of the auto-inhibitory sequence within the N-terminal domain of importin alpha. *J Biol Chem*. 278:21361-21369.

Hulsmann, B.B., A.A. Labokha, and D. Gorlich. 2012. The permeability of reconstituted nuclear pores provides direct evidence for the selective phase model. *Cell*. 150:738-751.

Hutchins, J.R., W.J. Moore, and P.R. Clarke. 2009. Dynamic localisation of Ran GTPase during the cell cycle. *BMC Cell Biol*. 10:66.

Isgro, T.A., and K. Schulten. 2005. Binding dynamics of isolated nucleoporin repeat regions to importin-beta. *Structure* 13(12):1869-1879.

Kabachinski, G., and T.U. Schwartz. 2015. The nuclear pore complex--structure and function at a glance. *J Cell Sci*. 128:423-429.

Kalab, P., K. Weis, and R. Heald. 2002. Visualization of a Ran-GTP gradient in interphase and mitotic Xenopus egg extracts. *Science*. 295:2452-2456.

Kapinos, L.E., B. Huang, C. Rencurel, and R.Y.H. Lim. 2017. Karyopherins regulate nuclear pore complex barrier and transport function. *J Cell Biol*. 216:3609-3624.

Kapinos, L.E., R.L. Schoch, R.S. Wagner, K.D. Schleicher, and R.Y.H. Lim. 2014. Karyopherin-centric control of nuclear pores based on molecular occupancy and

kinetic analysis of multivalent binding with FG nucleoporins. *Biophys J*. 106:1751-1762.

Kelley, J.B., and B.M. Paschal. 2007. Hyperosmotic stress signaling to the nucleus disrupts the Ran gradient and the production of RanGTP. *Mol Biol Cell*. 18:4365-4376.

Klebe, C., F.R. Bischoff, H. Ponstingl, and A. Wittinghofer. 1995a. Interaction of the nuclear GTP-binding protein Ran with its regulatory proteins RCC1 and RanGAP11. *Biochemistry*. 34:639-647.

Klebe, C., H. Prinz, A. Wittinghofer, and R.S. Goody. 1995b. The kinetic mechanism of Ran--nucleotide exchange catalyzed by RCC1. *Biochemistry*. 34:12543-12552.

Kobe, B. 1999. Autoinhibition by an internal nuclear localization signal revealed by the crystal structure of mammalian importin alpha. *Nat Struct Biol*. 6:388-397.

Konishi, H.A., S. Asai, T.M. Watanabe, and S.H. Yoshimura. 2017. In vivo analysis of protein crowding within the nuclear pore complex in interphase and mitosis. *Sci Rep*. 7:5709.

Kopito, R.B., and M. Elbaum. 2007. Reversibility in nucleocytoplasmic transport. *Proc Natl Acad Sci U S A*. 104:12743-12748.

Kosinski, J., S. Mosalaganti, A. von Appen, R. Teimer, A.L. DiGuilio, W. Wan, K.H. Bui, W.J. Hagen, J.A. Briggs, J.S. Glavy, E. Hurt, and M. Beck. 2016. Molecular architecture of the inner ring scaffold of the human nuclear pore complex. *Science*. 352:363-365.

Kutay, U., F.R. Bischoff, S. Kostka, R. Kraft, and D. Gorlich. 1997. Export of importin alpha from the nucleus is mediated by a specific nuclear transport factor. *Cell*. 90:1061-1071.

Li, P., S. Banjade, H.C. Cheng, S. Kim, B. Chen, L. Guo, M. Llaguno, J.V. Hollingsworth, D.S. King, S.F. Banani, P.S. Russo, Q.X. Jiang, B.T. Nixon, and M.K. Rosen. 2012.

Phase transitions in the assembly of multivalent signalling proteins. *Nature*. 483:336-340.

Lim, R.Y.H., B. Fahrenkrog, J. Koser, K. Schwarz-Herion, J. Deng, and U. Aebi. 2007. Nanomechanical basis of selective gating by the nuclear pore complex. *Science*. 318:640-643.

Lim, R.Y.H., B. Huang, and L.E. Kapinos. 2015. How to operate a nuclear pore complex by Kap-centric control. *Nucleus*. 6:366-372.

Lim, R.Y.H., N.P. Huang, J. Koser, J. Deng, K.H. Lau, K. Schwarz-Herion, B. Fahrenkrog, and U. Aebi. 2006. Flexible phenylalanine-glycine nucleoporins as entropic barriers to nucleocytoplasmic transport. *Proc Natl Acad Sci U S A*. 103:9512-9517.

Lowe, A.R., J.J. Siegel, P. Kalab, M. Siu, K. Weis, and J.T. Liphardt. 2010. Selectivity mechanism of the nuclear pore complex characterized by single cargo tracking. *Nature*. 467:600-603.

Lowe, A.R., J.H. Tang, J. Yassif, M. Graf, W.Y. Huang, J.T. Groves, K. Weis, and J.T. Liphardt. 2015. Importin-beta modulates the permeability of the nuclear pore complex in a Ran-dependent manner. *Elife*. 4.

Ma, J., A. Goryaynov, A. Sarma, and W. Yang. 2012. Self-regulated viscous channel in the nuclear pore complex. *Proc Natl Acad Sci U S A*. 109:7326-7331.

Macaulay, C., and D.J. Forbes. 1996. Assembly of the nuclear pore: biochemically distinct steps revealed with NEM, GTP gamma S, and BAPTA. *J Cell Biol*. 132:5-20.

Mahajan, R., C. Delphin, T. Guan, L. Gerace, and F. Melchior. 1997. A small ubiquitin-related polypeptide involved in targeting RanGAP11 to nuclear pore complex protein RanBP2. *Cell*. 88:97-107.

Maimon, T., N. Elad, I. Dahan, and O. Medalia. 2012. The human nuclear pore complex as revealed by cryo-electron tomography. *Structure*. 20:998-1006.

Mansfeld, J., S. Guttinger, L.A. Hawryluk-Gara, N. Pante, M. Mall, V. Galy, U. Haselmann, P. Muhlhausser, R.W. Wozniak, I.W. Mattaj, U. Kutay, and W. Antonin. 2006. The conserved transmembrane nucleoporin NDC1 is required for nuclear pore complex assembly in vertebrate cells. *Mol Cell*. 22:93-103.

Matunis, M.J., J. Wu, and G. Blobel. 1998. SUMO-1 modification and its role in targeting the Ran GTPase-activating protein, RanGAP11, to the nuclear pore complex. *J Cell Biol*. 140:499-509.

Maul, G.G., and L. Deaven. 1977. Quantitative determination of nuclear pore complexes in cycling cells with differing DNA content. *J Cell Biol*. 73:748-760.

Mehlin, H., B. Daneholt, and U. Skoglund. 1992. Translocation of a specific premessenger ribonucleoprotein particle through the nuclear pore studied with electron microscope tomography. *Cell*. 69:605-613.

Milles, S., K. Huy Bui, C. Koehler, M. Eltsov, M. Beck, and E.A. Lemke. 2013. Facilitated aggregation of FG nucleoporins under molecular crowding conditions. *EMBO Rep*. 14:178-183.

Nachury, M.V., and K. Weis. 1999. The direction of transport through the nuclear pore can be inverted. *Proc Natl Acad Sci U S A*. 96:9622-9627.

Nemergut, M.E., C.A. Mizzen, T. Stukenberg, C.D. Allis, and I.G. Macara. 2001. Chromatin docking and exchange activity enhancement of RCC1 by histones H2A and H2B. *Science*. 292:1540-1543.

Ohtsubo, M., H. Okazaki, and T. Nishimoto. 1989. The RCC1 protein, a regulator for the onset of chromosome condensation locates in the nucleus and binds to DNA. *J Cell Biol*. 109:1389-1397.

Otsuka, S., K.H. Bui, M. Schorb, M.J. Hossain, A.Z. Politi, B. Koch, M. Eltsov, M. Beck, and J. Ellenberg. 2016. Nuclear pore assembly proceeds by an inside-out extrusion of the nuclear envelope. *Elife*. 5.

Otsuka, S., and J. Ellenberg. 2018. Mechanisms of nuclear pore complex assembly - two different ways of building one molecular machine. *FEBS Lett*. 592:475-488.

Pante, N., and M. Kann. 2002. Nuclear pore complex is able to transport macromolecules with diameters of about 39 nm. *Mol Biol Cell*. 13:425-434.

Paradise, A., M.K. Levin, G. Korza, and J.H. Carson. 2007. Significant proportions of nuclear transport proteins with reduced intracellular mobilities resolved by fluorescence correlation spectroscopy. *J Mol Biol*. 365:50-65.

Patel, S.S., B.J. Belmont, J.M. Sante, and M.F. Rexach. 2007. Natively unfolded nucleoporins gate protein diffusion across the nuclear pore complex. *Cell*. 129:83-96.

Peters, R. 2005. Translocation through the nuclear pore complex: selectivity and speed by reduction-of-dimensionality. *Traffic*. 6:421-427.

Peters, R. 2009a. Functionalization of a nanopore: the nuclear pore complex paradigm. *Biochim Biophys Acta*. 1793:1533-1539.

Peters, R. 2009b. Translocation through the nuclear pore: Kaps pave the way. *Bioessays*. 31:466-477.

Popken, P., A. Ghavami, P.R. Onck, B. Poolman, and L.M. Veenhoff. 2015. Size-dependent leak of soluble and membrane proteins through the yeast nuclear pore complex. *Mol Biol Cell*. 26:1386-1394.

Rabe, B., A. Vlachou, N. Pante, A. Helenius, and M. Kann. 2003. Nuclear import of hepatitis B virus capsids and release of the viral genome. *Proc Natl Acad Sci U S A*. 100:9849-9854.

Rasala, B.A., C. Ramos, A. Harel, and D.J. Forbes. 2008. Capture of AT-rich chromatin by ELYS recruits POM121 and NDC1 to initiate nuclear pore assembly. *Mol Biol Cell*. 19:3982-3996.

Reichelt, R., A. Holzenburg, E.L. Buhle, Jr., M. Jarnik, A. Engel, and U. Aebi. 1990. Correlation between structure and mass distribution of the nuclear pore complex and of distinct pore complex components. *J Cell Biol*. 110:883-894.

Ribbeck, K., and D. Gorlich. 2001. Kinetic analysis of translocation through nuclear pore complexes. *EMBO J*. 20:1320-1330.

Ribbeck, K., and D. Gorlich. 2002. The permeability barrier of nuclear pore complexes appears to operate via hydrophobic exclusion. *EMBO J*. 21:2664-2671.

Ribbeck, K., G. Lipowsky, H.M. Kent, M. Stewart, and D. Gorlich. 1998. NTF2 mediates nuclear import of Ran. *EMBO J*. 17:6587-6598.

Rothballer, A., and U. Kutay. 2013. Poring over pores: nuclear pore complex insertion into the nuclear envelope. *Trends Biochem Sci*. 38:292-301.

Rout, M.P., J.D. Aitchison, M.O. Magnasco, and B.T. Chait. 2003. Virtual gating and nuclear transport: the hole picture. *Trends Cell Biol*. 13:622-628.

Rout, M.P., and G. Blobel. 1993. Isolation of the yeast nuclear pore complex. *J Cell Biol*. 123:771-783.

Sachdev, R., C. Sieverding, M. Flotenmeyer, and W. Antonin. 2012. The C-terminal domain of Nup93 is essential for assembly of the structural backbone of nuclear pore complexes. *Mol Biol Cell*. 23:740-749.

Sakiyama, Y., A. Mazur, L.E. Kapinos, and R.Y.H. Lim. 2016. Spatiotemporal dynamics of the nuclear pore complex transport barrier resolved by high-speed atomic force microscopy. *Nat Nanotechnol*. 11:719-723.

Sampathkumar, P., S.J. Kim, P. Upla, W.J. Rice, J. Phillips, B.L. Timney, U. Pieper, J.B. Bonanno, J. Fernandez-Martinez, Z. Hakhverdyan, N.E. Ketaren, T. Matsui, T.M. Weiss, D.L. Stokes, J.M. Sauder, S.K. Burley, A. Sali, M.P. Rout, and S.C. Almo. 2013. Structure, dynamics, evolution, and function of a major scaffold component in the nuclear pore complex. *Structure*. 21:560-571.

Schoch, R.L., L.E. Kapinos, and R.Y.H. Lim. 2012. Nuclear transport receptor binding avidity triggers a self-healing collapse transition in FG-nucleoporin molecular brushes. *Proc Natl Acad Sci U S A*. 109:16911-16916.

Schwoebel, E.D., B. Talcott, I. Cushman, and M.S. Moore. 1998. Ran-dependent signal-mediated nuclear import does not require GTP hydrolysis by Ran. *J Biol Chem*. 273:35170-35175.

Shaulov, L., R. Gruber, I. Cohen, and A. Harel. 2011. A dominant-negative form of POM121 binds chromatin and disrupts the two separate modes of nuclear pore assembly. *J Cell Sci*. 124:3822-3834.

Siebrasse, J.P., and R. Peters. 2002. Rapid translocation of NTF2 through the nuclear pore of isolated nuclei and nuclear envelopes. *EMBO Rep*. 3:887-892.

Smith, A.E., B.M. Slepchenko, J.C. Schaff, L.M. Loew, and I.G. Macara. 2002. Systems analysis of Ran transport. *Science*. 295:488-491.

Stewart, M. 2007. Molecular mechanism of the nuclear protein import cycle. *Nat Rev Mol Cell Biol*. 8:195-208.

Stewart, M., H.M. Kent, and A.J. McCoy. 1998. The structure of the Q69L mutant of GDP-Ran shows a major conformational change in the switch II loop that accounts for its failure to bind nuclear transport factor 2 (NTF2). *J Mol Biol*. 284:1517-1527.

Stoffler, D., B. Feja, B. Fahrenkrog, J. Walz, D. Typke, and U. Aebi. 2003. Cryo-electron tomography provides novel insights into nuclear pore architecture: implications for nucleocytoplasmic transport. *J Mol Biol*. 328:119-130.

Strambio-De-Castillia, C., M. Niepel, and M.P. Rout. 2010. The nuclear pore complex: bridging nuclear transport and gene regulation. *Nat Rev Mol Cell Biol*. 11:490-501.

Strawn, L.A., T. Shen, N. Shulga, D.S. Goldfarb, and S.R. Wente. 2004. Minimal nuclear pore complexes define FG repeat domains essential for transport. *Nat Cell Biol*. 6:197-206.

Talamas, J.A., and M.W. Hetzer. 2011. POM121 and Sun1 play a role in early steps of interphase NPC assembly. *J Cell Biol*. 194:27-37.

Timney, B.L., B. Raveh, R. Mironska, J.M. Trivedi, S.J. Kim, D. Russel, S.R. Wente, A. Sali, and M.P. Rout. 2016. Simple rules for passive diffusion through the nuclear pore complex. *J Cell Biol*. 215:57-76.

Tran, E.J., and S.R. Wente. 2006. Dynamic nuclear pore complexes: life on the edge. *Cell*. 125:1041-1053.

Vetter, I.R., C. Nowak, T. Nishimoto, J. Kuhlmann, and A. Wittinghofer. 1999. Structure of a Ran-binding domain complexed with Ran bound to a GTP analogue: implications for nuclear transport. *Nature*. 398:39-46.

Vetter, I.R., and A. Wittinghofer. 2001. The guanine nucleotide-binding switch in three dimensions. *Science*. 294:1299-1304.

Vietri, M., K.O. Schink, C. Campsteijn, C.S. Wegner, S.W. Schultz, L. Christ, S.B. Thoresen, A. Brech, C. Raiborg, and H. Stenmark. 2015. Spastin and ESCRT-III coordinate mitotic spindle disassembly and nuclear envelope sealing. *Nature*. 522:231-235.

Vollmer, B., M. Lorenz, D. Moreno-Andres, M. Bodenhofer, P. De Magistris, S.A. Astrinidis, A. Schooley, M. Flotenmeyer, S. Leptihn, and W. Antonin. 2015. Nup153 Recruits

the Nup107-160 Complex to the Inner Nuclear Membrane for Interphasic Nuclear Pore Complex Assembly. *Dev Cell*. 33:717-728.

Vollmer, B., A. Schooley, R. Sachdev, N. Eisenhardt, A.M. Schneider, C. Sieverding, J. Madlung, U. Gerken, B. Macek, and W. Antonin. 2012. Dimerization and direct membrane interaction of Nup53 contribute to nuclear pore complex assembly. *EMBO J*. 31:4072-4084.

von Appen, A., J. Kosinski, L. Sparks, A. Ori, A.L. DiGuilio, B. Vollmer, M.T. Mackmull, N. Banterle, L. Parca, P. Kastritis, K. Buczak, S. Mosalaganti, W. Hagen, A. Andres-Pons, E.A. Lemke, P. Bork, W. Antonin, J.S. Glavy, K.H. Bui, and M. Beck. 2015. In situ structural analysis of the human nuclear pore complex. *Nature*. 526:140-143.

Vujica, S., C. Zelmer, R. Panatala, and R.Y.H. Lim. 2016. Nucleocytoplasmic Transport: A Paradigm for Molecular Logistics in Artificial Systems. *Chimia (Aarau)*. 70:413-417.

Wagner, R.S., L.E. Kapinos, N.J. Marshall, M. Stewart, and R.Y.H. Lim. 2015. Promiscuous binding of Karyopherinbeta1 modulates FG nucleoporin barrier function and expedites NTF2 transport kinetics. *Biophys J*. 108:918-927.

Walther, T.C., H.S. Pickersgill, V.C. Cordes, M.W. Goldberg, T.D. Allen, I.W. Mattaj, and M. Fornerod. 2002. The cytoplasmic filaments of the nuclear pore complex are dispensable for selective nuclear protein import. *J Cell Biol*. 158:63-77.

Wen, W., J.L. Meinkoth, R.Y. Tsien, and S.S. Taylor. 1995. Identification of a signal for rapid export of proteins from the nucleus. *Cell*. 82:463-473.

Whittaker, G.R., M. Kann, and A. Helenius. 2000. Viral entry into the nucleus. *Annu Rev Cell Dev Biol*. 16:627-651.

Winey, M., D. Yarar, T.H. Giddings, Jr., and D.N. Mastronarde. 1997. Nuclear pore complex number and distribution throughout the Saccharomyces cerevisiae cell cycle by three-

dimensional reconstruction from electron micrographs of nuclear envelopes. *Mol Biol Cell*. 8:2119-2132.

Yamada, J., J.L. Phillips, S. Patel, G. Goldfien, A. Calestagne-Morelli, H. Huang, R. Reza, J. Acheson, V.V. Krishnan, S. Newsam, A. Gopinathan, E.Y. Lau, M.E. Colvin, V.N. Uversky, and M.F. Rexach. 2010. A bimodal distribution of two distinct categories of intrinsically disordered structures with separate functions in FG nucleoporins. *Mol Cell Proteomics*. 9:2205-2224.

Yang, W., and S.M. Musser. 2006. Nuclear import time and transport efficiency depend on importin beta concentration. *J Cell Biol*. 174:951-961.

Yasuda, Y., Y. Miyamoto, T. Saiwaki, and Y. Yoneda. 2006. Mechanism of the stress-induced collapse of the Ran distribution. *Exp Cell Res*. 312:512-520.

Yokoyama, N., N. Hayashi, T. Seki, N. Pante, T. Ohba, K. Nishii, K. Kuma, T. Hayashida, T. Miyata, U. Aebi, and et al. 1995. A giant nucleopore protein that binds Ran/TC4. *Nature*. 376:184-188.

Kapβ1 enrichment attenuates Ran permeability at the nuclear pore complex

---

Adapted from

Karyopherin enrichment at the nuclear pore complex attenuates Ran permeability

Suncica Barbato, Larisa E. Kapinos, Chantal Rencurel, and Roderick Y.H. Lim

Published in Journal of Cell Science, 2020;133(3)

2Kap β 1 enrichment attenuates Ran permeability at the nuclear pore complex

2.1Role of the selective transport barrier in the maintenance of RanGTP/GDP gradient

An understanding of how NPCs reconcile physical size exclusion with biochemical selectivity to mediate NCT remains incoherent. One peculiarity that remains unexplained concerns Ran, which is vital for controlling the site of cargo release and accumulation as well as for the recycling of Kaps (Gorlich et al., 1995a), (Gorlich et al., 1996a). This underpins NCT directionality across the NE and is regulated by a gradient of its two nucleotide-bound forms, Ran-guanosine triphosphate (RanGTP) and Ran-guanosine diphosphate (RanGDP), which are enriched in the nucleus and cytoplasm, respectively (Hutchins et al., 2009), (Kalab et al., 2002), (Kelley and Paschal, 2007), (Smith et al., 2002). It should be noted that Ran (being 25 kDa in size) is smaller than the nonspecific size cutoff, and neither RanGDP nor RanGTP interact with the FG-repeats (Rexach and Blobel, 1995). Hence, it remains unknown why an uncontrolled mixing of RanGTP and RanGDP at NPCs in unable to establish the Ran gradient. Importantly, NCT directionality is lost as a consequence of irregularities in the Ran gradient (Nachury and Weis, 1999).

NLS-cargo•Kapα•Kapβ1 complexes that traverse NPCs are disassembled when RanGTP binds to Kapβ1 in the nucleus (Chi et al., 1996), (Gorlich et al., 1996b), (Rexach and Blobel, 1995). This event imparts a ratcheting mechanism that facilitates the nuclear retention of NLS-cargoes, whose retrograde transport is hindered in the absence of FG-Nup binding. On the other hand, RanGTP•Kapβ1 retains its interactions with the FG-Nups to return through

NPCs (Kapinos et al., 2017). Upon reaching the cytoplasmic periphery, GTP is hydrolyzed to (Ran)GDP by RanGTPase activating protein (RanGAP1), which releases Kapβ1 to seek out the next NLS-cargo (Stewart, 2007). However, although Ran is highly mobile (Abu-Arish et al., 2009), it does not diffuse through the NPC like other nonspecific molecules of similar size (Timney et al., 2016). Instead, RanGDP requires a dedicated importer, NTF2 (i.e., nuclear transport factor 2) (Ribbeck et al., 1998), (Smith et al., 1998), which shuttles it back through NPCs to the nucleus. Upon re-entry, a chromatin-bound enzyme known as RanGEF (guanine nucleotide exchange factor, also called regulator of chromatin condensation or RCC1) (Klebe et al., 1995b), (Renault et al., 2001) then recharges RanGDP to RanGTP to complete the cycle. Meanwhile, RanGTP•exportin•NES cargo complexes that form in the nucleus are disassembled following GTP hydrolysis by RanGAP1 in the cytoplasm (Macara, 2001). In this manner, NCT cargo delivery and Kap recycling are energetically driven by RanGAP1/GEF and maintained by the controlled exchange of RanGTP and RanGDP across NPCs (Gorlich et al., 1996a), (Abu-Arish et al., 2009), (Izaurralde et al., 1997), (Kalab et al., 2006), (Kalab et al., 2002).

As a matter of fact, Kapβ1 generally enriches the FG-Nups at steady state (Kapinos et al., 2014), (Schoch et al., 2012), (Vovk et al., 2016), (Wagner et al., 2015), (Zahn et al., 2016) and in NPCs (Gorlich et al., 1995b), (Kassianidou et al., 2019), (Lim et al., 2015), (Lowe et al., 2015). Depleting this Kapβ1 pool abolishes the NPC barrier function against nonspecific cargoes (Kapinos et al., 2017). Accordingly, we proposed that Kaps might impart a form of "Kap-centric" control in NPCs (i) to reinforce the NPC barrier against nonspecific cargoes and (ii) to facilitate fast Kapβ1 transport kinetics (Lim et al., 2015).

Here, we explore the implications of Kap-centric control in preventing the uncontrolled exchange of Ran across NPCs. Our results show that the FG-Nups alone do not optimally restrict its movement through NPCs lacking Kaps. Instead, the presence of Kapβ1 enables the selective partitioning of RanGTP and RanGDP into the NPC, but not passive molecules of similar size (e.g., GFP). This partitioning is underpinned by binding interactions with Kapβ1 at the pore, which is stronger for RanGTP and weaker for RanGDP. Nevertheless, the largest outflow occurs for RanGTP, which follows from the formation of RanGTP•Kapβ1 and its hydrolysis to RanGDP•Kapβ1, being the more weakly bound state. Finally, our work explains why selective transport of RanGDP is mediated by NTF2, which does so to prevent RanGDP•Kapβ1 complex formation. On this basis, Kaps might further serve to regulate NCT by selectively partitioning Ran within NPCs so as to prevent its uncontrolled mixing across the NE.

2.2Kap depletion weakens the NPC barrier against RanGDP

As we previously reported (Kapinos et al., 2017), a pool of endogenous Kapβ1 (endoKapβ1) and Kapα (endoKapα) (collectively termed endoKaps) is generally retained at the NE after digitonin permeabilization (**Figure 2-1 A**). Therefore, we initially wanted to know if endoKaps had an impact on the movement of RanGDP through NPCs (**Figure 2-1 B**). This was compared against permeabilized cells that were significantly reduced of endoKaps in NPCs after an incubation in Ran mix (Gorlich et al., 1995b), (Kapinos et al., 2017), which resulted in a ~50% endoKapβ1 and ~80% endoKapα reduction in the nucleus and NE, respectively (**Figure 2-1 B-C**). Next, we incubated both samples in 5 μM exoRanGDP for 1 h until equilibration was reached within the nucleus and its exterior. This was followed by a

short PBS wash (3 x 5 min) to investigate the extent of exoRanGDP nuclear retention in the presence and absence of endoKaps. In comparison to the permeabilized cell control (and under the same time conditions), exoRanGDP was reduced by ~50% in both the nucleus and NE when endoKaps were reduced (**Figure 2-1 B-C**). This observation suggests that the presence of endoKaps in NPCs impedes the outflow of exoRanGDP from the nucleus.

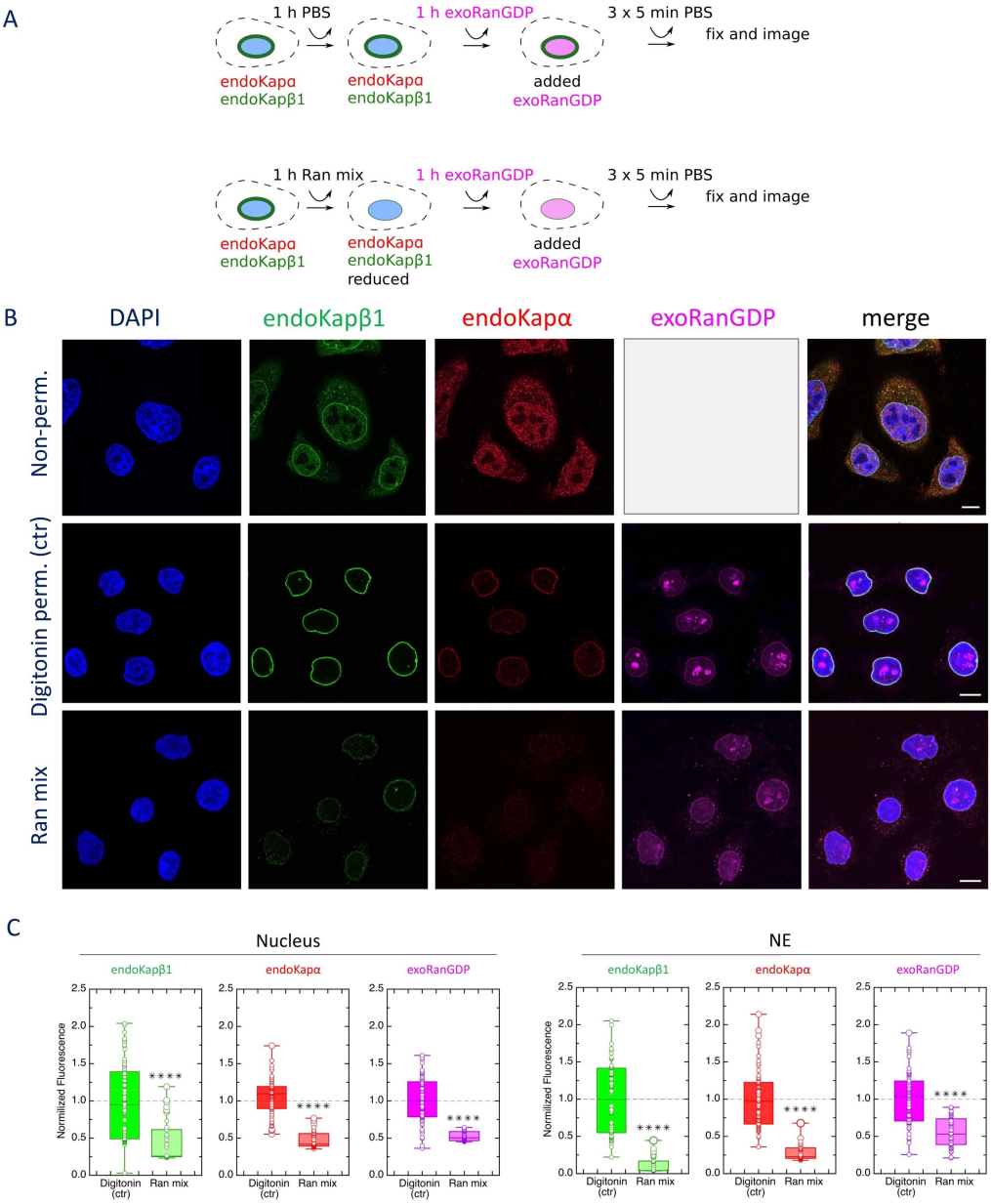

Figure 2-1 Depleting Kapβ1 from the NPC liberates RanGDP from the nucleus

*(A) Experimental sequence. (B) Immunofluorescence reveals the accumulation of endoKapβ1 at the NE before and after digitonin permeabilization, signifying its retention in NPCs. Following its equilibration inside the nucleus, more exoRanGDP is liberated out of Ran mix-treated nuclei, which reduces endoKapβ1 from NPCs. Bars, 10 µm. (C) Fluorescence quantification of endoKapβ1, endoKapα and exoRanGDP in digitonin-permeabilized cells with and without Ran mix. n ≥ 3, with a total of 120, 63 and 39 cells for non-permeabilized cells, digitonin-permeabilized cells (i.e., control) and Ran mix, respectively. ****, P < 0.0001; Student's t-test. Box plots denote the median, first, and third quartiles. Error bars denote standard deviation, including outliers. See Table 2-1 for details. Reproduced from (Barbato and Kapinos et al., 2020).*

2.3Kapβ1, but not Kapα·Kapβ1, restricts RanGDP diffusion through NPCs

To test this hypothesis, we filled endoKap-reduced nuclei with exoRanGDP, followed by 10 μM exogenous Kapβ1 (exoKapβ1) to check if exoRanGDP retention was mediated by the exoKapβ1 that had re-populated the NPCs (**Figure 2-2 A**). These were compared against samples re-populated with exoKapα•Kapβ1 (20 μM:10 μM). As expected, exoKapβ1 and exoKapα•Kapβ1 stained the NE in both cases. Much to our surprise, exoRanGDP retention was the lowest in nuclei harboring exoKapα•Kapβ1, being 25% less than control samples that were incubated in PBS lacking exoKaps (**Figure 2-2 B-C**). This difference signified that exoKapα•Kapβ1 did not impede exoRanGDP outflow as effectively as standalone exoKapβ1 at the NPC, which was 20% more effective than control (**Figure 2-2 B-C**). Nevertheless, we did obtain exoRanGDP signal at the NE of control cells, which suggested residual binding with endoKaps or other NPC components (Gorlich et al., 1996b), (Partridge and Schwartz, 2009), (Schrader et al., 2008). Based on these observations, we rationalized that the NPC might only effectively impede exoRanGDP movement based on its biochemical interactions with the Kaps.

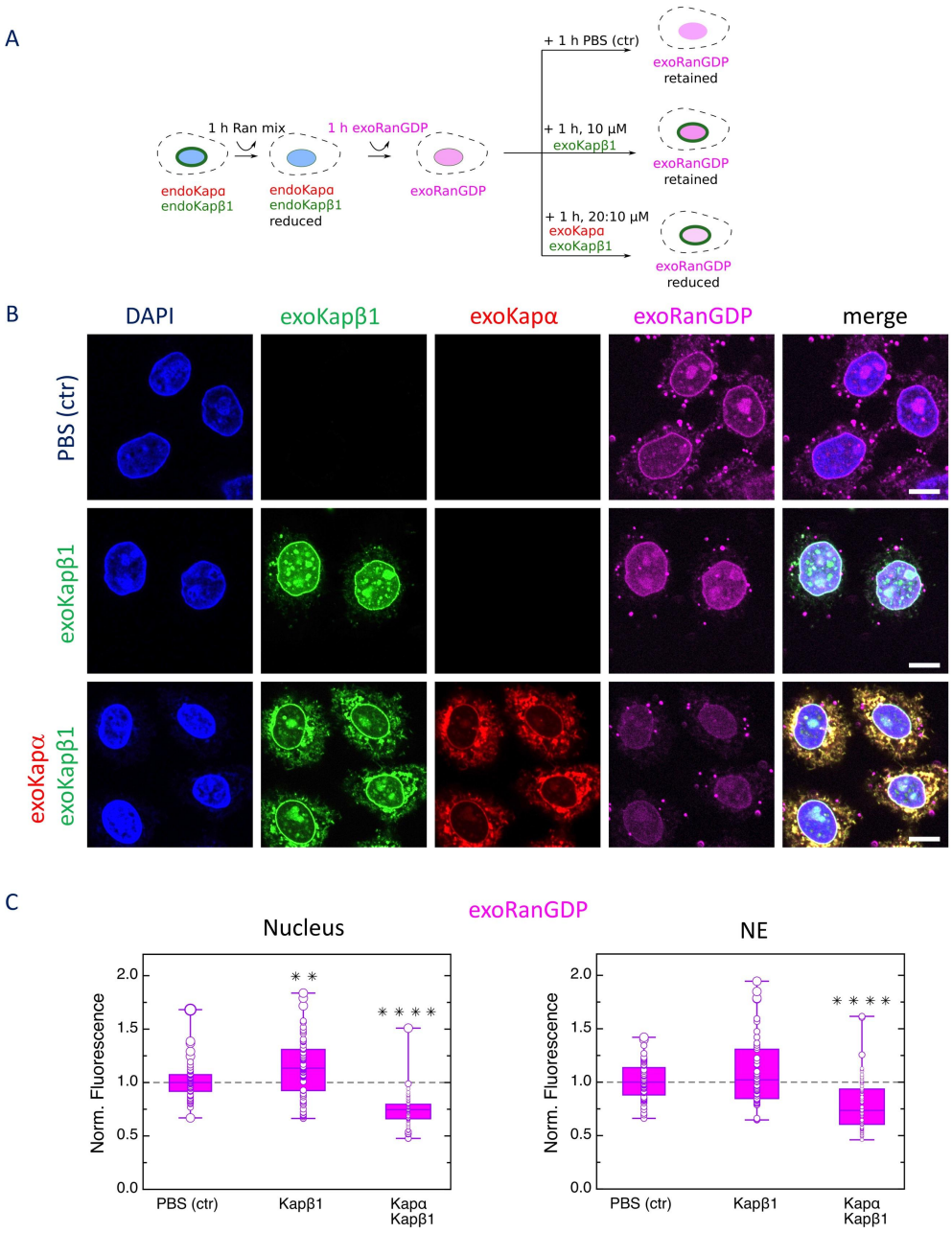

Figure 2-2 Binding to Kapβ1 restricts RanGDP diffusion through NPCs

*(A) Experimental sequence. (B) ExoRanGDP is retained in Ran mix-treated nuclei after being repopulated with exoKapβ1 because of their binding at NPCs. For comparison, exoKapα•Kapβ1 does not impede the outflow of exoRanGDP as they do not bind. Bar, 10 µm. (C) Fluorescence quantification of exoRanGDP in the nucleus and NE at each of the above conditions. n = 3 with a total of 56, 65 and 70 cells for PBS control, 10 µM exoKapβ1 and (20:10) µM exoKapα•Kapβ1 complex, respectively. **, P < 0.01; ****, P < 0.0001; Student's t-test. Box plots denote the median, first, and third quartiles. Error bars denote standard deviation, including outliers. See Table 2-1 for details. Reproduced from (Barbato and Kapinos et al., 2020).*

Subsequently, binding affinity measurements of exoRanGDP and the mutant RanQ69L•GDP against exoKapβ1 gave K_d = 0.5 ± 0.07 µM or K_d = 1.3 ± 0.15 µM, respectively (**Figure 2-3**). This result was consistent with values in the literature (Forwood et al., 2008), (Lonhienne et al., 2009). For comparison, Kap α •Kapβ1 binding is comparably stronger (K_d = 0.2 µM) (Bednenko et al., 2003), (Catimel et al., 2001), (Kapinos et al., 2017), potentially explaining why exoRanGDP retention is lowest in nuclei harboring exoKapα•Kapβ1, as it is unable to outcompete exoKapα for exoKapβ1. In comparison, NPCs in control nuclei may harbor free importins and exportins that can bind to exoRanGDP. Indeed, the nuclear and NE exoRanGDP signal is ~30% higher for exoKapβ1 compared to exoKapα•Kapβ1 (**Figure 2-2 B-C**). Thereafter, we hypothesized that exoKapβ1 might act as a biochemical barrier against exoRanGDP in the NPC. Conversely, a lack of binding with exoKapα•Kapβ1 facilitates a larger outflow of exoRanGDP from the nucleus.

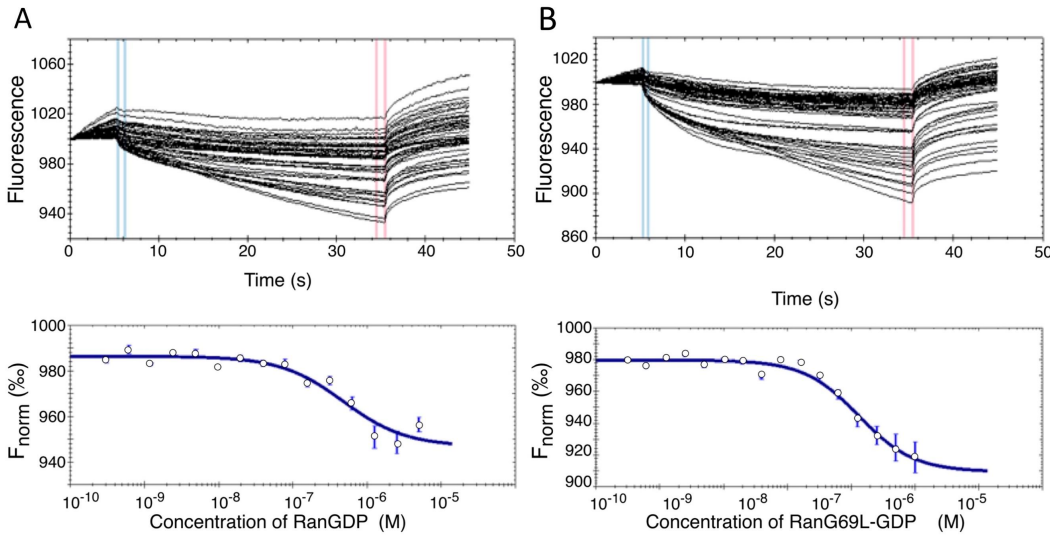

Figure 2-3 Microscale thermophoresis binding affinity measurements
(A) K_d = 453 ± 74.4 nM for RanGDP-Kapβ1 binding. (B) K_d = 1300 ± 147nM for RanQ69L-GDP-Kapβ1 binding. n = 3. Reproduced from (Barbato and Kapinos et al., 2020).

To validate this argument, we used GFP (ca. 26 kDa), which is about the same size as Ran but neither binds to the FG-Nups nor Kaps and therefore should not be retained at the NE. In both cases, GFP was undetectable, indicating that neither exoKapβ1 nor exoKapα•Kapβ1 could stem the outflow of GFP from the nucleus (**Figure 2-4**). Interestingly, this finding is consistent with in vivo observations of small passive cargoes of equivalent size (Abu-Arish et al., 2009), (Timney et al., 2016). Hence, this observation shows that the NPC cutoff for nonspecific molecules does not preclude Kap occupancy at the pore.

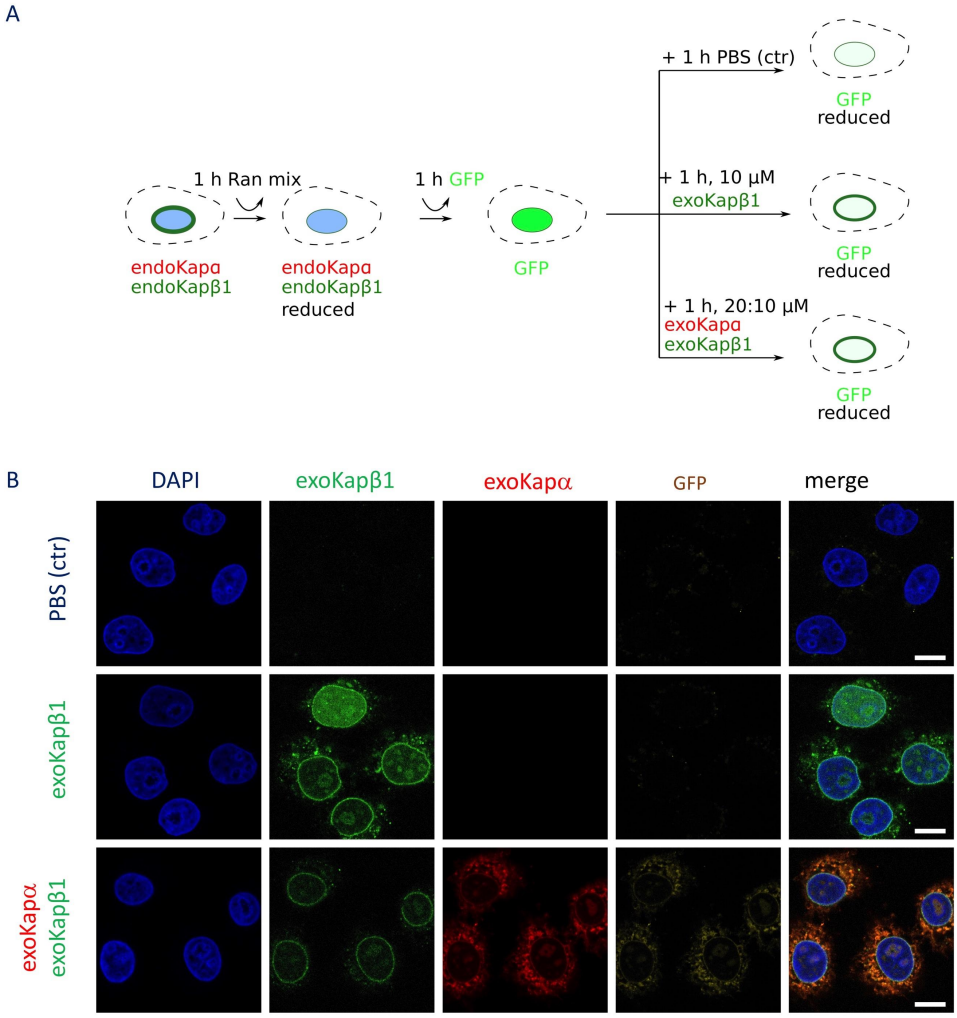

Figure 2-4 Kapβ1 is ineffective as a barrier against GFP

(A) Experimental sequence. (B) Neither NPC-bound pools of exoKapβ1 nor exoKapα•Kapβ1 are able to stem the outflow of GFP from the nucleus. Note: GFP quantification was not possible because of the low signal obtained in each experiment. Reproduced from (Barbato and Kapinos et al., 2020).

2.4RanGTP diffusion depends on GTP hydrolysis

RanGDP is rapidly converted by RanGEF into RanGTP (k_{cat} = 3.5 s^{-1}) (Klebe et al., 1995a), which binds Kapβ1 in the nucleus to displace Kapα during NCT. Given that RanGTP•Kapβ1 binding is significantly stronger (K_d = 0.035 μM) (Bednenko et al., 2003), (Hahn and Schlenstedt, 2011), (Kapinos et al., 2017) than RanGDP, we wondered how its efflux would differ. Upon verifying that RanGEF (and RanGAP1) was present following permeabilization (**Figure 2-5**), we again entrapped exoRanGDP by incubating endoKap-reduced nuclei with 10 μM exoKapβ1 or exoKapα•Kapβ1 (20 μM:10 μM) but followed this with an energy regenerating mixture comprising of 2 mM GTP, 0.1 mM ATP, 4 mM creatine phosphate, 20 U/mL creatine kinase (Ribbeck et al., 1998) to enable RanGEF activity (**Figure 2-6**).

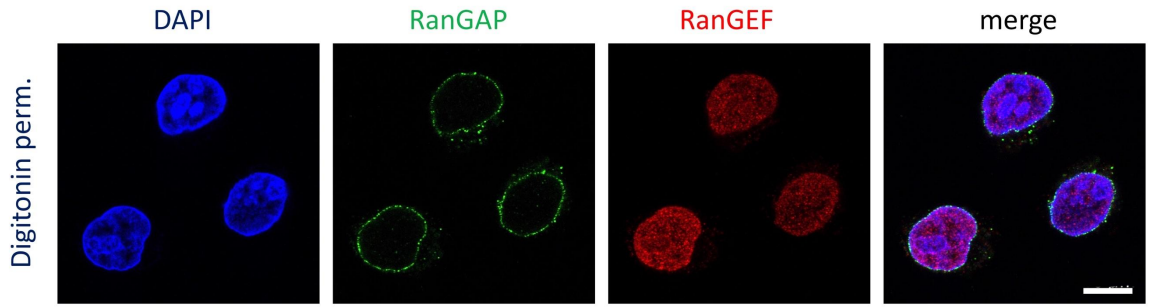

Figure 2-5 Immunostaining of RanGAP1 and RanGEF in HeLa cells
RanGAP1 and RanGEF are present following digitonin permeabilization. See Methods for details. Reproduced from (Barbato and Kapinos et al., 2020).

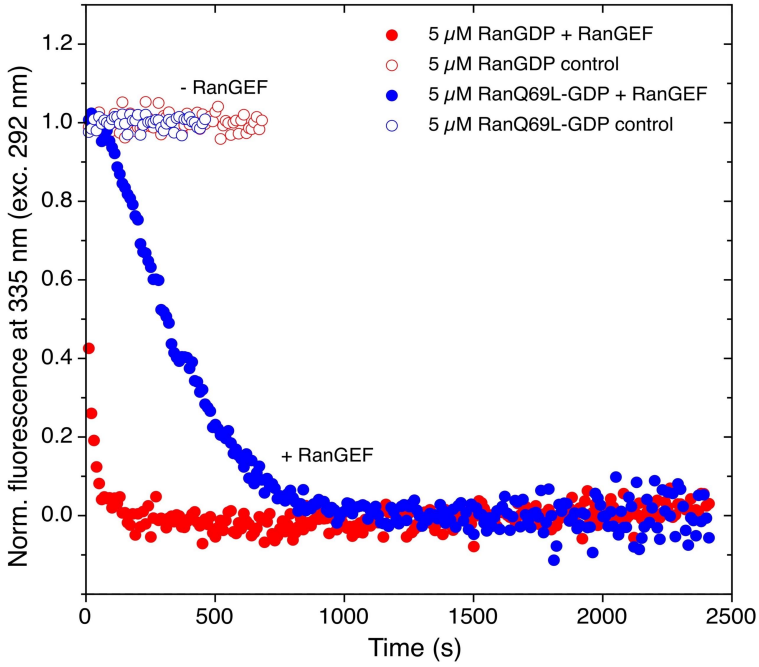

Figure 2-6 RanGEF activity assay

RanGEF rapidly converts RanGDP into Ran(Mant)GTP. This conversion rate is similar for the conversion of RanQ69L-GDP to RanQ69L-(Mant)GTP, albeit requiring a longer reaction time. See Methods for details. Reproduced from (Barbato and Kapinos et al., 2020).

Whereas exoRanGDP was withheld by exoKapβ1 because of its binding (**Figure 2-2**), we observed a dramatic reduction of 50% inside of the nucleus and at the NE with energy mix, indicating that exoRanGDP was switched into exoRanGTP (**Figure 2-7 B-D**). Indeed, the same was true in terms of the nuclear signal when exoKapα•Kapβ1 was used, except that the NE signal was slightly higher. Still, because both exoRanGDP•Kapβ1 and exoRanGTP•Kapβ1 bind the FG-Nups, we questioned whether exoRanGTP efflux was promoted by the action of RanGAP1, which hydrolyses GTP at a rate of k_{cat} = 2.1 s^{-1} (Klebe et al., 1995a).

To validate this, we used a RanQ69L mutant that could also be converted into GTP form by RanGEF (**Figure 2-6**) but that could not be hydrolyzed by RanGAP1 (Klebe et al., 1995a).

Similarly to exoRanGDP (**Figure 2-2**), exoKapβ1 impedes the outflow of RanQ69L•GDP, leading to signal increase in the NE and nucleus (**Figure 2-8**) because of their binding (**Figure 2-3**). Likewise, RanQ69L-GDP leaked out nonspecifically in the presence of exoKapα•Kapβ1 compared to control (**Figure 2-8**). Markedly, however, when energy mix was added, the nuclear signal for RanQ69L•GTP was only slightly reduced, by 10% (**Figure 2-9**), in comparison to exoRanGTP (ca. 50%; **Figure 2-7 D**) with respect to control. Hence, the absence of hydrolysis abrogates the release of RanQ69L-GTP from the nucleus, which remains bound to Kapβ1 inside NPCs.

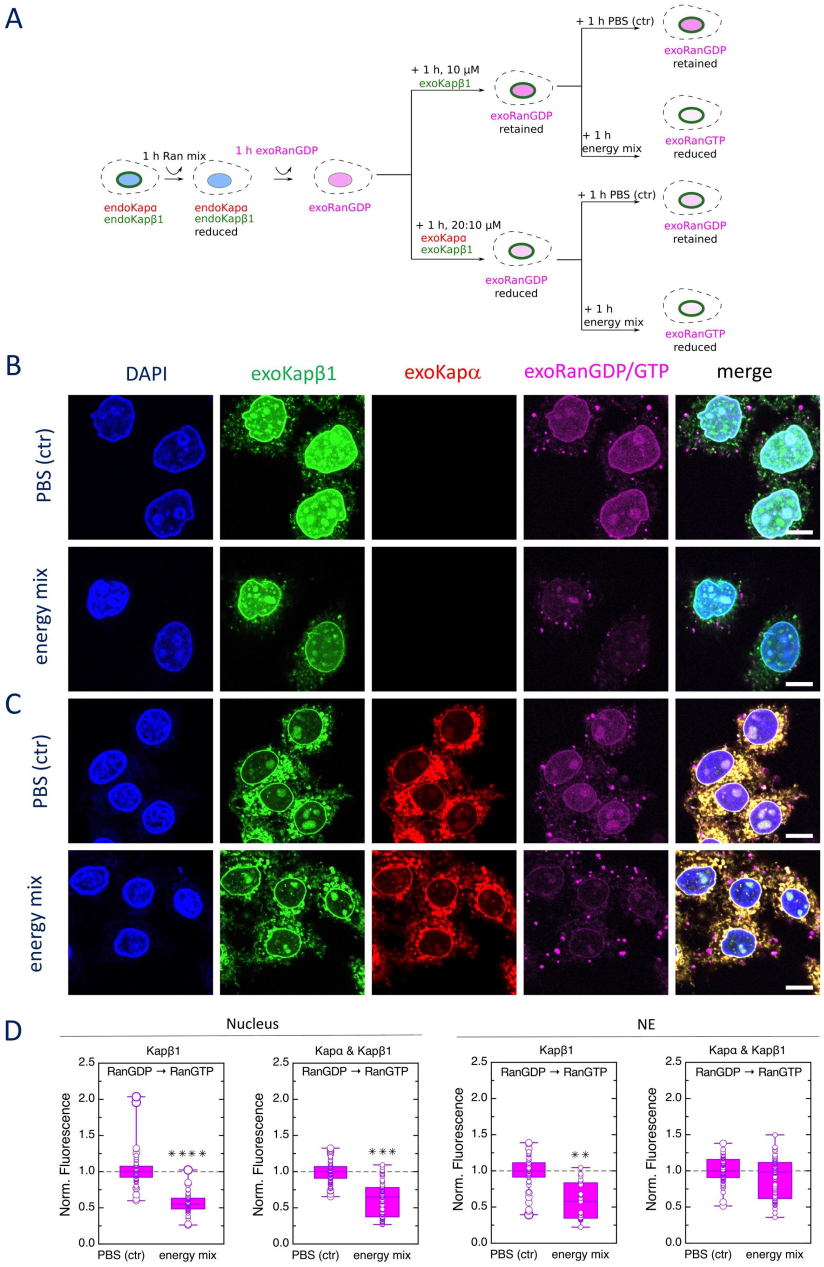

Figure 2-7 RanGTP efflux requires Kapβ1-binding and GTP hydrolysis

*(A) Experimental sequence. (B) In the absence of energy mix, exoRanGDP is retained because of binding with exoKapβ1 at NPCs. When energy mix is added, RanGEF converts exoRanGDP to exoRanGTP, which leaves the nucleus in spite of binding to exoKapβ1 at NPCs because of GTP hydrolysis by RanGAP1. To compare, the non-hydrolyzable mutant RanQ69L-GTP is retained in the nucleus. Bar, 10 µm. (C) Replacing exoKapβ1 with exoKapα•Kapβ1 resulted in similar observations as (B). Bar, 10 µm. (D) Fluorescence quantification of exoRanGDP (and/or exoRanGTP after energy mix) in the nucleus and NE at each of the above conditions. For exoKapβ1, n = 3, with a total of 65 and 55 cells for PBS control and "energy mix" experiments, respectively. For exoKapα•Kapβ1, n = 3 with a total of 85 and 77 cells for PBS control and "energy mix" experiments, respectively. **, P < 0.01; ***, P < 0.001; ****, P < 0.0001; Student's t-test. Box plots denote the median, first, and third quartiles. Error bars denote standard deviation, including outliers. See Table 2-1 for details. Reproduced from (Barbato and Kapinos et al., 2020).*

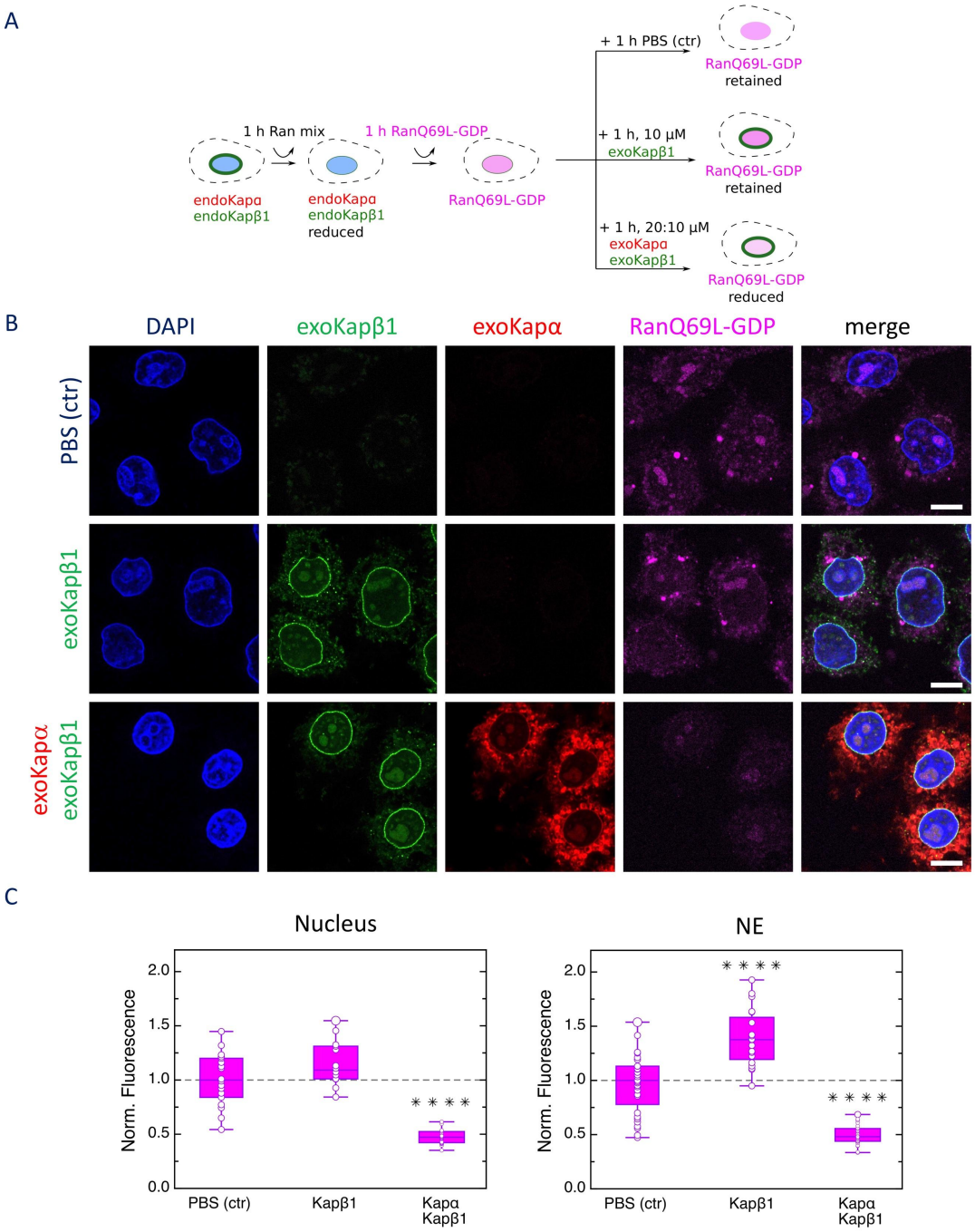

Figure 2-8 Binding to Kapβ1 restricts RanQ69L-GDP diffusion through NPCs

*(A) Experimental sequence. (B) ExoRanQ69L-GDP is retained in Ran mix-treated nuclei after being repopulated with exoKapβ1 because of its binding at NPCs. For comparison, exoKapα•Kapβ1 does not impede the outflow of exoRanQ69L-GDP because they do not bind. Bar, 10 µm. (C) Fluorescence quantification of exoRanQ69L-GDP in the nucleus and NE at each of the above conditions. n = 3 with a total of 18, 14 and 22 cells for PBS control, 10 µM exoKapβ1 and (20:10) µM exoKapα•Kapβ1, respectively. **, P < 0.01; ****, P < 0.0001; Student's t-test. Box plots denote the median, first, and third quartiles. Error bars denote standard deviation, including outliers. See Table 2-1 for details. Reproduced from (Barbato and Kapinos et al., 2020).*

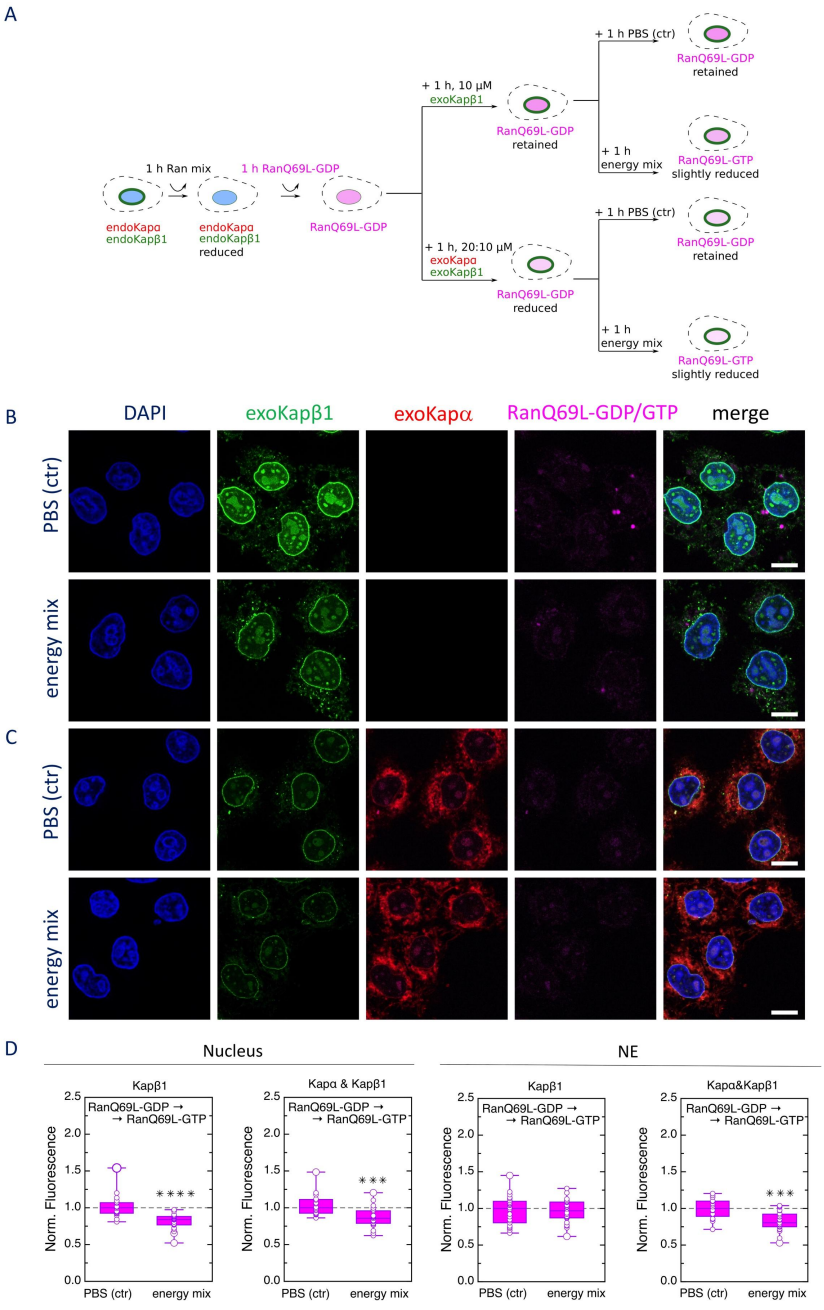

Figure 2-9 RanQ69L-GTP is retained in the nucleus in the absence of GTP hydrolysis

*(A) Experimental sequence. (B) In the absence of energy mix, RanQ69L-GDP is retained because of binding with exoKapβ1 at NPCs. RanGEF converts RanQ69L-GDP to RanQ69L-GTP when energy mix is added. However, RanQ69L-GTP is largely retained in the nucleus because it cannot hydrolyze GTP. Scale bar, 10 μm. (C) Replacing exoKapβ1 with exoKapα•Kapβ1 resulted in similar observations as (B). Bar, 10 μm. (D) Fluorescence quantification of RanQ69L-GDP (and/or RanQ69L-GTP after energy mix) in the nucleus and NE at each of the above conditions. For exoKap β 1, n = 3, with a total of 20 and 22 cells for PBS control and energy mix experiments, respectively. For exoKapα•Kapβ1, n = 3, with a total of 16 and 22 cells for PBS control and energy mix experiments, respectively. ***, P < 0.001; ****, P < 0.0001; Student's t-test. Box plots denote the median, first, and third quartiles. Error bars denote standard deviation, including outliers. See Table 2-1 for details. Reproduced from (Barbato and Kapinos et al., 2020).*

2.5NTF2 facilitates RanGDP re-import into the nucleus

So far, we have shown that Kapβ1 modulates the passage of Ran through the NPC and that this modulation depends on the bound nucleotide. To replenish the nuclear Ran pool, RanGDP is known to recruit NTF2 for its re-import into the nucleus (Ribbeck et al., 1998). We therefore sought to functionally verify this fact by incorporating 4 μM exogenous NTF2 (exoNTF2) in addition to energy mix in our transport assay (**Figure 2-10 A**). Remarkably, the exoRanGDP signal in the nucleus increased almost two-fold over the control in comparison to its reduction when NTF2 was absent (**Figure 2-10 B-C**). Hence, this finding confirms that NTF2 is necessary to replenish exoRanGDP in the nucleus following the hydrolysis of exoRanGTP by RanGAP1 at the NPC cytoplasmic periphery.

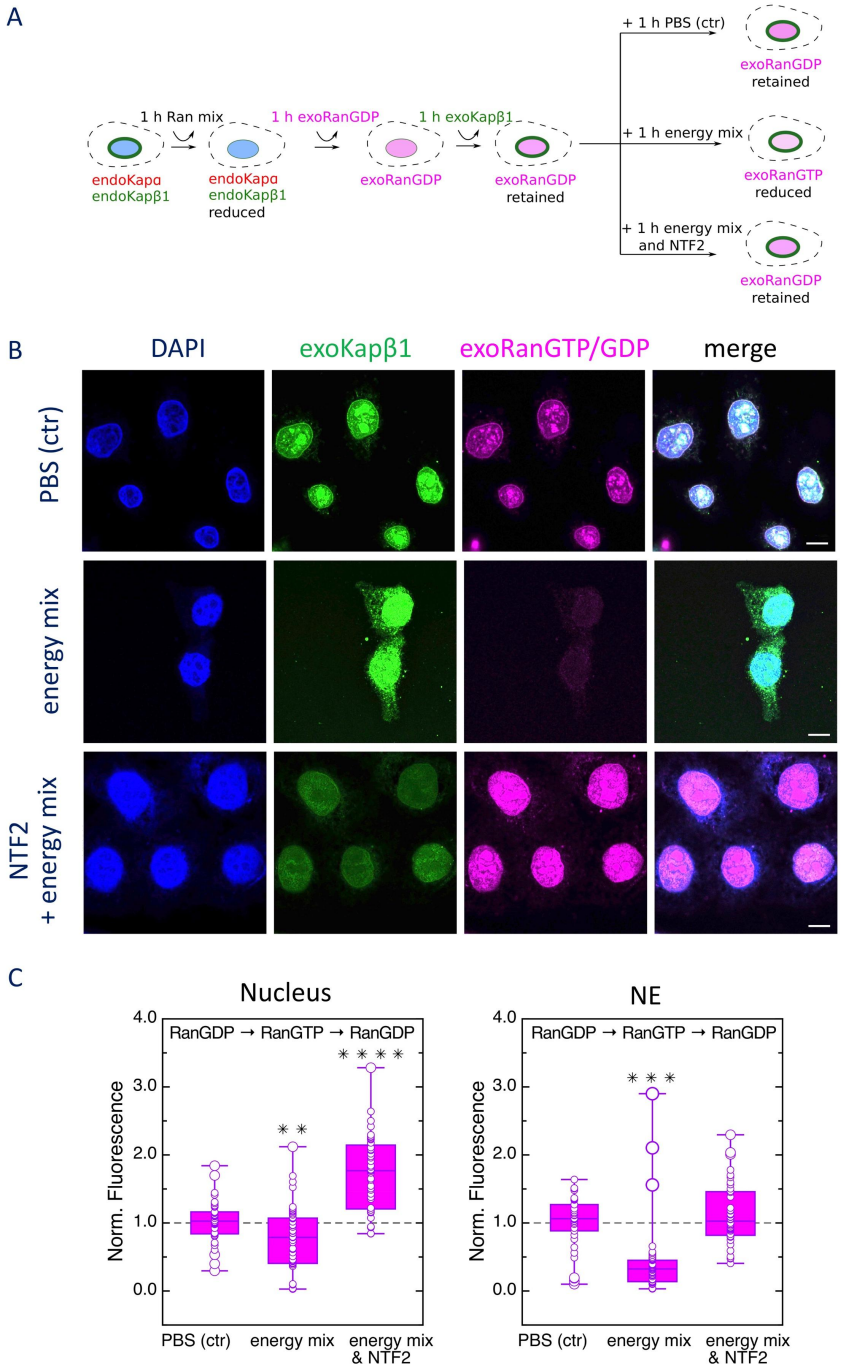

Figure 2-10 NTF2 facilitates RanGDP import into the nucleus

*(A) Experimental sequence. (B) Energy mix converts exoRanGDP to exoRanGTP. This is subsequently lost from the nucleus when exoRanGTP is hydrolyzed to exoRanGDP in the presence of exoKap β1 (Fig 3). Thereafter, adding NTF2 facilitates exoRanGDP import back into the nucleus. Bar, 10 µm. (C) Fluorescence quantification of exoRanGDP (and/or exoRanGTP after energy mix) in the nucleus and NE at each of the above conditions. n = 3 with a total of 39, 53 and 44 cells for PBS control, energy mix, and energy mix plus NTF2 experiments, respectively. **, P < 0.01; ****, P < 0.0001; Student's t-test. Box plots denote the median, first, and third quartiles. Error bars denote standard deviation, including outliers. See Table 2-1 for details. Reproduced from (Barbato and Kapinos et al., 2020).*

Specific condition (compared to the respective control)		p-values	
		Nucleus	NE
Figure 2-1	endoKapβ1: Ran mix vs. digitonin perm. (ctr)	0.0001	0.0001
	endoKapα: Ran mix vs. digitonin perm. (ctr)	0.0001	0.0001
	exoRanGDP: Ran mix vs. digitonin perm. (ctr)	0.0001	0.0001
Figure 2-2	exoRanGDP: exoKapβ1 vs. PBS (ctr)	0.0068	0.089
	exoRanGDP: exoKapα•Kapβ1 vs. PBS (ctr)	0.0001	0.0001
Figure 2-7	exoRanGDP w/ exoKapβ1: Energy mix vs. PBS (ctr)	0.0001	0.0034
	exoRanGDP w/ exoKapα•Kapβ1: Energy mix vs. PBS (ctr)	0.0008	0.12
Figure 2-8	RanQ69L-GDP: exoKapβ1 vs. PBS (ctr)	0.088	0.0001
	RanQ69L-GDP: exoKapα•Kapβ1 vs. PBS (ctr)	0.0001	0.0001
Figure 2-9	RanQ69L-GDP w/ exoKapβ1: Energy mix vs. PBS (ctr)	0.0001	0.9
	RanQ69L-GDP w/ exoKapα•Kapβ1: Energy mix vs. PBS (ctr)	0.0008	0.0004
Figure 2-10	exoRanGDP w/ exoKapβ1: Energy mix vs. PBS (ctr)	0.002	0.0001
	exoRanGDP w/ exoKapβ1: Energy mix + NTF2 vs. PBS (ctr)	0.0001	0.22

Table 2-1 Summary of Student's t-test

*P > 0.05 denotes that the observed differences are not significant; P < 0.05 denotes significant differences between the median values of the two independent data sets. *, P <0.05; **, P < 0.01; ***, P < 0.001; ****, P < 0.0001 are used to indicate the significance in the box plots shown in the figures. Reproduced from (Barbato and Kapinos et al., 2020).*

2.6Implications of Ran partitioning in NPCs

We teased apart conditions under which NPCs might regulate Ran transport. Clearly, the *in vivo* behavior of Ran depends on the distribution of the different Kapβ1 complexes that co-exist at the NPC; whose distribution is presently unknown. Still, certain qualitative predictions can be made from the current findings. First and foremost, Ran is smaller than the nonspecific NPC limit (Paine et al., 1975), (Popken et al., 2015), (Timney et al., 2016) and does not bind to the FG-Nups in either nucleotide-bound state. Hence, its transport regulation to establish the Ran gradient and NCT directionality is inconsistent with NPC models that invoke FG-Nup behavior to explain barrier function (**Figure 2-11**) (Frey and Gorlich, 2007), (Labokha et al., 2013), (Lim et al., 2007), (Rout et al., 2000), (Yamada et al., 2010). Instead, this involves Kapβ1 that serves as a *bona fide* constituent of the NPC barrier mechanism as we proposed in terms of Kap-centric control (Kapinos et al., 2017), (Kapinos et al., 2014), (Lim et al., 2015). Hence, our results predict that the absence of Kapβ1 at the pore precludes Ran partitioning leading to uncontrolled mixing across the NE.

On the basis of their interactions, the selective partitioning of Ran in the NPC depends on its nucleotide-bound form and the specific Kapβ1 complexes that reside within it (**Figure 2-11**). Therefore, we note that this "barrier" is biochemical in nature and not based on physical size exclusion, as is generally invoked for large nonspecific cargoes (Kapinos et al., 2017). At the pore, RanGDP is hindered by weak interactions with standalone Kapβ1 (Forwood et al., 2008), (Lonhienne et al., 2009) to form RanGDP•Kapβ1, which remains bound to the FG-Nups. This explains why RanGDP is retained in NPCs compared to other small nonspecific molecules that lack either Kapβ1 or FG-Nup binding (i.e., GFP) (Timney et al., 2016).

Consequently, RanGDP may remain within the NPCs long enough to be converted into RanGTP by RanGEF. Conversely, RanGDP is not retained by Kapα•Kapβ1 at the NPC because of its lack of binding.

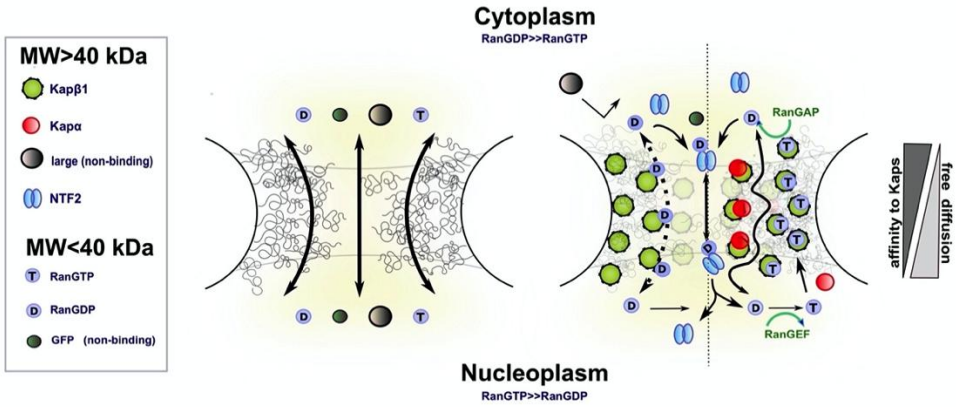

Figure 2-11 Kapβ1 controls Ran partitioning in NPCs
Left - An uncontrolled mixing of RanGDP, RanGTP and nonspecific cargoes is predicted to occur when NPCs lack Kaps. Right – Model describing how Kaps might selectively control Ran partitioning in the NPC as described in (A). Dashed line = weak binding. Solid lines = diffusion. See text for details. Reproduced from (Barbato and Kapinos et al., 2020).

In contrast, RanGTP binds to standalone Kapβ1 as well as Kapα•Kapβ1 thereby leading to the release of Kapα. As opposed to its uncontrolled diffusion, RanGTP is retained and cannot easily depart from the NPC in RanGTP•Kapβ1 form because of FG-Nup binding. To do so, GTP hydrolysis by RanGAP1 is required to facilitate its departure from the NPC cytoplasmic periphery by converting a strongly bound species (RanGTP•Kapβ1) to a weakly bound species (RanGDP•Kapβ1). This is evidenced in the increased retention of non-hydrolyzable RanQ69L-GTP at the pore. Being a weak complex, RanGDP may be further outcompeted and displaced by incoming Kapα at the cytoplasmic periphery. Taken together, this finding suggests that GTP hydrolysis plays a regulatory role in releasing RanGTP from the nucleus.

Surprisingly, the biochemical barrier provided by Kapβ1 does not have an impact on other small molecules, such as GFP, which may still permeate the NPC. Such a scenario may apply to RanGDP (i) following RanGTP hydrolysis or (ii) if Kapα•Kapβ1 dominates at the NPC. However, it would be rapidly shuttled back into the nucleus by NTF2, which binds RanGDP with a K_d = 75-240 nM. This is even stronger than RanGDP•Kapβ1 and may even serve to displace RanGDP from Kapβ1. As a matter of fact, RanGDP•NTF2 import (Kubitscheck et al., 2005) is considerably faster (~5 ms) than freely diffusing RanGDP (Ribbeck et al., 1998) or other small nonspecific molecules (Timney et al., 2016), resulting in active translocations that are estimated to be 260 Ran per NPC per second (Smith et al., 2002). Moreover, Kapβ1 appears to expedite the FG-Nup binding kinetics of NTF2 (Wagner et al., 2015). In this way, any loss of RanGDP within the cytoplasm is minimized by NTF2 thereby ensuring a high Ran concentration in the nucleus.

To conclude, we found that Kapβ1 selectively partitions Ran in the NPC. Minimizing its free diffusion not only prevents the uncontrolled mixing of RanGTP and RanGDP across the NE but also maximizes the efficiency of energy conversion that drives NCT directionality. This finding highlights another potential feature of Kap-centric control besides (i) reinforcing the FG-Nups against large nonspecific cargoes and (ii) promoting the facilitated diffusion of Kap-cargo complexes. More generally, our findings support a view whereby NPCs may prevent an uncontrolled leakage of small cargoes that specifically interact with it (Frey et al, 2018). Hence, it might be important to consider how Kaps influence Ran behavior at the NPC together with the enzymatic activity of RanGAP1 and RanGEF (Becskei and Mattaj, 2003), (Gorlich et al., 2003), (Kopito and Elbaum, 2009), (Riddick and Macara, 2005), (Smith et al., 2002).

2.7Materials and Methods

2.7.1Permeabilized cell assay

HeLa cells were washed with PBS and then permeabilized with 40 µg/mL digitonin (5 min incubation time). After permeabilization, the cells were washed with PBS three times for 5 min. Then, the cells were incubated with Ran mix (2 mM GTP, 0.1 mM ATP, 4 mM creatine phosphate, 20 U/mL creatine kinase, 5 µM RanGDP, 4 µM NTF2, and 1 mM DTT) for 1 h. Afterward, the cells were washed with PBS three times for 5 min each. Then 5 µM RanGDP-AlexaFluor 647 (degree of labelling: DOL = 1) or 5 µM RanQ69L-GDP-AlexaFluor 647 was added to cells for 1 h at room temperature. Depending on the assay, some samples underwent a triple washing step in PBS for 5 min each. Next, permeabilized cells were immediately fixed with 4% formalin, stained with DAPI, mounted on the sample glass using Vectashield (Vector Labs) and imaged. For the exogenous Kap repopulation assays, the cells were not washed after exoRanGDP incubation but instead were directly incubated with exoKapβ1, exoKapα•Kapβ1 or PBS for 1 h at room temperature. Subsequently, the cells were washed and fixed, except when energy mix (2 mM GTP, 0.1 mM ATP, 4 mM creatine phosphate, 20 U/mL creatine kinase) (Lowe et al., 2015) was added for 30 min, or when PBS was added as a control. After a triple washing step in PBS for 5 min each, the cells were also immediately fixed with 4% formalin and mounted on the microscope slide using Vectashield medium. For the NTF2 assay, the same procedure used for the energy mix-based assay was followed but with the addition of NTF2 with energy mix.

2.7.2Immunofluorescence

HeLa cells were washed with PBS and then permeabilized with 40 ug/mL digitonin. After permeabilization, the cells were washed with PBS three times for 5 min each. Upon washing,

cells were incubated in primary antibody solution for 1 h at room temperature. For detection of endoKapα we used goat anti-Kapα (Santa Cruz Biotechnology) diluted 1:50. For detection of endoKapβ we used mouse anti-Kapβ (Abcam) diluted 1:200. For detection of RanGEF we used mouse anti-RanGEF (Sigma) diluted 1:50. For detection of RanGAP1 we used goat anti-RanGAP1 (Everest Biotech) diluted 1:50. All dilutions were made in 1x PBS/5% BSA solution. Next, cells were washed with 1x PBS/5% BSA solution three times for 5 min. Afterward, cells were incubated with 1:400 diluted fluorescently tagged secondary antibodies: anti-mouse-AlexaFluor-568 (Abcam) and anti-goat-AlexaFluor-488 (Abcam). In addition, DAPI solution was added. Subsequently, the cells were again washed three times with 1x PBS/5% BSA solution and then fixed with 4% formalin.

2.7.3Protein expression and purification

Five different proteins were used in this work: Kap β 1, Kapα, Ran WT, Ran Q69L and NTF2. All proteins were purified on an Åkta rotein urificat ion ystem Äkta urifier 00/10 ystem, E ealthcare). he inal urity f ll he roteins as nalyzed y 2% AGE t .1% DS nd heir oncentration as etermined y bsorpt ion easurements t 80 m.

2.7.3.1Kapβ1

A full-length human Kap β 1 was cloned, expressed and purified as described elsewhere (Kapinos et al., 2014). Briefly, the 876 residues long full-length human Kapβ1 was amplified by PCR and cloned into a NcoI-BamHI digested pETM-11 expression vector with an N-terminal His6-tag and TEV-cleavage site (MKH-HHHHHPMSDYDIPTTENLYFQGA). An

His-tagged Kapβ1 was grown at 37°C to OD600 0.5 in *E. coli* BL21 (DE3) cells, expressed overnight at 22°C and induced by 0.5 mM IPTG. The cells were collected and lysed with the addition of lysozyme (1h at 4°C, 10 mg/3000 ml bacterial culture) in buffer (10 mM Tris, pH 7.5/100 mM NaCl/1 mM DTT/ 10 mM Imidazole) that additionally contained DNase, Pefabloc and other protein inhibitors (Roche Complete EDTA Free). Just before the centrifugation, cell lysate was sonicated at 40% for 5 min (3 sec on, 4 sec off). The lysates were spun down at 25000 g for 1 h, after which the supernatant was applied onto a Ni-NTA column (cOmplete His-tag purification column, Roche) in buffer (10 mM Tris, pH 7.5/100mM NaCl/1 mM DTT/ 10 mM Imidazole). The recombinant Kapβ1 was eluted using imidazole gradient (10 mM to 500 mM). The Kapβ1-rich fractions were pooled and purified using size exclusion (HiLoad 16/60 Superdex 200 prep grade, GE Healthcare) in buffer (10 mM Tris, pH 7.5/100mM NaCL/1 mM DTT). The collected fractions of the purified Kapβ1were pooled together, concentrated to 15–20 μM. The protein was shock-frozen using liquid nitrogen and stored at −80°C.

2.7.3.2Kapα

A full-length human Kapα construct (Addgene template pCMVTNT-T7-KPNA2; plasmid 26678) was cloned into the pQE70 vector using EcoRI–BamII restriction enzymes with His6 tag at their C-terminus with a short linker (-GSRSHHHHHH) that does not affect the complex formation of this protein with Kapβ1. An His-tagged Kapα was grown at 37°C to OD600 0.5 in *E. coli* BL21 (DE3) cells and expressed overnight at 22°C induced by 0.5 mM IPTG. The cells were collected and lysed with the addition of lysozyme (60 min, 10 mg/3000 ml bacterial culture) in buffer (50 mM Na-Pi pH 7.5 / 200 mM NaCl / 10 mM Imidazole / 1% Tween 20 / 2 mM beta-Mercapto / 10% Glycerol), which also contained Dnase, Pefabloc and

other protein inhibitors (Roche Complete EDTA Free). Just before the centrifugation, cell lysate was sonicated at 40% for 5 min (3 sec on, 4 sec off). The lysates were spun down at 25000 g for 1 h, after which the supernatant was applied onto a Ni-NTA column (cOmplete His-tag purification column, Roche) in buffer (50 mM Na-Pi pH 7.5 / 200 mM NaCl / 10 mM Imidazole / 1% Tween 20 / 2 mM beta-Mercapto / 10% Glycerol). This procedure resulted in the elution of recombinant Kapα using an imidazole gradient from 10 mM to 500 mM. Finally, Kapα monomers were separated and isolated using a Superdex 200 column (20 mM Tris pH 7.5 / 100 mM NaCl / 2 mM DTT / 10% Glycerol), and the collected fractions were stored at −80°C.

2.7.3.3Ran WT and Q69L

A plasmid (pQE32) with a full-length RanQ69L construct (the non-hydrolyzing mutant of Ra n) was a gift of U. Kutay (ETH Zurich, Zurich, Switzerland). BL21 competent cells were tran sformed with the construct and expressed at 24°C overnight after being induced by 0.5 M IPT G. The cells were collected and lysed for 1 h at 4°C using the following buffer: 50 mM Hepe s-KOH, pH 7, 100 mM NaCl, 5 mM DTT, 5 mM MgCl2, and 20 mM imidazole with additio n of 40 µl DNase (10 mg/ml), Pefobloc, Roche cOmplete EDTA free and lysozyme. Just befo re the centrifugation, cell lysate was sonicated at 40% for 5 min (3 sec on, 4 sec off), after wh ich the lysates were spun down at 25000 g for 1 h. Finally, Ran WT and RanQ69L were purif ied using a nickel-nitrilotriacetic acid (Ni- NTA) column (Roche) in an imidazole gradient (2 0–500 mM), after which the proteins were dialyzed into a 10 mM Hepes buffer, pH 7.2 with 200 mM NaCl for 1 h at 4°C. In order to add GDP or GTP nucleotides, the purified proteins were incubated for 30 min at 4°C with 10 mM EDTA and 1 mM nucleotides, respectively. A 25 mM of excess MgCl2 was added ensuring MgCl2 and GTP or GDP binding to nucleotide-

free Ran. Loaded proteins were dialyzed into PBS buffer, pH 7.2 (GIBCO by Life Sciences), in the presence of 1 mM MgCl2 and isolated using an Åkta urifier n olumn Superdex 5 iLoad 6/60; E). he urified rotein as hock-frozen sing iquid itrogen nd tored t 80 C. ypical tock oncentrations f oth roteins ere ∼25–30 μM.

2.7.3.4NTF2

The 127 residues long full-length rat NTF2 coding sequence was cloned into the NdeI and XhoI sites of the T7 expression vector pET15b with an N-terminal His6-tag (MGSSHHHHHHSSGLVPRGSHM). The *E. coli* strain BL21 (DE3) CodonPlus RIL was transformed with the construct and grown at 37°C to OD600 0.5 and expressed overnight at 22°C induced by 0.5 mM IPTG. Cells were collected and lysed by incubation with lysozyme (1h at 4°C) in buffer (10 mM Tris, pH 7.5/100 mM NaCl/1 mM DTT/10mM Imidazole), which additionally contained Dnase, Pefabloc and protein inhibitors. After lysis, before the centrifugation, cell lysates were sonicated at 40% for 5 min (3 sec on, 4 sec off), and cell lysates were then spun down at 25000 g for 1h at 4°C. A Ni-NTA column (cOmplete His-tag purification column, Roche) was used for supernatant using Tris-based buffer (10 mM Tris, pH 7.5/100mM NaCl/1 mM DTT, 10 mM Imidazole), resulting in NTF2 elution using an Imidazole gradient from 10 mM to 500 mM. NTF2-rich fractions were pooled and run through a size exclusion column (HiLoad 16/60 Superdex S-75, GE Healthcare) in phosphate-buffered saline (GIBCO PBS, Lifetechnologies). Purified protein was shock-frozen using liquid nitrogen and stored at -80 °C. Typical stock concentrations of NTF2 were ∼250–300 μM.

2.7.4Protein labelling

Recombinant proteins were labeled with fluorescent dyes (1:5 ratio) for 2 h at room temperature in light-protected vials. AlexaFluor 647 maleimide (Invitrogen) was used to label Ran WT or RanQ69L. AlexaFluor 488 maleimide (Invitrogen) was used to label Kapβ1. Atto 550 maleimide (Sigma Aldrich) was used to label Kap α. Spin columns (GE Healthcare, Lifesciences) were used to remove excessive dye. The degree of the labelling (DOL) was calculated following Nanodrop UV-Vis spectrometry to measure the respective dye and protein absorptions.

2.7.5RanGEF activity assay

A Synergy H1 Hybrid Multi-Mode Monochromator Fluorescence Microplate Reader (BioTek) was used to measure the enzymatic activity of RanGEF to exchange RanGDP to RanGTP (Klebe et al., 1995a). 1 µl of 3 µM RanGEF (final concentration: 30 nM) was added to 100 µl of 5 µM RanGDP (WT or Q69L mutant) and 200 µM (Mant)GTP (Sigma) in PBS buffer at 25°C (Fig S4). As control, we repeated the experiments without RanGEF in order to monitor the non-catalyzed rate of the GDP-GTP exchange. The fluorescent signal was monitored at two wavelengths: 335 nm (excitation at 292 nm; internal tryptophan fluorescence) and 450 nm (excitation at 370 nm; Mant nucleotide fluorescence). Fluorescence change was normalized by control experiments lacking RanGEF.

2.7.6Confocal imaging and image analysis

Fluorescence images were obtained at room temperature using an LSM700 upright confocal microscope with an oil-immersed 63x objective and multialkali PMT detector type. Fluorescence intensity quantification was performed using CellProfiler software. DAPI

staining was used to define a region of interest (ROI). In order to define the NE, the DAPI ROI was reduced by 5 pixels and simultaneously expanded by 5 pixels (Pixel Size (XY): 0.04 (µm) x 0.04 (µm)). The region between these two selections was assigned as "NE ROI," and the area inside of the reduced ROI was assigned as "nucleus ROI." These regions were then used to quantify the mean fluorescence intensity of exoRan at NE and inside the nucleus, respectively. In each case during the calculation of the fraction of exoRan, the Ran fluorescence intensity was normalized by the signal obtained with the PBS-treated sample as a control. The analyzed cell numbers are specified in the figure legend.

2.7.7Microscale electrophoresis (MST)

The efficiency of the recombinantly expressed RanGDP or RanQ69L-GDP binding to Kapβ1 was verified using microscale thermophoresis (MST). To 100 nM of the Kapβ1 labeled with maleimide AlexaFluor488 (DOL = 2), an increasing concentration of RanGDP or RanQ69L-GDP was added. The final test solutions contained 50 nM of Kapβ1-488 and the following Ran concentrations: 0.00031 µM, 0.000625 µM, 0.00125 µM, 0.0025 µM, 0.005, µM, 0.01 µM, 0.019 µM, 0.039 µM, 0.078 µM, 0.156 µM, 0.3125 µM, 0.625 µM, 1.25 µM, 2.5 µM, 5 µM 10 µM. These solutions were loaded into the glass capillaries (Monolith NT.115 capillary, standard treatment MO-K002, NanoTemper), and the change of the normalized fluorescence (‰ F_{norm}) was measured (60% laser power, 100% LED power, 30 sec laser on / 10 sec laser off) using Nanotemper Monolith NT.115 (NanoTemper).

2.8References

Abu-Arish, A., P. Kalab, J. Ng-Kamstra, K. Weis, and C. Fradin. 2009. Spatial distribution and mobility of the Ran GTPase in live interphase cells. *Biophys J*. 97:2164-2178.

Barbato, S., L.E. Kapinos, C. Rencurel, and R.Y.H. Lim. 2020. Karyopherin enrichment at the nuclear pore complex attenuates Ran permeability. *J. Cell Science* 133(3).

Bayliss, R., T. Littlewood, and M. Stewart. 2000. Structural basis for the interaction between FxFG nucleoporin repeats and importin-beta in nuclear trafficking. *Cell*. 102:99-108.

Bayliss, R., T. Littlewood, L.A. Strawn, S.R. Wente, and M. Stewart. 2002. GLFG and FxFG nucleoporins bind to overlapping sites on importin-beta. *J. Biol. Chem.* 277:50597-50606.

Becskei, A., and L.W. Mattaj. 2003. The strategy for coupling the RanGTP gradient to nuclear protein export. *Proceedings of the National Academy of Sciences of the United States of America*. 100:1717-1722.

Bednenko, J., G. Cingolani, and L. Gerace. 2003. Importin beta contains a COOH-terminal nucleoporin binding region important for nuclear transport. *J Cell Biol*. 162:391-401.

Boulikas, T. 1994. Putative nuclear-localization signals (NLS) in protein transcription factors. *J Cell Biochem*. 55:32-58.

Catimel, B., T. Teh, M.R. Fontes, I.G. Jennings, D.A. Jans, G.J. Howlett, E.C. Nice, and B. Kobe. 2001. Biophysical characterization of interactions involving importin-alpha during nuclear import. *J. Biol. Chem.* 276:34189-34198.

Chi, N.C., E.J.H. Adam, G.D. Visser, and S.A. Adam. 1996. RanBP1 stabilizes the interaction of Ran with p97 in nuclear protein import. *J. Cell Biol.* 135:559-569.

Cingolani, G., C. Petosa, K. Weis, and C.W. Muller. 1999. Structure of importin-beta bound to tbe IBB domain of importin-alpha. *Nature*. 399:221-229.

Cokol, M., R. Nair, and B. Rost. 2000. Finding nuclear localization signals. *EMBO Rep*. 1:411-415.

Eibauer, M., M. Pellanda, Y. Turgay, A. Dubrovsky, A. Wild, and O. Medalia. 2015. Structure and gating of the nuclear pore complex. *Nat. Comm.* 6.

Forwood, J.K., T.G. Lonhienne, M. Marfori, G. Robin, W. Meng, G. Guncar, S.M. Liu, M. Stewart, B.J. Carroll, and B. Kobe. 2008. Kap95p binding induces the switch loops of RanGDP to adopt the GTP-bound conformation: implications for nuclear import complex assembly dynamics. *J Mol Biol*. 383:772-782.

Frey, S., and D. Gorlich. 2007. A saturated FG-repeat hydrogel can reproduce the permeability properties of nuclear pore complexes. *Cell*. 130:512-523.

Gorlich, D., and U. Kutay. 1999. Transport between the cell nucleus and the cytoplasm. *Ann Rev Cell Dev Biol*. 15:607-660.

Gorlich, D., N. Pante, U. Kutay, U. Aebi, and F.R. Bischoff. 1996a. Identification of different roles for RanGDP and RanGTP in nuclear protein import. *EMBO J*. 15:5584-5594.

Gorlich, D., N. Pante, U. Kutay, U. Aebi, and F.R. Bischoff. 1996b. Identification of different roles for RanGDP and RanGTP in nuclear protein import. *Embo Journal*. 15:5584-5594.

Gorlich, D., M.J. Seewald, and K. Ribbeck. 2003. Characterization of Ran-driven cargo transport and the RanGTPase system by kinetic measurements and computer simulation. *EMBO J*. 22:1088-1100.

Gorlich, D., F. Vogel, A.D. Mills, E. Hartmann, and R.A. Laskey. 1995a. Distinct functions for the 2 importin subunits in nuclear-protein import. *Nature*. 377:246-248.

Gorlich, D., F. Vogel, A.D. Mills, E. Hartmann, and R.A. Laskey. 1995b. Distinct functions for the two importin subunits in nuclear protein import. *Nature*. 377:246-248.

Grossman, E., O. Medalia, and M. Zwerger. 2012. Functional architecture of the nuclear pore complex. *Annu Rev Biophys*. 41:557-584.

Hahn, S., and G. Schlenstedt. 2011. Importin beta-type nuclear transport receptors have distinct binding affinities for Ran-GTP. *Biochem Biophys Res Commun*. 406:383-388.

Hutchins, J.R., W.J. Moore, and P.R. Clarke. 2009. Dynamic localisation of Ran GTPase during the cell cycle. *BMC Cell Biol*. 10:66.

Isgro, T.A., and K. Schulten. 2005. Binding dynamics of isolated nucleoporin repeat regions to importin-beta. *Structure*. 13:1869-1879.

Izaurralde, E., U. Kutay, C. von Kobbe, I.W. Mattaj, and D. Gorlich. 1997. The asymmetric distribution of the constituents of the Ran system is essential for transport into and out of the nucleus. *EMBO J*. 16:6535-6547.

Kalab, P., A. Pralle, E.Y. Isacoff, R. Heald, and K. Weis. 2006. Analysis of a RanGTP-regulated gradient in mitotic somatic cells. *Nature*. 440:697-701.

Kalab, P., K. Weis, and R. Heald. 2002. Visualization of a Ran-GTP gradient in interphase and mitotic Xenopus egg extracts. *Science*. 295:2452-2456.

Kapinos, L.E., B. Huang, C. Rencurel, and R.Y.H. Lim. 2017. Karyopherins regulate nuclear pore complex barrier and transport function. *J Cell Biol*. 216:3609-3624.

Kapinos, L.E., R.L. Schoch, R.S. Wagner, K.D. Schleicher, and R.Y.H. Lim. 2014. Karyopherin-centric control of nuclear pores based on molecular occupancy and kinetic analysis of multivalent binding with FG nucleoporins. *Biophys J*. 106:1751-1762.

Kassianidou, E., J. Kalita, and R.Y.H. Lim. 2019. The role of nucleocytoplasmic transport in mechanotransduction. *Exp Cell Res*. 377:86-93.

Kelley, J.B., and B.M. Paschal. 2007. Hyperosmotic stress signaling to the nucleus disrupts the Ran gradient and the production of RanGTP. *Mol Biol Cell*. 18:4365-4376.

Kim, S.J., J. Fernandez-Martinez, I. Nudelman, Y. Shi, W.Z. Zhang, B. Raveh, T. Herricks, B.D. Slaughter, J.A. Hogan, P. Upla, I.E. Chemmama, R. Pellarin, I. Echeverria, M. Shivaraju, A.S. Chaudhury, J.J. Wang, R. Williams, J.R. Unruh, C.H. Greenberg, E.Y. Jacobs, Z.H. Yu, M.J. de la Cruz, R. Mironska, D.L. Stokes, J.D. Aitchison, M.F. Jarrold, J.L. Gerton, S.J. Ludtke, C.W. Akey, B.T. Chait, A. Sali, and M.P. Rout. 2018. Integrative structure and functional anatomy of a nuclear pore complex. *Nature*. 555:475-+.

Kimura, M., and N. Imamoto. 2014. Biological significance of the importin-beta family-dependent nucleocytoplasmic transport pathways. *Traffic*. 15:727-748.

Klebe, C., F.R. Bischoff, H. Ponstingl, and A. Wittinghofer. 1995a. Interaction of the nuclear GTP-binding protein Ran with its regulatory proteins RCC1 and RanGAP11. *Biochemistry*. 34:639-647.

Klebe, C., H. Prinz, A. Wittinghofer, and R.S. Goody. 1995b. The kinetic mechanism of Ran--nucleotide exchange catalyzed by RCC1. *Biochemistry*. 34:12543-12552.

Kopito, R.B., and M. Elbaum. 2009. Nucleocytoplasmic transport: a thermodynamic mechanism. *HFSP J*. 3:130-141.

Kubitscheck, U., D. Grunwald, A. Hoekstra, D. Rohleder, T. Kues, J.P. Siebrasse, and R. Peters. 2005. Nuclear transport of single molecules: dwell times at the nuclear pore complex. *J. Cell Biol.* 168:233-243.

Labokha, A.A., S. Gradmann, S. Frey, B.B. Hulsmann, H. Urlaub, M. Baldus, and D. Gorlich. 2013. Systematic analysis of barrier-forming FG hydrogels from Xenopus nuclear pore complexes. *Embo Journal*. 32:204-218.

Lim, R.Y.H., B. Huang, and L.E. Kapinos. 2015. How to operate a nuclear pore complex by Kap-centric control. *Nucleus*. 6:366-372.

Lim, R.Y.H., B. Fahrenkrog, J. Koser, K. Schwarz-Herion, J. Deng, and U. Aebi. 2007. Nanomechanical basis of selective gating by the nuclear pore complex. *Science*. 318:640-643.

Lonhienne, T.G., J.K. Forwood, M. Marfori, G. Robin, B. Kobe, and B.J. Carroll. 2009. Importin-beta is a GDP-to-GTP exchange factor of Ran: implications for the mechanism of nuclear import. *J Biol Chem*. 284:22549-22558.

Lowe, A.R., J.H. Tang, J. Yassif, M. Graf, W.Y. Huang, J.T. Groves, K. Weis, and J.T. Liphardt. 2015. Importin-beta modulates the permeability of the nuclear pore complex in a Ran-dependent manner. *Elife*. 4.

Macara, I.G. 2001. Transport into and out of the nucleus. *Microbiol. Mol. Biol. Rev.* 65:570-+.

Nachury, M.V., and K. Weis. 1999. The direction of transport through the nuclear pore can be inverted. *Proc Natl Acad Sci U S A*. 96:9622-9627.

Paine, P.L., L.C. Moore, and S.B. Horowitz. 1975. Nuclear-envelope permeability. *Nature*. 254:109-114.

Partridge, J.R., and T.U. Schwartz. 2009. Crystallographic and Biochemical Analysis of the Ran-binding Zinc Finger Domain. *Journal of Molecular Biology*. 391:375-389.

Popken, P., A. Ghavami, P.R. Onck, B. Poolman, and L.M. Veenhoff. 2015. Size-dependent leak of soluble and membrane proteins through the yeast nuclear pore complex. *Mol Biol Cell*. 26:1386-1394.

Pumroy, R.A., and G. Cingolani. 2015. Diversification of importin-alpha isoforms in cellular trafficking and disease states. *Biochemical Journal*. 466:13-28.

Renault, L., J. Kuhlmann, A. Henkel, and A. Wittinghofer. 2001. Structural basis for guanine nucleotide exchange on Ran by the regulator of chromosome condensation (RCC1). *Cell*. 105:245-255.

Rexach, M., and G. Blobel. 1995. Protein import into nuclei - association and dissociation reactions involving transport substrate, transport factors, and nucleoporins. *Cell*. 83:683-692.

Ribbeck, K., G. Lipowsky, H.M. Kent, M. Stewart, and D. Gorlich. 1998. NTF2 mediates nuclear import of Ran. *EMBO J*. 17:6587-6598.

Riddick, G., and I.G. Macara. 2005. A systems analysis of importin-{alpha}-{beta} mediated nuclear protein import. *J. Cell Biol.* 168:1027-1038.

Rout, M.P., J.D. Aitchison, A. Suprapto, K. Hjertaas, Y.M. Zhao, and B.T. Chait. 2000. The yeast nuclear pore complex: Composition, architecture, and transport mechanism. *J. Cell Biol.* 148:635-651.

Sakiyama, Y., A. Mazur, L.E. Kapinos, and R.Y.H. Lim. 2016. Spatiotemporal dynamics of the nuclear pore complex transport barrier resolved by high-speed atomic force microscopy. *Nat Nanotechnol*. 11:719-723.

Schoch, R.L., L.E. Kapinos, and R.Y.H. Lim. 2012. Nuclear transport receptor binding avidity triggers a self-healing collapse transition in FG-nucleoporin molecular brushes. *Proc Natl Acad Sci U S A*. 109:16911-16916.

Schrader, N., C. Koerner, K. Koessmeier, J.-A. Bangert, A. Wittinghofer, R. Stoll, and I.R. Vetter. 2008. The crystal structure of the Ran-Nup153ZnF2 complex: a general Ran docking site at the nuclear pore complex. *Structure*. 16:1116-1125.

Smith, A., A. Brownawell, and I.G. Macara. 1998. Nuclear import of Ran is mediated by the transport factor NTF2. *Curr Biol*. 8:1403-1406.

Smith, A.E., B.M. Slepchenko, J.C. Schaff, L.M. Loew, and I.G. Macara. 2002. Systems analysis of Ran transport. *Science*. 295:488-491.

Stewart, M. 2007. Molecular mechanism of the nuclear protein import cycle. *Nature Reviews Molecular Cell Biology*. 8:195-208.

Timney, B.L., B. Raveh, R. Mironska, J.M. Trivedi, S.J. Kim, D. Russel, S.R. Wente, A. Sali, and M.P. Rout. 2016. Simple rules for passive diffusion through the nuclear pore complex. *J Cell Biol*. 215:57-76.

Tran, E.J., T.A. Bolger, and S.R. Wente. 2007. SnapShot: Nuclear transport. *Cell*. 131.

von Appen, A., J. Kosinski, L. Sparks, A. Ori, A.L. DiGuilio, B. Vollmer, M.T. Mackmull, N. Banterle, L. Parca, P. Kastritis, K. Buczak, S. Mosalaganti, W. Hagen, A. Andres-Pons, E.A. Lemke, P. Bork, W. Antonin, J.S. Glavy, K.H. Bui, and M. Beck. 2015. In situ structural analysis of the human nuclear pore complex. *Nature*. 526:140-+.

Vovk, A., C. Gu, M.G. Opferman, L.E. Kapinos, R.Y.H. Lim, R.D. Coalson, D. Jasnow, and A. Zilman. 2016. Simple biophysics underpins collective conformations of the intrinsically disordered proteins of the Nuclear Pore Complex. *eLife*. 5.

Wagner, R.S., L.E. Kapinos, N.J. Marshal, M. Stewart, and R.Y.H. Lim. 2015. Promiscuous binding of karyopherin beta 1 modulates FG nucleoporin barrier function and expedites NTF2 transport kinetics. *Biophys. J.* 108:918-927.

Xu, D.R., A. Farmer, G. Collett, N.V. Grishin, and Y.M. Chook. 2012. Sequence and structural analyses of nuclear export signals in the NESdb database. *Molecular Biology of the Cell*. 23:3677-3693.

Xu, L., and A. Massague. 2004. Nucleocytoplasmic shuttling of signal transducers. *Nat Rev Mol Cell Biol*. 5:209-219.

Yamada, J., J.L. Phillips, S. Patel, G. Goldfien, A. Calestagne-Morelli, H. Huang, R. Reza, J. Acheson, V.V. Krishnan, S. Newsam, A. Gopinathan, E.Y. Lau, M.E. Colvin, V.N. Uversky, and M.F. Rexach. 2010. A bimodal distribution of two distinct categories of intrinsically disordered structures with separate functions in FG nucleoporins. *Mol. Cell. Proteomics*. 9:2205-2224.

In vitro reconstitution of Pom121 and Ndc1 into liposomes

Adapted from

Nucleocytoplasmic Transport: A Paradigm for Molecular Logistics in Artificial Systems

Suncica Vujica, Christina Zelmer, Radhakrishnan N. Panatala, and Roderick Y.H. Lim

Published in CHIMIA International Journal for Chemistry, 2016;70(6):413–417

And

Nuclear Pore Membrane Proteins Self-Assemble into Nanopores

Radhakrishnan Panatala, Suncica Barbato, Toshiya Kozai, Jinghui Luo, Larisa E. Kapinos, and Roderick Y.H. Lim

Published in Biochemistry, 2019;58(6):484–488

3*In vitro* reconstitution of Pom121 and Ndc1 into liposomes

3.1Introduction

Living cells are the machines of life (Goodsell, 2009). The sophistication of eukaryotic cells is underscored by the prevalence of organelles that encapsulate different contents within specialized membrane-bound microenvironments (Cooper and Hausman, 2000). This separation from the bulk intracellular space facilitates the coexistence of diverse biochemical reactions that culminate into synergistic cellular functions. However, for this to proceed, specific proteins have to be sorted and delivered to exact locations within the complex cellular milieu (i.e., protein targeting) (Blobel, 2000), which is physically unprecedented. To illustrate this, the gene expression is mediated by the spatial separation of transcription and translation that occurs in the nucleus and cytoplasm, respectively.

From an abiological perspective, artificial organelles, molecular factories and nanoreactors are membrane-bound molecular systems that are envisaged to replicate or harness the efficacy and complexity of the cellular function (Leduc et al., 2007). This constitutes a shift from a "one-flask one-reaction" paradigm to a system where cross-regulated reactions take place under spatiotemporal control (Drexler, 1999). However, this change introduces basic logistical challenges that remain unaddressed. For instance, it is unclear how the various proteins and enzymes (henceforth termed "molecular modules") are recruited into an artificial organelle to drive such cross-reactions. Nature has found a solution to the problem of molecular logistics in the context of NCT regulation. Accordingly, we propose that an

analogous system may be harnessed to regulate molecular logistics in artificial organelles and other biosynthetic systems.

3.2Molecular Factories

Molecular compartments can be constructed from lipid membranes that form liposomes (Engelman, 2005), (van Meer et al., 2008) or from amphiphilic polymers that form polymeric membranes and vesicles, known as “polymersomes” (Klok and Lecommandoux, 2001), (Kowal et al., 2013). Based on their enhanced mechanical and chemical stability (Discher and Eisenberg, 2002), polymer-based membranes are increasingly being favored for use as building blocks of biomimetic membranes (LoPresti et al., 2009). Since their discovery, the encapsulation efficacy of polymersomes has been shown to protect sugars, enzymes and proteins against proteolytic attack (Meier et al., 2000), (Nardin et al., 2001). Several transmembrane proteins have been successfully inserted into the polymeric membrane to render the polymersome permeable to ions and small molecules (Garni et al., 2017). Importantly, this permeability allows for a product or substrate to be exchanged with the outside environment so as to support *in situ* reactions within the encapsulated entities (Balasubramanian et al., 2010). For instance, the insertion of gramicidin and ionomycin into the polymersome membrane enables the transport of monovalent (H^+, Na^+ and K^+) (Lomora et al., 2015a) and divalent cations ($Ca2^+$) (Lomora et al., 2015b), respectively. Moreover, electrical and chemical gradients have been generated by irradiating and activating polymersomes harboring light-driven proton pumps, such as bacteriorhodopsin (Choi and Montemagno, 2007) and proteorhodopsin (Hua et al., 2011). The reconstitution of aquaporin-0 (AQP0) further has yielded intrinsically osmoregulatory polymersomes that have been able to transport water molecules across their polymeric membranes (Stoenescu et al., 2004).

To transport larger molecules, α-hemolysin, which bears an inner channel diameter of ~2.6 nm, has enabled the exchange of ions and vital molecules (i.e., ATP) (Nallani et al., 2011), while molecules of up to 600 Da could traverse the ~3.3 nm-diameter outer membrane protein F (OmpF) and diffuse into the polymersomes (Nardin et al., 2001). To further bio-catalyze reactions, (Einfalt et al., 2015) OmpF was chemically modified with a molecular cap that acted as a pH responsive gate that could be thus opened by lowering the pH. In this manner, a modified OmpF-bearing polymersome served as a nanoreactor, converting the influx of chromogenic substrate 3,3`,5,5`-tetramethylbenzidine (TMB) using a pre-encapsulated model enzyme horseradish peroxidase (HRP) within its lumen. Furthermore, entrapping antioxidant enzymes within a polymeric membrane that was leaky to reactive oxygen species (ROS) could effectively accelerate the ROS detoxification within cells under oxidative stress (Tanner et al., 2013). As a step toward multicompartmentalization, two different nanoreactors bearing two different enzymes could be encapsulated into a larger polymersome (Klyszejko et al., 2008) and be used to control a cascade reaction across the compartmental boundaries (Tanner et al., 2013).

In spite of the abovementioned breakthroughs, the transport into proteopolymersomes is largely restricted to ions and small molecules based on size exclusion, as defined by the inner diameter of the membrane proteins. In contrast, an ideal molecular factory would resemble a cell, where a number of molecular modules would perform different activities (**Figure 3-1**).

However, if a more cell-like system is to be envisaged, it will be necessary to transport diverse substances into and out of a proteopolymersome, depending on the following questions:

(i)How many different types of molecular modules, enzymes and essential proteins are needed to construct a functional “molecular factory”?

(ii)What are the optimal concentrations needed for such molecular modules to function?

(iii)How large are the molecular modules under consideration, and how should they be encapsulated or imported?

(iv)How will the transport of essential reactants, ligands and metabolites be regulated?

(v)How will the reaction by-products be removed from the proteopolymersome interior and moved to the external environment?

(vi)What can be used as an energy source to sustain the longevity and turnover of such reactions?

Hence, this emphasizes the need for a more advanced form of molecular logistics that goes beyond passive diffusion and the constraints imposed by size exclusion. Such a molecular logistic system should facilitate the continuous transport of large and small cargoes, from proteins to metabolites based on biochemical specificity and not size exclusion *per se*. Moreover, this process should include an energy supply so as to dictate the directionality of transport in order to accumulate cargoes within the proteopolymersome (i.e., against concentration gradients) as well as to ensure an efficient turnover of the reaction by-products. Quite remarkably, these key ingredients constitute the NCT regulation in eukaryotic cells.

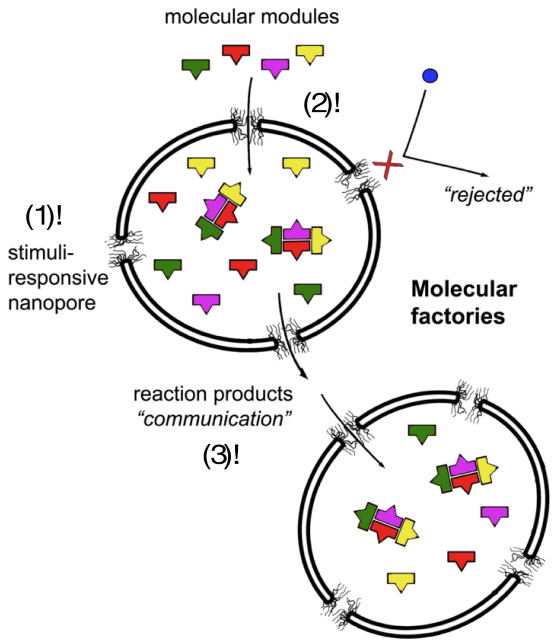

Figure 3-1 Cartoon depicting nano-porous molecular factories that can selectively accumulate molecular modules for the compartmentalized control of enzymatic reactions

A molecular factory should harbor (bio)chemically selective nanopores (1) that are able to selectively transport molecular modules from outside (2) for a reaction within a factory and later on, re-use the reaction products for the feedback regulation and communication between factories (3). Reproduced from (Vujica et al., 2016).

3.3NPC mimics

The mechanism of NCT highlights several hierarchical principles (Terry et al., 2007) that surpass the basic encapsulation/size exclusion and that may be applied to artificial systems. In fact, solid-state nanopores and polymeric membranes that incorporate FG-Nups (artificial NPCs) have been shown to exert NPC-like properties (Jovanovic-Talisman et al., 2009), (Kowalczyk et al., 2011). FG-Nup-functionalized surfaces have also been shown to reconstitute selective transport in two-dimensions (Schleicher et al., 2014). Accordingly, this presents a molecular logistics paradigm for regulating transport and communication between artificial organelles (i.e., "artificial nuclei"), which can be broken down into the following constituent parts:

1. NPC-like selective nanopores that are wide enough (> 10 nm) to accommodate a diverse range of molecular entrants of varying sizes. To prevent unwanted infiltration, each nanopore should be assembled with a stimuli-responsive "barrier" that regulates the permeability and porosity of the artificial nuclei. *A priori* the barrier repels nonspecific entities but facilitates the translocation of molecular "keys" (see below) based on biochemical recognition. This imparts a property of anti-fouling that prevents nonspecific macromolecules from clogging the pores within a complex milieu (Wu et al., 2008). Thus, biosynthetic alternatives to the FG-Nups might include chemically derived biorecognition polymers (Barbey et al., 2009).
2. Kap-like molecular "keys" that gain selective and exclusive access through the nanopore by exerting specific biochemical interactions with the stimuli-responsive barrier. Additionally, such "keys" have to recognize and bind molecular cargoes (i.e., the main molecules of interest) (see below). Possible candidates include bispecific antibodies (Pluckthun and Pack, 1997) or antibody variants (Chan and Carter, 2010).
3. A suite of cargoes (e.g., molecular modules, enzymes or other essential proteins) that do not interact with the stimuli-responsive barrier but instead bear signal-specific tags (e.g., NLS) that the molecular keys recognize and bind to. In this manner, cargoes traverse the nanopore by "hitchhiking" along with the molecular key.
4. Employing a "host," such as RanGTP, inside the artificial nuclei that facilitates cargo release from the key upon entering the luminal space. After encapsulation, an outflow of cargo is minimized for the same reason that a key was required to enter the artificial nucleus in the first place.
5. An energy source that provides feedback recycles the keys and replenishes the "host." This source provides the driving force to ensure transport directionality, continuity and accumulation against concentration gradients.

The most challenging task in the construction of such molecular machines is to create functional NPC-like pores (sufficiently large) in the mobile micro-sized vesicles, such as in giant liposomes or polymersomes. One of the possibilities to manage this task is to create a minimalistic NPC still constructed from the essential nucleoporins. With this in mind, we decided to use the trans-membrane nucleoporins (TM-Nups), Pom121 and Ndc1, which we expected to be sufficient to assemble the pre-NPC pores.

3.4Cell-Free membrane protein expression and their incorporation into liposomes

We took inspiration from how NPCs perform the transport function in eukaryotic cells, and we explored the first steps toward developing membrane-bound molecular factories that translocate specific cargoes. We exploited the knowledge of TM-Nups and reconstituted two of the most conserved members into soybean phospholipid liposomes (Madrid et al., 2006). In yeast, the Ndc1 interaction network with other POMs (Pom152 and Pom34) and soluble Nups (Nup53 and Nup59) was shown to be crucial for NPC assembly and maintenance (Onischenko et al., 2009). Whether those interactions involve extensive lipid remodeling to initiate the NPC biogenesis remains an open question. Hence, in order to develop an NPC-inspired molecular factory, we used a wheat-germ-based *in vitro* transcription and translation system to efficiently express and incorporate Pom121 and Ndc1 into synthetic liposomes (**Figure 3-2)** (Goren et al., 2009).

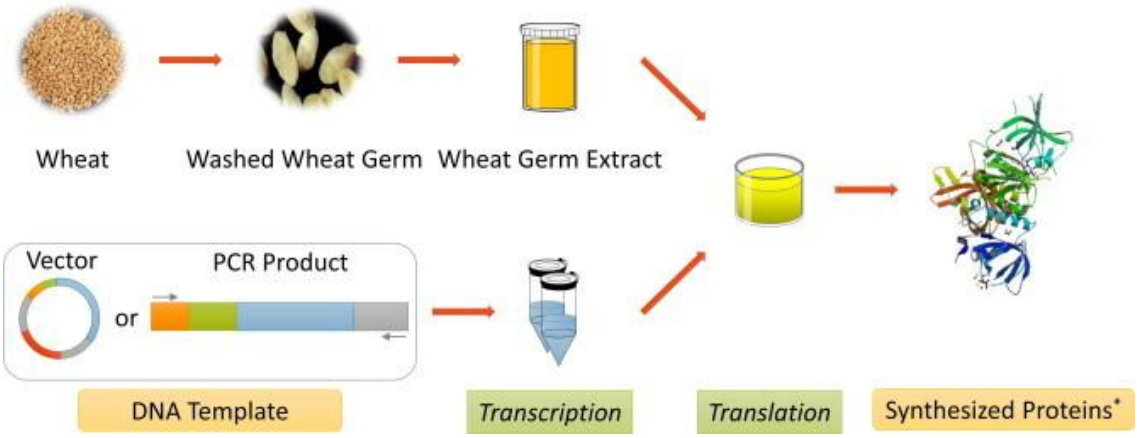

Figure 3-2 Outline of wheat germ cell-free expression system

Wheat germ extract is prepared from the wheat, while DNA template is transcribed in a tube. Two components mix together during translation reaction. The outcome is a protein. Reproduced from (Harbers, 2014).

3.4.1Proteoliposome preparation

The full-length coding region of Ndc1-eGFP and Pom121 was amplified by PCR from parental plasmid using two primers (**Table 3-1**) containing SgfI and PmeI restriction sites.

Pom121	
Forward Primer	GCC GCGATCGC ATGTCTCCGGCGGCTGCGGC
Reverse Primer	GCC GTTTAAAC CTA ATGGTGATGGTGATGATG CCCCGCCTCCTTGGG
Ndc1	
Forward Primer	GCC GCGATCGC ATGGCCACGGCCGTGAGCC
Reverse Primer	GCC GTTTAAAC CTTGTACAGCTCGTCCATG

Table 3-1 Primers used for Pom121 and Ndc1 amplification

Afterward, the PCR products were digested with SgfI and PmeI and cloned into a wheat-germ-based pEU-Flexi expression vector: pEU-C-His_FV with Bar-CAT cassette at the EcoICRI and SgfI sites (**Table 3-2**)

Restriction enzyme	Restriction site
SgfI	5'...GCGAT CGC...3'
PmeI	5'...GTTT^AAAC...3'
EcoICRI	5'…GAG^CTC… 3'

Table 3-2 Restriction enzymes used for Pom121 and Ndc1 digestion

The sequence of the inserted fragment was confirmed by DNA sequencing. The same procedure was followed for Pom121.

As for the DNA amplification, the *E. coli* strain *DH5alpha* was transformed with either the pEu-Ndc1-eGFP-C-6 His construct or the pEu-Pom121-C-6His construct. Both constructs carried an antibiotic resistant gene, which confers resistance to Ampicillin. The transformed *DH5alpha* cells were grown in the presence of Ampicillin at 37°C overnight. In order to grow a sufficient number of bacteria to isolate enough of the plasmid DNA, we used a liquid culture with Luria broth (LB) medium. Subsequently, the colonies were picked and used to pre-inoculate 3 mL LB medium with 100 µg/ml of Ampicillin. After 6 h at 37°C, the pre-inoculate was used to inoculate 150 mL of LB medium with 100 µg/ml Ampicillin and left at 37°C for 16 h. The next step was to isolate the DNA using the ZymoPURE™ Midi PrepKit (Zymo Research, USA). To confirm the quality of DNA, we measured the absorbance and the respective A260/A280 was within a range of 1.5–2.5.

A highly purified plasmid DNA is a prerequisite for successful *in vitro* transcription and translation. Hence, the obtained plasmids were further purified by proteinase-K treatment in order to remove the RNase. In both cases, the plasmids were treated with proteinase-K (Sigma Aldrich, USA) for at least 1 h at 37°C in 1x proteinase-K buffer. The 10x buffer used with proteinase K is 100 mM Tris-HCL, pH 8.0, containing 50 mM EDTA and 1% (w/v)

SDS. The Proteinase K solution was prepared with the addition of 0.5 mg of proteinase K to 1 mL of 10x proteinase K buffer.

An additional purification step, which consisted of removing the remaining proteins, was accomplished with 1:1 phenol/chloroform solution (Sigma) followed by precipitation with sodium acetate and ethanol. A phenol-chloroform extraction is a liquid-liquid extraction. It separates mixtures of molecules according to their different solubilities in two different immiscible liquids. As a last step, the DNA pellet was dissolved by adjusting the volume of the Mili-Q water (18.2 MΩ-cm) in order to obtain a final concentration of 1 μg/μL, which served as a template for mRNA production.

In vitro transcription was performed at 37°C for 6 h according to the CellFree Sciences (CFS) protocol. In brief, an SP6 promoter drives the expression of the gene of interest in a pEU Flexi vector. 100 ng/μL of purified plasmid was incubated for 6 h at 37°C with 1x transcription buffer, 2.5 mM NTP mix and 60 units each of RNA polymerase and RNasin (i.e., RNAse inhibitor). The NTP mix contained ATP, GTP, CTP and UTP. During the transcription reaction, the RNA polymerase produced mRNA as the main product and pyrophosphate (PPi) as by-product, with $Mg2^{+}$ as cofactor. Hence, during a successful transcription a white precipitate of magnesium pyrophosphate was formed. The newly produced mRNA served as a template for the translation reaction happening in the next step.

In a test phase, the translation was performed using two different methods (**Figure 3-3**). Given that the yield was higher with the bilayer method, we continued using it throughout the whole study. The reaction mixture and its components were layered at the bottom followed

by an undisturbed layering of SUB-AMIX solution (1x) on the top. The reaction mixture was composed by mRNA, 1x SUB-AMIX solution (translation buffer), wheat germ extract (WGE7240, 60 O.D.), asolectin liposomes (10 mg/mL) and creatine kinase (40 ng/µL). The SUB-AMIX solution is a translation buffer containing amino acids, ATP and the cofactors needed to carry out the translation reaction. The rationale behind these selections is that such a diffusion system enables a continuous supply of substrates while removing small by-products through a phase between the two mixtures (translation and substrate mixtures). In our case, given that Ndc1 has the eGFP tag, we incubated the entire reaction mixture in the dark for 20 h at 15°C.

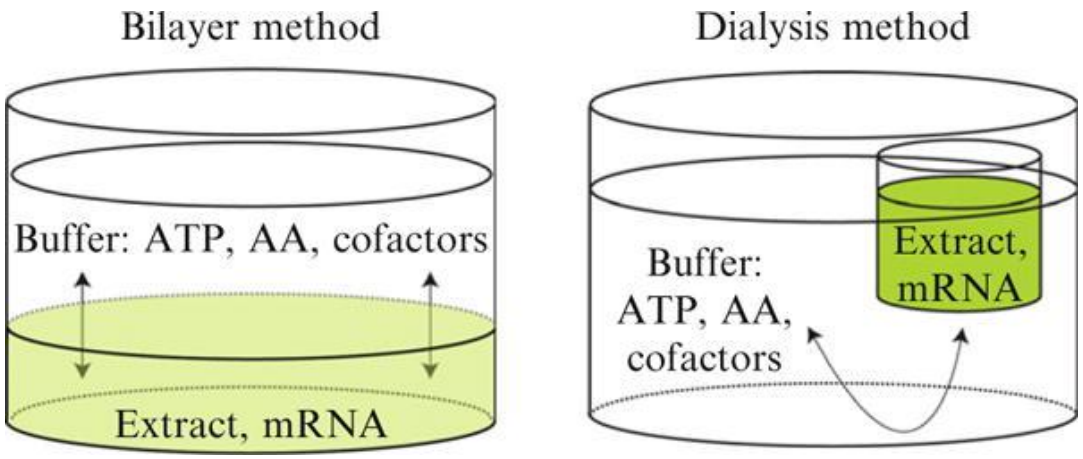

Figure 3-3 Schematic representation of two cell-free translation methods

The bilayer mode reaction method is based on a two-layers solutions approach: The bottom solution contains mRNA and cell-free extract, while the upper layer solution contains mRNA and cell-free extract. The upper layer solution consists of translation components. In a similar manner, the dialysis method consists of two separated systems, where the outer system supplies the energy with amino acids and cofactors through the membrane to an mRNA located in an inner system, together with the wheat-germ extract. Reproduced from (Goren et al., 2009).

3.4.2Purification of proteoliposomes

The newly produced proteoliposomes were separated and purified from the soluble components of the wheat germ extract by Accudenz (Accurate Chemical and Scientific Corporation, Westbury, U.S.A.)-based density gradient ultracentrifugation (**Figure 3-4**). The

total translation product was treated with 0.3 M KCl for 5 min at room temperature (RT), followed by layering of the total mix at the bottom of a clear ultracentrifuge tube (total volume of 5 mL). An equal volume of 80% Accudenz (prepared in 25 mM HEPES pH 7.5, 100 mM NaCl, 10% glycerol; hereafter, gradient buffer) was thoroughly mixed with the translation mix. This layer was followed by the layering of 3 mL of 30% Accudenz on top of the freshly prepared 40% Accudenz bottom gradient. Finally, 1 mL of gradient buffer was layered to form an overall step gradient composed of three layers. All the samples were spun at 217000 g (45000 rpm) for 4 h at 4°C in an MLS50 swing out bucket rotor fitted in a table-top ultracentrifuge (Beckman Coulter, U.S.A.). The spin resulted in a gradient with the densest material at the bottom of the tubes and the proteoliposomes at the interface between the 30% Accudenz and the gradient buffer layers. The fractions were collected from the top without disturbing the bottom layers. The fractions were analyzed for purity and protein quantity by SDS-PAGE followed by either Coomassie staining or immunoblotting using the appropriate antibody (anti-Pom121: ab190015, Abcam; anti-Ndc1: GTX120091, GeneTex; anti-His6: ab9108, Abcam).

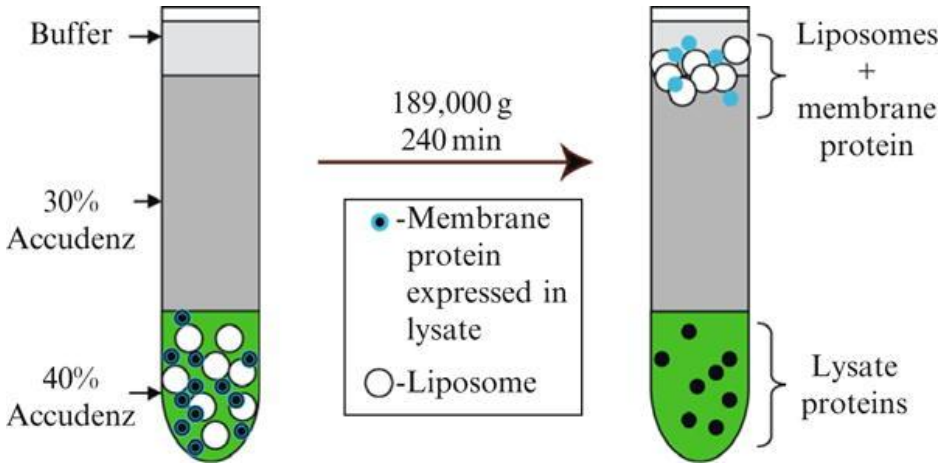

Figure 3-4 Purification of proteoliposomes

The three layers of composed gradient, upon ultracentrifugation, allow separation of vesicles depending on their weight. This separation results in light liposomes and proteoliposomes floating at the top, while heavier fractions, such as non-incorporated proteins and by-products of the translation reaction, stay at the bottom. Reproduced from (Goren et al., 2009).

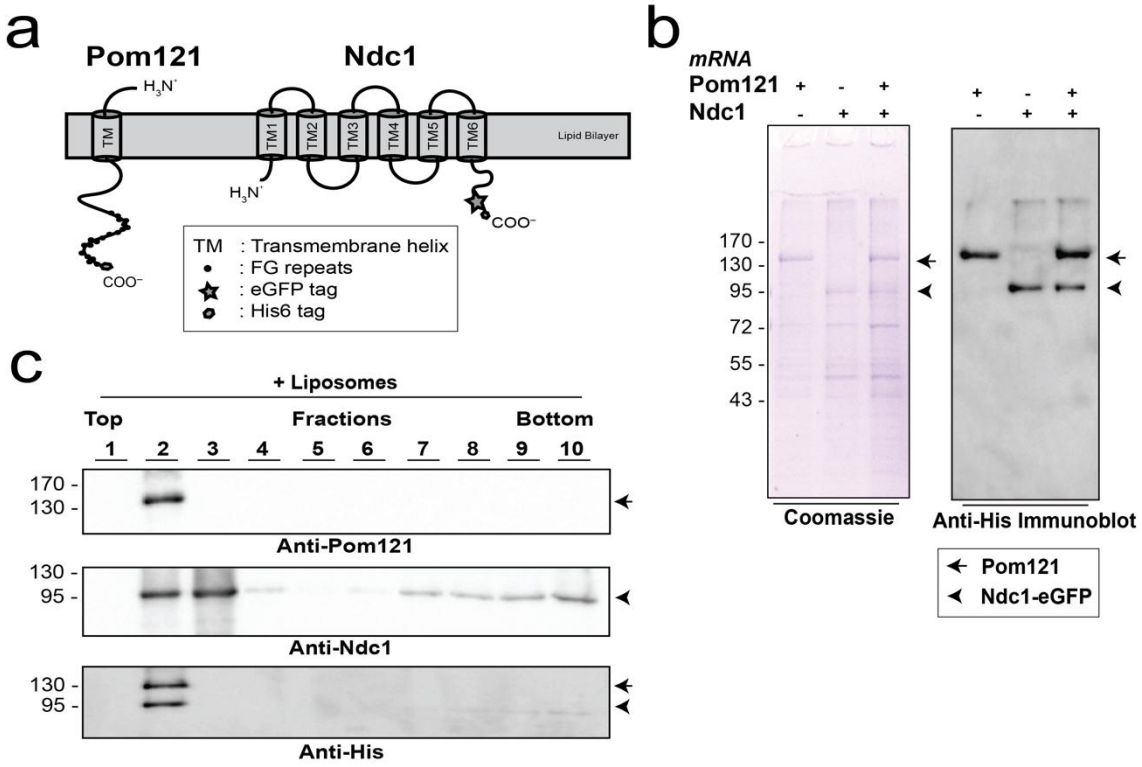

Figure 3-5 Biochemical assay to validate protein incorporation

3.4.3Biochemical validation of protein incorporation

(A) Membrane topology of Pom121 and Ndc1-eGFP fusion proteins. (B) Coomassie staining and anti-His immunoblot show expression and co-expression of full-length Pom121 and Ndc1-eGFP. (B) Accudenz-based density gradient liposome floatation assay shows that most of the expressed protein is membrane incorporated and floats in the lighter top fractions. Non-membrane associated proteins are present in the dense bottom fractions. Reproduced from (Panatala et al., 2019).

To begin, we tested the expression of the full-length Pom121 and Ndc1, both tagged with His6 fusion tag at their C-termini and an Ndc1 bearing an additional eGFP tag. Pom121 is a single-pass TM Nup, which has approximately 50 amino acid residues of its N-terminus exposed into the PNS (perinuclear space). Downstream of its transmembrane domain (TMD), there is a long C-terminus, which bears additional features like nuclear localization signal (NLS), NE binding domain (NEBD) and an FG domain exhibiting 24 FG repeats that present themselves in the central channel of the NPC. On the other hand, Ndc1 is a multi-pass TM

Nup with six TMDs, and both its N- and C-termini are exposed to the central channel (**Figure 3-5 A**).

Both full-length proteins were the most abundant upon expression using an SP6-derived mRNA when compared to other wheat-germ-based contaminating proteins, which were not overexpressed. Of note, there were two protein bands around 50 kDa and 70 kDa (**Figure 3-5 B**), which were enriched in the proteoliposome purified fractions. This appeared to be even more evident when Pom121 and Ndc1 were co-expressed, leading specific interacting partners of both Pom121 and Ndc1 to bear the same pool of proteoliposomes (Mitchell et al., 2010), (Vollmer et al., 2012). The corresponding immunoblots against His6-tag confirmed the expression of the full-length fusion proteins (**Figure 3-5 B**).

To address whether the *in vitro* expressed Pom121 and Ndc1 are incorporated into the liposomal membrane, the total translation products were incubated with 500 mM KCl for 10 min at room temperature to remove any peripherally associated membrane protein. The reaction mix was then subjected to high-speed density gradient centrifugation upon loading it at the bottom of an Accudenz step gradient. (**Figure 3-5 C)** shows that the majority of Pom121 and Ndc1 was recovered from the top fractions of the density gradient, which also contained the bulk of the exogenously added liposomes. This recovery was also the case when the proteins were co-translated. Taken together, these experiments indicate that the newly expressed Pom121 and Ndc1 were incorporated into the liposomal membrane and hence floated along with liposome fractions.

3.5Proteoliposome profiling

Alongside membrane protein production, various methods may be used to characterize proteoliposomes and to check protein yield. Western blot and mass spectrometry (MS) are limited to a bulk analysis of vesicles (Nyblom et al., 2007), (Yang et al., 1997). Thus, they are not suited for accurate quantification of the phenotypic heterogeneity of proteoliposomes. Using protein content to draw conclusions on the number of vesicles is misleading given that each vesicle can have a different size and protein abundance. Moreover, imaging techniques, such as electron microscopy, X-ray diffraction or atomic force microscopy (AFM), allow phenotypic analysis of individual vesicles (Yuana et al., 2010), (Aldick et al., 2009) but hinder the analysis of a large number of vesicles necessary to investigate their heterogeneity: This makes an accurate quantification complicated and liable to large statistical error. All the aforementioned methods are not feasible for single-vesicle analysis since they provide only qualitative information and even more importantly since they do not reproduce the physiological (native) related environment (e.g., disregard of the membrane curvature effect (Iversen et al., 2015)).

Since the simultaneous, high-throughput quantitative and qualitative analysis of a large number of individual liposomes results in multi-dimensional information, we converged on flow cytometry (FCM) as a method that would allow the profiling of a heterogeneous mixture of vesicles. FCM, in fact, is a powerful technique that enables one to measure both light scatter and fluorescence properties of individual objects suspended in a continuous flow. In brief, the forward scatter (FCS) of a laser light is measured to determine the size of an object, while the side scatter (SSC) gives information about the granularity and the internal

complexity of the sample. Furthermore, the fluorescence is measured and the respective generated signal intensity are dependent on the amount of fluorophore (**Figure 3-6**).

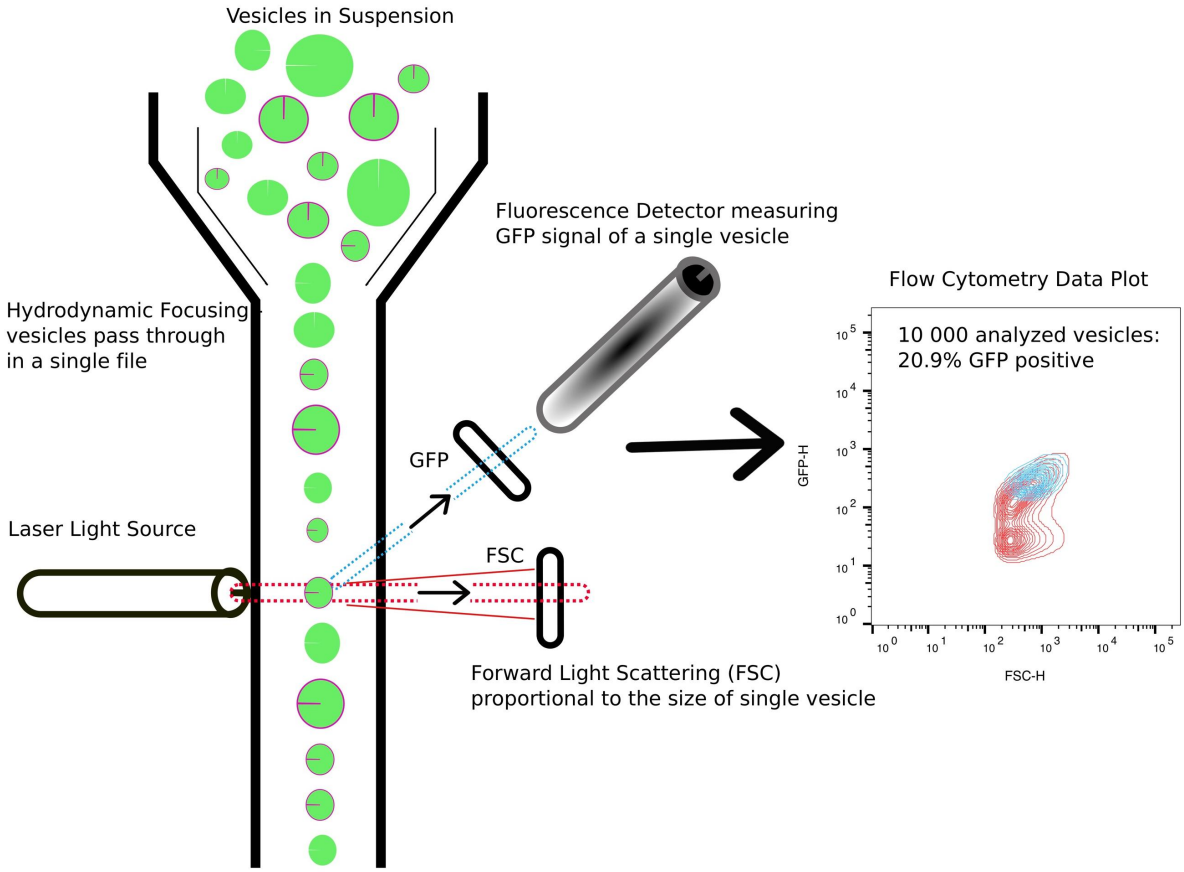

Figure 3-6 Schematic representation of a FCM experiment

FCM is used to profile proteoliposomes. Hydrodynamic focusing aligns vesicles to pass in a single file in front of a laser light source. FSC of a laser light measures the size of a vesicle, while fluorescence detector measures GFP signal. FSC is plotted on the x-axis with GFP fluorescence plotted on the y-axis.

In order to study the incorporation efficiency of Pom121 and Ndc1 at the level of a single vesicle, we used FCM measurements to analyze single liposomes and proteoliposomes in a high throughput fashion. For detection purposes, we produced giant liposomes and giant proteoliposomes (GLs and GPLs) using an ITO-based electroformation device, introducing Nile Red dye to stain the lipid membrane.

3.6Electroformation of proteoliposomes

The production of giant proteoliposomes from protein-containing single unilamellar vesicles (SUVs) is the same as growing pure lipid giants from SUVs but with the obvious challenge of protecting the proteins from dehydration (Garten et al., 2015). The drying of the lipid mixture causes the formation of a multi-lamellar stack of membranes, which then move apart and form GLs when rehydrated. We generated GPLs by partially dehydrating proteoSUVs and by rehydrating them with a "low-salt" buffer (**Figure 3-7**) adapted from (Garten et al., 2015)).

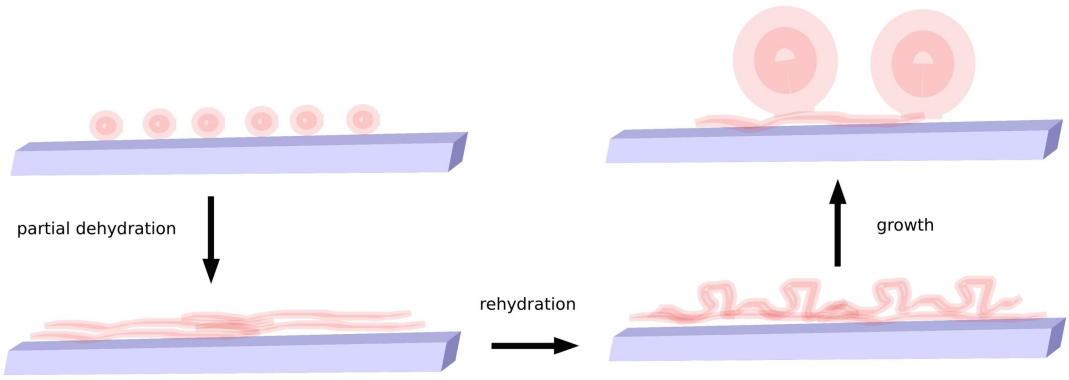

Figure 3-7 Scheme of growing GPLs by electroformation
Proteoliposomes are deposited onto the ITO-coated conductance side and left to partially dehydrate. Next, the rehydration step is performed by addition of the growth buffer, after which, the standard protocol is applied to grow GPLs.

We used an ITO (indium tin oxide) glass-slide-based vesicle formation device from Nanion Technologies. A set of two glass slides were wiped clean with 70% ethanol and MQ water. An O-ring supplied by the company was painted with vacuum grease, which aids in sealing the ring on the glass slide and forms a chamber to be fixed in a desired position on the slide. Next, 15 µM of Nile Red (N1142, Thermo Fisher Scientific), previously dissolved and stored

in methanol at 4°C, were deposited as 0.2 µL drops onto the ITO-coated conductance side (measured using a multimeter). The drops were allowed to dry at room temperature in the dark for 30–60 min, followed by passing a stream of nitrogen gas to remove any remaining methanol. Liposomes and proteoliposomes were dialyzed into a filter-sterilized SUV buffer containing 5 mM NaCl, 1 mM HEPES (pH 7.4) and 2 mM sucrose. 30 µL of liposomes/proteoliposomes were applied as 2–3 µL drops on the freshly dried Nile Red deposit. The samples were left under observation every 5 min to partially dehydrate at room temperature in the dark. Following this, a gentle introduction of 150 µL of growth buffer (5 mM NaCl, 1 mM HEPES pH 7.4 and 400 mM sucrose) was added into the chamber. To prevent the collapse of the freshly formed vesicles, a higher concentration of osmoticants, such as sucrose or sorbitol, were used in the growth buffer. The second ITO slide (conductance side facing the buffer) was placed over the chamber; no air was trapped, and the chamber was sealed. A standard protocol by Nanion Technologies was followed for GL/GPL production for 150 min at 37 °C. The duly produced GLs and GPLs were unstable in the ITO chamber after production. Hence, they were immediately aspirated into an amber-colored microcentrifuge tube of 1.5 mL. HEPES and NaCl were added to a final concentration of 10 mM and 100 mM, respectively. They were either used immediately or stored at 4°C before the FCM measurements.

3.7Incorporation efficiency of Pom121 and Ndc1 into liposomes

There is much merit to the idea that FCM can be used to measure submicron particles in a manner similar to that carried out during the analysis of the whole cell (Lannigan et al., 2016). Quantification and profiling of membrane-derived vesicles by FCM led to the development of a) a simple method for enumerating phosphatidylserine-exposing extracellular vesicles

(EVs) (Arraud et al., 2015), b) size profiling and counting of bacterial outer-membrane vesicles (Wieser et al., 2014), c) a fluorescence-based detection of EVs for accurate measurement of their size and number, demonstrating that FCM can detect a significantly higher number of EVs than what can be achieved with light-scatter-based techniques (Stoner et al., 2016). In addition, a fluorescence-based, high-resolution, FCM-based method has been developed for quantitative and qualitative analysis of nanosized membrane vesicles, enabling the identification of exosome subsets and phenotyping of individual exosomes produced by dendritic cells (DCs) undergoing different modes of activation (Nolte-'t Hoen et al., 2012).

Furthermore, there are many developments in FCM usage for evolutionary studies, such as the synthesis of functional GFP mutants in the liposomes (Yu et al., 2001), studies on the influence of outer chemical composition on internal GFP synthesis (Nishimura et al., 2012) and the measurement of *in vitro* translation of GFP inside individual liposomes in a high-throughput format to assess an eventual effect of the compartment on the biochemical reaction (Sunami et al., 2006). In addition to extensive FCM and FACS GFP-related studies, FCM has also been used to analyze the structural properties of giant liposomes formed by different methods (Nishimura et al., 2009).

Given that a flow cytometric approach allows for the rapid screening of engineered proteins, a similar approach has been used for the *in vitro* evolution of α-hemolysin (a membrane protein derived from *Staphylococcus aureus*) by entrapping different α-hemolysin DNA mutants with the PURE system into liposomes and subsequently measuring their pore-forming activity (Fujii et al., 2013).

Besides the characterization of EVs and *in vitro* screening methods, FCM has been applied to develop a novel assay to quantify interactions between proteins and membrane lipids as well (Temmerman and Nickel, 2009).

For our purposes, we used FCM to measure the incorporation yield of membrane proteins into liposomes. First, we selected single fluorescent vesicles by detection of forward scatter, side scatter and Nile Red signal. Importantly, as described above, the forward scatter light (FSC) is measured to determine the size of the object, while the side scatter light (SSC) gives information about the granularity and the internal complexity of the sample. Within the sorted Nile Red positive vesicles, we looked for eGFP fluorescence-positive because it indicates a sub-fraction of the vesicles with the Ndc1 incorporation. Hence, we could determine Ndc1 abundance on a lipid membrane in a single measurement. We analyzed the Ndc1-Pom121-GPLs and the Ndc1-GPLs, where GLs served as control. For every sample, we detected approximately > 90% of Nile Red labelled single vesicles. Out of those, the Ndc1-eGFP signal intensity provided a ~30% yield for Pom121-Ndc1-GPLs and 10% for Ndc1-GPLs, whereas blank giant-liposome (GL) controls gave null results (**Figure 3-8**).

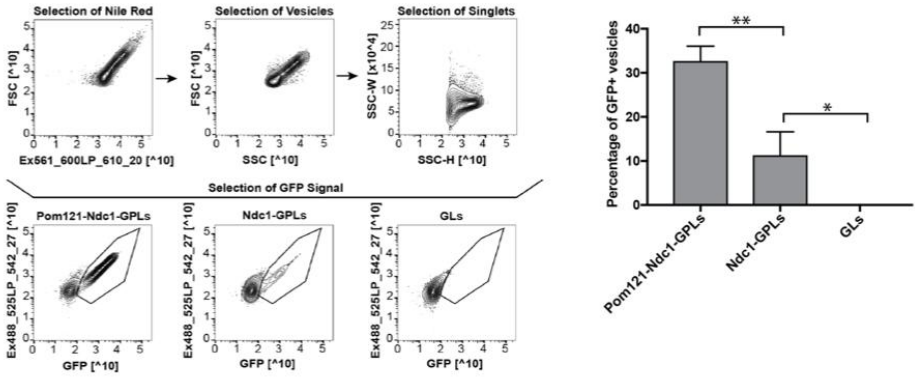

Figure 3-8 Flow cytometry evaluation of GLs and GPLs

Detection of Nile Red labelled GPLs (upper panel) by fluorescence, forward scattering (FSC), and side scattering (SSC). Subsequent analysis of Ndc1-eGFP with and without Pom121 (lower panel). GLs show no fluorescence. Histogram showing average yield of GFP obtained under each condition. N = 10000 data points for n = 3. Reproduced from (Panatala et al., 2019).

3.8Visualization of giant proteoliposomes

Next, we used confocal microscopy to visualize giant proteoliposomes. First, an O-paper ring was used to create a chamber within a glass slide. Then, the GPLs were placed into a chamber within a glass slide and covered with the cover slip. Next, the entire setup was turned upside down and left in the dark at room temperature to allow the GPLs to settle down. A sample was taken under the microscope LSM800, and an oil-immersion objective was used to image the eGFP GPLs. Imaging was performed by simultaneously using two wavelengths, 488 nm and 555 nm, to excite GFP and Nile Red, respectively. The rationale behind this procedure was to minimize the imaging time. One needs to note that the GPLs in our setup were not immobilized, hence their movement made imaging difficult. The immobilization of the GPLs was impossible because of already fragile membrane after protein reconstitution. In addition, because of the high polydispersity of the sample, the real challenge was to identify giant vesicles containing Pom121 and Ndc1. However, the images that we could obtain reveal morphology of the GPLs, showing most of them as having a circular shape, as shown in **Figure 3-9**. Interestingly, the GFP fluorescence on the GPL rim is punctate, which might indicate that the Pom121-Ndc1 incorporation is not homogenous but rather is localized to parts of the membrane.

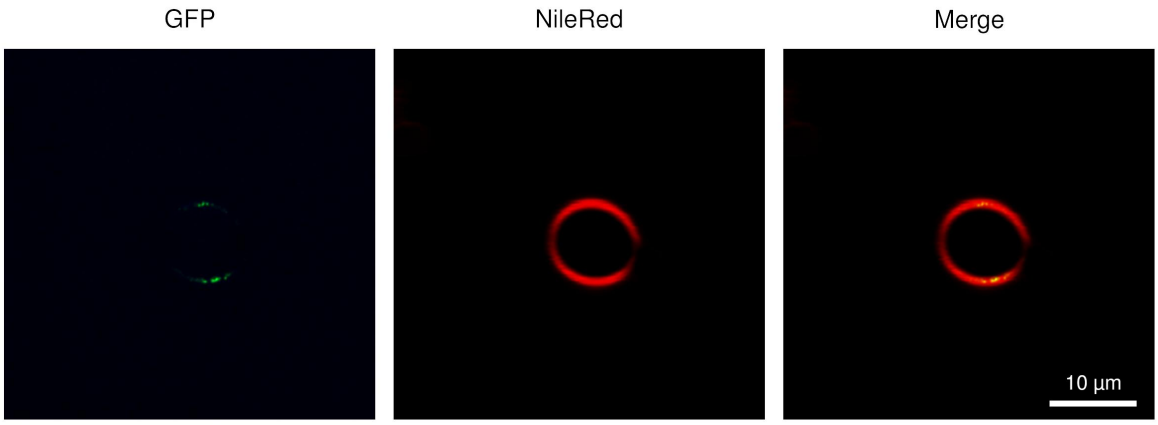

Figure 3-9 Pom121-Ndc1 giant proteoliposomes under confocal microscope
The Nile Red dyed lipid membrane is easily detectable, while the GFP signal is punctuated and appears only within a few membrane sections.

3.9Imaging Pom121/Ndc1 nanopores by high-speed AFM

(Note to reader: This section is a kind contribution from Toshiya Kozai).

Subsequently, both GLs and GPLs were spread onto freshly cleaned glass and examined by high-speed atomic force microscopy (HS-AFM) to check for the formation of nanopores following membrane reconstitution. At the nanoscale, HS-AFM revealed numerous pore-like perforations in the Pom121-Ndc1-PL membrane (**Figure 3-10 A**) that were not present in the blank liposome controls. Interestingly, each pore was enclosed by a ring-like structure above the membrane surface (**Figure 3-10 B**). Each ring suggests that the individual Pom121-Ndc1 sub-complexes assembled into a corral-like arrangement. Their average pore dimensions were 5.8 ± 1.4 nm, 19.5 ± 3.7 nm and 37.3 ± 6.1 nm for height (H_{pore}), inner diameter (*i.d.*) and outer diameter (*o.d.*), respectively (**Figure 3-10 B**). Moreover, the ring height (H_{rim}) and thickness of the surrounding membrane (H_{mem}) were 3.2 ± 1.4 nm and 2.5 ± 0.6 nm, respectively, as measured from the top of each ring and bottom of each pore to the membrane

surface. Here, H_{mem} appears smaller than the expected thickness of the lipid bilayer (Nagle and Tristram-Nagle, 2000). This observation may be due to a limited penetration of the HS-AFM tip into the pore or to the fact that the Pom121-Ndc1 pore formation might cause a local deformation (compression) of the lipid bilayer that surrounds it (Gilbert, 2016). In addition, we sometimes observed elongated pores (or "slits") (**Figure 3-10 C**) with similar H_{pore}, *i.d.* and *o.d.* values, thereby suggesting that the slits might originate from conjoined pores, as summarized in **Figure 3-10 D**.

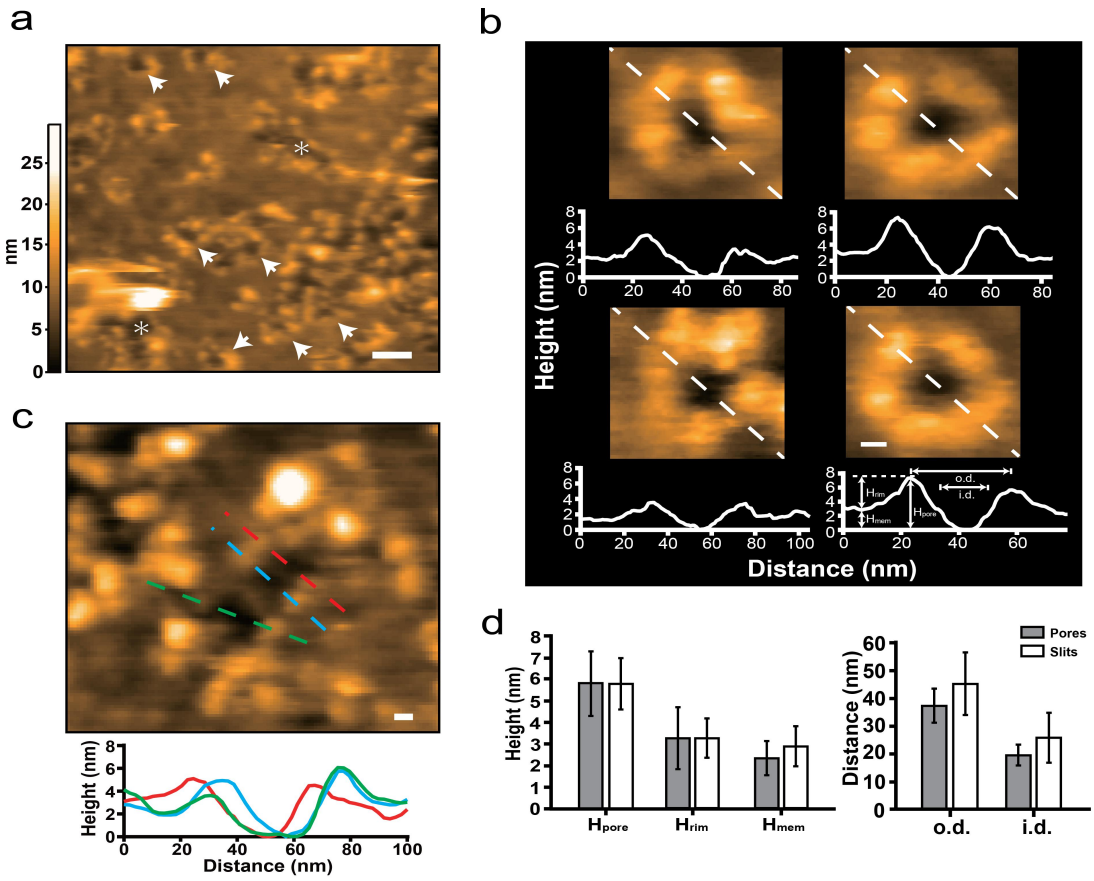

Figure 3-10 Imaging Pom121/Ndc1 nanopores by HS-AFM

(A) Zoomed-out HS-AFM image showing the PL membrane perforated with several Pom121-Ndc1 pores (white arrow heads). Asterisks denote conjoined pores (i.e., "slits"). Scale bar = 50 nm. (B) Height and diameter profiles of four representative pores. Pore height as well as inner and outer diameter are given by H_{pore}, i.d. and o.d., respectively, as shown in the cross-sectional profile. Scale bar = 10 nm. (C) Image and cross-sectional profiles of a member slit. Scale bar = 10 nm. (D) Histograms provide an overview of the dimensions of pores and slits. Reproduced from (Panatala et al., 2019).

3.10 Nanopore characterization using single channel electrical measurements

(Note to reader: This section is a kind contribution from Radhakrishnan Panatala and Jinghui Luo).

Finally, we applied single-channel electrical measurements (Bayley and Martin, 2000) to verify that the TM-Nups formed aqueous pores that punctured the lipid membrane (**Figure 3-11**). In the absence of pores, such as in the blank liposomes, the membrane exhibited a property of zero conductance. Similar results were obtained for Pom121- or Ndc1-only PLs, which did not show any evidence of pore formation. In marked contrast, Pom121-Ndc1 PLs exhibited an overall staircase-like behavior (Bode et al., 2017) that ascended until reaching the detection limit of the instrument. Importantly, each upward "step" signified the emergence of a new pore, although local fluctuations suggest more complex behavior (Sekiya et al., 2018), such as the opening and closing of multiple pores. Moreover, each step could be used to estimate a theoretical pore size (Cruickshank et al., 1997), giving 3.8 ± 2.0 nm, which is in approximate agreement with our HS-AFM results. For completeness, it is noteworthy to mention that pore formation neither occurred when blank liposomes were added to Pom121-PLs and Ndc1-PLs nor during sequential additions of Ndc1-PLs to Pom121-PLs. However, the electrical signal was destabilized when Pom121-PLs were introduced to Ndc1-PLs, which may suggest that Pom121 facilitates a rearrangement of Ndc1 in the membrane. Still, it remains to be ascertained how the sequential addition of Pom121 and Ndc1 favors the pore formation.

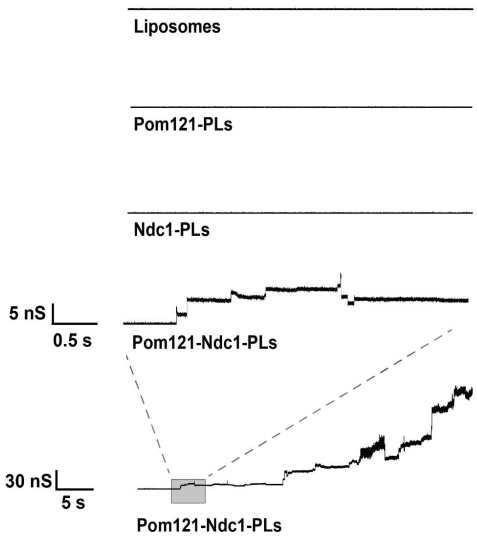

Figure 3-11 Characterization of pores using single channel electrical measurements
Ascending staircase-like conductance behaviour indicates that the numbers of Pom121-Ndc1 pores are increasing over time. Each upward "step" signifies the emergence of a new pore but local fluctuations indicate stochastic behaviour during protein insertion. A controls,blank liposomes, Pom121-PLs and Ndc1-PLS did not form pores. Reproduced from (Panatala et al., 2019).

3.11 Conclusions

Our findings suggest that the reconstitution of Pom121 and Ndc1 results in porous proteoliposomes. Remarkably, our FCM data shows that the membrane incorporation efficiency of Ndc1 increases upon its complexation with Pom121, indicating that Pom121 facilitates this process. To our knowledge, this is the first study reporting the usage of in vitro-expressed membrane proteins, where one protein favors the incorporation of a second protein into the liposomal membrane. The HS-AFM data revealed that the morphological features of the Pom121-Ndc1 pore show a fair resemblance to native NPCs (Sakiyama et al., 2016). As expected, because of the lack of other structural and functional elements from native NPCs, the dimensions of the Pom121-Ndc1 pores were smaller both in diameter and in height. The single channel electrical recordings show that only those proteoliposomes with both proteins co-expressed can fuse with the bilayer lipid membrane and lead to the pore

formation. Also, these observations show that with increasing time, the conductance reaches an overload, which depicts the dynamicity of pore formation. An important future direction based on this work could investigate how the transmembrane domains (TMDs) of both proteins are arranged in the lipid bilayer with regard to the pore axis and whether there is a correlation between the number of sub-complex rings and the pore diameter. Besides well-established DNA origami (Gopfrich et al., 2016) and solid-state pores (Kowalczyk et al., 2011), our data suggests that Pom121-Ndc1 proteoliposomes may provide a *de novo* platform to construct NPC mimics.

3.12 Materials and Methods

3.12.1Flow cytometry

Proteoliposome characterization was performed using a BD LSRFortessa™ (BD Biosciences, San Jose, CA). The flow rate was set to low (approximately 8–12 µL/min). Forward scatter (FSC) and side scatter (SSC) were measured in log scale, and the threshold was set to 200 for FSC and SSC. The FSC and SSC voltages were adjusted to the highest value, ensuring the majority of background noise was excluded. Nile Red was excited with a 561 nm laser, and the emission signal was collected through a 610/20 nm bandpass filter. The GFP was excited with a 488 nm laser, while the emission was collected through a 512/25 nm bandpass pass filter. All the vesicles were diluted 20 times in 1xPBS prior to measurement. 10000 events were collected per sample. Data was analyzed, and figures were generated using the FlowJo® software.

3.12.2Confocal microscopy

The proteoliposomes were imaged using Zeiss Point Scanning Confocal LSM800 Inverted with PLAN APO oil-immersive 63x objective (NA = 1.40), using Zen Blue software. Two laser lines were used: 488 nm and 550 nm, both solid-state types (10 mW). Both laser powers and gains were adjusted in order to minimize any crosstalk. Figures were generated using OMERO software.

3.12.3HS-AFM

All experiments were conducted using a commercial HS-AFM 1.0 system (RIBM, Japan) featuring a standard scanner with a maximum scan speed of 50 ms per frame. Pristine NT-

AC10 Quantum cantilevers (Nanotools) (7 μm long, 2 μm wide, 80 nm thick and a tip radius of ~3 nm) were used. Supplier specifications indicate that these cantilevers have a nominal spring constant of 0.1 Nm^{-1} and a resonance frequency of 1.2 MHz in air. Liposomes or proteoliposomes were adsorbed onto freshly cleaned (with RCA buffer, sonication and plasma) glass. After an adsorption time of 30 min, the sample was washed several times in buffer solution (100 mM NaCl, 25 mM HEPES, pH 7.5) to remove weakly bound adsorbates. Buffer solutions were freshly made using MQ water (18.2 MΩ-cm). Several liposomes and proteoliposomes were scanned and visualized. However, we observed that the image resolution varied with the tip quality, stability and sample roughness and the images shown here are representative of the most highly resolved data.

3.12.4Single channel electrical recordings

Recordings of the planar lipid bilayers were conducted at RT in an apparatus with two Delrin compartments. The compartments were separated into *cis*- (connected with a ground electrode) and *trans*- (connected with a voltage electrode) sides by a polytetrafluoroethylene (PTFE) film with a 100 μm aperture and 25 μm thickness (Good Fellow Inc., #FP301200). A mixture of DOPC (1,2-dioleoyl-sn-glycero-3-phosphocholine, Avanti Polar Lipids, Inc.) and DOPG (1,2-Dioleoyl-sn-glycero-3-phosphoglycerol, Avanti Polar Lipids, Inc.) at a ratio of 4:1 was dissolved in pentane at a concentration of 20 mg/mL. The film was pretreated in 2% (v/v) hexadecane in pentane, and 10 μL of the lipid mixture was applied to form lipid bilayers across the aperture in electrolyte solution (20 mM HEPES buffer, pH 7.4 with 150 mM NaCl). Following the above steps, either liposomes or proteoliposomes were added into the *trans* side next to the film for the electrical recordings that were performed with two Ag/AgCl electrodes at a voltage of -50 mV. The currents were recorded for 20 minutes to check for

any interaction between proteoliposomes and lipid bilayers. All the current recordings were amplified and digitized by an Axopatch 200B (Molecular Devices) and a Digidata 1440 A (Molecular Devices), respectively, followed by a 2 kHz low-pass Bessel filter. Data were analyzed with the pClamp 10.7 software (Molecular Devices). The estimates of pore diameters were calculated based on the model by (Cruickshank et al., 1997).

3.13 References

Aldick, T., Bielaszewska, M., Uhlin, B. E., Humpf, H. U., Wai, S. N. and Karch, H. (2009). Vesicular stabilization and activity augmentation of enterohaemorrhagic Escherichia coli haemolysin. *Mol Microbiol* 71, 1496-508.

Arraud, N., Gounou, C., Linares, R. and Brisson, A. R. (2015). A simple flow cytometry method improves the detection of phosphatidylserine-exposing extracellular vesicles. *J Thromb Haemost* 13, 237-47.

Balasubramanian, V., Onaca, O., Enea, R., Hughes, D. W. and Palivan, C. G. (2010). Protein delivery: from conventional drug delivery carriers to polymeric nanoreactors. *Expert opinion on drug delivery* 7, 63-78.

Barbey, R., Lavanant, L., Paripovic, D., Schuwer, N., Sugnaux, C., Tugulu, S. and Klok, H. A. (2009). Polymer brushes via surface-initiated controlled radical polymerization: synthesis, characterization, properties, and applications. *Chem Rev* 109, 5437-527.

Bayley, H. and Martin, C. R. (2000). Resistive-Pulse Sensing-From Microbes to Molecules. *Chem Rev* 100, 2575-2594.

Blobel, G. (2000). Protein targeting (Nobel lecture). *Chembiochem* 1, 86-102.

Bode, D. C., Baker, M. D. and Viles, J. H. (2017). Ion Channel Formation by Amyloid-beta42 Oligomers but Not Amyloid-beta40 in Cellular Membranes. *J Biol Chem* 292, 1404-1413.

Chan, A. C. and Carter, P. J. (2010). Therapeutic antibodies for autoimmunity and inflammation. *Nat Rev Immunol* 10, 301-16.

Choi, H.-J. and Montemagno, C. D. (2007). Light-driven hybrid bioreactor based on protein-incorporated polymer vesicles. *Nanotechnology, IEEE Transactions on* 6, 171-176.

Cooper, G. M. and Hausman, R. E. (2000). The cell: Sinauer Associates Sunderland.

Cruickshank, C. C., Minchin, R. F., Le Dain, A. C. and Martinac, B. (1997). Estimation of the pore size of the large-conductance mechanosensitive ion channel of Escherichia coli. *Biophys J* 73, 1925-31.

Discher, D. E. and Eisenberg, A. (2002). Polymer vesicles. *Science* 297, 967-73.

Drexler, K. E. (1999). Building molecular machine systems. *Trends in Biotechnology* 17, 5-7.

Einfalt, T., Goers, R., Dinu, I. A., Najer, A., Spulber, M., Onaca-Fischer, O. and Palivan, C. G. (2015). Stimuli-triggered activity of nanoreactors by biomimetic engineering polymer membranes. *Nano letters* 15, 7596-7603.

Engelman, D. M. (2005). Membranes are more mosaic than fluid. *Nature* 438, 578-80.

Fujii, S., Matsuura, T., Sunami, T., Kazuta, Y. and Yomo, T. (2013). In vitro evolution of alpha-hemolysin using a liposome display. *Proc Natl Acad Sci U S A* 110, 16796-801.

Garni, M., Thamboo, S., Schoenenberger, C. A. and Palivan, C. G. (2017). Biopores/membrane proteins in synthetic polymer membranes. *Biochim Biophys Acta Biomembr* 1859, 619-638.

Garten, M., Aimon, S., Bassereau, P. and Toombes, G. E. (2015). Reconstitution of a transmembrane protein, the voltage-gated ion channel, KvAP, into giant unilamellar vesicles for microscopy and patch clamp studies. *J Vis Exp*, 52281.

Gilbert, R. J. (2016). Protein-lipid interactions and non-lamellar lipidic structures in membrane pore formation and membrane fusion. *Biochim Biophys Acta* 1858, 487-99.

Goodsell, D. S. (2009). The machinery of life: Springer Science & Business Media.

Gopfrich, K., Li, C. Y., Ricci, M., Bhamidimarri, S. P., Yoo, J., Gyenes, B., Ohmann, A., Winterhalter, M., Aksimentiev, A. and Keyser, U. F. (2016). Large-Conductance Transmembrane Porin Made from DNA Origami. *ACS Nano* 10, 8207-14.

Goren, M. A., Nozawa, A., Makino, S., Wrobel, R. L. and Fox, B. G. (2009). Cell-free translation of integral membrane proteins into unilamelar liposomes. *Methods Enzymol* 463, 647-73.

Harbers, M. (2014). Wheat germ systems for cell-free protein expression. *FEBS Lett* 588, 2762-73.

Hua, D., Kuang, L. and Liang, H. (2011). Self-directed reconstitution of proteorhodopsin with amphiphilic block copolymers induces the formation of hierarchically ordered proteopolymer membrane arrays. *J Am Chem Soc* 133, 2354-7.

Iversen, L., Mathiasen, S., Larsen, J. B. and Stamou, D. (2015). Membrane curvature bends the laws of physics and chemistry. *Nat Chem Biol* 11, 822-5.

Jovanovic-Talisman, T., Tetenbaum-Novatt, J., McKenney, A. S., Zilman, A., Peters, R., Rout, M. P. and Chait, B. T. (2009). Artificial nanopores that mimic the transport selectivity of the nuclear pore complex. *Nature* 457, 1023-1027.

Klok, H. A. and Lecommandoux, S. (2001). Supramolecular materials via block copolymer self‐assembly. *Advanced Materials* 13, 1217-1229.

Klyszejko, A. L., Shastri, S., Mari, S. A., Grubmüller, H., Muller, D. J. and Glaubitz, C. (2008). Folding and assembly of proteorhodopsin. *Journal of molecular biology* 376, 35-41.

Kowal, J., Zhang, X., Dinu, I. A., Palivan, C. G. and Meier, W. (2013). Planar Biomimetic Membranes Based on Amphiphilic Block Copolymers. *ACS Macro Letters* 3, 59-63.

Kowalczyk, S. W., Kapinos, L., Blosser, T. R., Magalhães, T., van Nies, P., Lim, R. Y. H. and Dekker, C. (2011). Single-molecule transport across an individual biomimetic nuclear pore complex. *Nature nanotechnology* 6, 433-438.

Lannigan, J., J, P. N. and Zucker, R. (2016). Measurement of extracellular vesicles and other submicron size particles by flow cytometry. *Cytometry A* 89, 109-10.

Leduc, P. R., Wong, M. S., Ferreira, P. M., Groff, R. E., Haslinger, K., Koonce, M. P., Lee, W. Y., Love, J. C., McCammon, J. A., Monteiro-Riviere, N. A. et al. (2007). Towards an in vivo biologically inspired nanofactory. *Nat Nanotechnol* 2, 3-7.

Lomora, M., Garni, M., Itel, F., Tanner, P., Spulber, M. and Palivan, C. G. (2015a). Polymersomes with engineered ion selective permeability as stimuli-responsive nanocompartments with preserved architecture. *Biomaterials* 53, 406-414.

Lomora, M., Itel, F., Dinu, I. A. and Palivan, C. G. (2015b). Selective ion-permeable membranes by insertion of biopores into polymersomes. *Physical Chemistry Chemical Physics* 17, 15538-15546.

LoPresti, C., Lomas, H., Massignani, M., Smart, T. and Battaglia, G. (2009). Polymersomes: nature inspired nanometer sized compartments. *Journal of Materials Chemistry* 19, 3576-3590.

Madrid, A. S., Mancuso, J., Cande, W. Z. and Weis, K. (2006). The role of the integral membrane nucleoporins Ndc1p and Pom152p in nuclear pore complex assembly and function. *J Cell Biol* 173, 361-71.

Meier, W., Nardin, C. and Winterhalter, M. (2000). Reconstitution of channel proteins in (polymerized) ABA triblock copolymer membranes. *Angewandte Chemie International Edition* 39, 4599-4602.

Mitchell, J. M., Mansfeld, J., Capitanio, J., Kutay, U. and Wozniak, R. W. (2010). Pom121 links two essential subcomplexes of the nuclear pore complex core to the membrane. *J Cell Biol* 191, 505-21.

Nagle, J. F. and Tristram-Nagle, S. (2000). Structure of lipid bilayers. *Biochim Biophys Acta* 1469, 159-95.

Nallani, M., Andreasson-Ochsner, M., Tan, C.-W. D., Sinner, E.-K., Wisantoso, Y., Geifman-Shochat, S. and Hunziker, W. (2011). Proteopolymersomes: In vitro production of a membrane protein in polymersome membranes. *Biointerphases* 6, 153-157.

Nardin, C., Widmer, J., Winterhalter, M. and Meier, W. (2001). Amphiphilic block copolymer nanocontainers as bioreactors. *The European Physical Journal E* 4, 403-410.

Nishimura, K., Hosoi, T., Sunami, T., Toyota, T., Fujinami, M., Oguma, K., Matsuura, T., Suzuki, H. and Yomo, T. (2009). Population analysis of structural properties of giant liposomes by flow cytometry. *Langmuir* 25, 10439-43.

Nishimura, K., Matsuura, T., Nishimura, K., Sunami, T., Suzuki, H. and Yomo, T. (2012). Cell-free protein synthesis inside giant unilamellar vesicles analyzed by flow cytometry. *Langmuir* 28, 8426-32.

Nolte-'t Hoen, E. N., van der Vlist, E. J., Aalberts, M., Mertens, H. C., Bosch, B. J., Bartelink, W., Mastrobattista, E., van Gaal, E. V., Stoorvogel, W., Arkesteijn, G. J. et al. (2012). Quantitative and qualitative flow cytometric analysis of nanosized cell-derived membrane vesicles. *Nanomedicine* 8, 712-20.

Nyblom, M., Oberg, F., Lindkvist-Petersson, K., Hallgren, K., Findlay, H., Wikstrom, J., Karlsson, A., Hansson, O., Booth, P. J., Bill, R. M. et al. (2007). Exceptional overproduction of a functional human membrane protein. *Protein Expr Purif* 56, 110-20.

Onischenko, E., Stanton, L. H., Madrid, A. S., Kieselbach, T. and Weis, K. (2009). Role of the Ndc1 interaction network in yeast nuclear pore complex assembly and maintenance. *J Cell Biol* 185, 475-91.

Panatala, R., Barbato, S., Kozai, T., Luo, J., Kapinos, L. E. and Lim, R. Y. H. (2019). Nuclear Pore Membrane Proteins Self-Assemble into Nanopores. *Biochemistry* 58, 484-488.

Pluckthun, A. and Pack, P. (1997). New protein engineering approaches to multivalent and bispecific antibody fragments. *Immunotechnology* 3, 83-105.

Sakiyama, Y., Mazur, A., Kapinos, L. E. and Lim, R. Y. H. (2016). Spatiotemporal dynamics of the nuclear pore complex transport barrier resolved by high-speed atomic force microscopy. *Nat Nanotechnol* 11, 719-23.

Schleicher, K. D., Dettmer, S. L., Kapinos, L. E., Pagliara, S., Keyser, U. F., Jeney, S. and Lim, R. Y. H. (2014). Selective transport control on molecular velcro made from intrinsically disordered proteins. *Nature nanotechnology* 9, 525-530.

Sekiya, Y., Sakashita, S., Shimizu, K., Usui, K. and Kawano, R. (2018). Channel current analysis estimates the pore-formation and the penetration of transmembrane peptides. *Analyst* 143, 3540-3543.

Stavru, F., Hulsmann, B. B., Spang, A., Hartmann, E., Cordes, V. C. and Gorlich, D. (2006). NDC1: a crucial membrane-integral nucleoporin of metazoan nuclear pore complexes. *J Cell Biol* 173, 509-19.

Stoenescu, R., Graff, A. and Meier, W. (2004). Asymmetric ABC‐Triblock Copolymer Membranes Induce a Directed Insertion of Membrane Proteins. *Macromolecular bioscience* 4, 930-935.

Stoner, S. A., Duggan, E., Condello, D., Guerrero, A., Turk, J. R., Narayanan, P. K. and Nolan, J. P. (2016). High sensitivity flow cytometry of membrane vesicles. *Cytometry A* 89, 196-206.

Sunami, T., Sato, K., Matsuura, T., Tsukada, K., Urabe, I. and Yomo, T. (2006). Femtoliter compartment in liposomes for in vitro selection of proteins. *Anal Biochem* 357, 128-36.

Talamas, J. A. and Hetzer, M. W. (2011). POM121 and Sun1 play a role in early steps of interphase NPC assembly. *J Cell Biol* 194, 27-37.

Tanner, P., Balasubramanian, V. and Palivan, C. G. (2013). Aiding nature's organelles: artificial peroxisomes play their role. *Nano Lett* 13, 2875-83.

Temmerman, K. and Nickel, W. (2009). A novel flow cytometric assay to quantify interactions between proteins and membrane lipids. *J Lipid Res* 50, 1245-54.

Terry, L. J., Shows, E. B. and Wente, S. R. (2007). Crossing the nuclear envelope: hierarchical regulation of nucleocytoplasmic transport. *Science* 318, 1412-6.

van Meer, G., Voelker, D. R. and Feigenson, G. W. (2008). Membrane lipids: where they are and how they behave. *Nat Rev Mol Cell Biol* 9, 112-24.

Vollmer, B., Schooley, A., Sachdev, R., Eisenhardt, N., Schneider, A. M., Sieverding, C., Madlung, J., Gerken, U., Macek, B. and Antonin, W. (2012). Dimerization and direct membrane interaction of Nup53 contribute to nuclear pore complex assembly. *EMBO J* 31, 4072-84.

Wieser, A., Storz, E., Liegl, G., Peter, A., Pritsch, M., Shock, J., Wai, S. N. and Schubert, S. (2014). Efficient quantification and characterization of bacterial outer membrane derived nano-particles with flow cytometric analysis. *Int J Med Microbiol* 304, 1032-7.

Wu, P., Castner, D. G. and Grainger, D. W. (2008). Diagnostic devices as biomaterials: a review of nucleic acid and protein microarray surface performance issues. *J Biomater Sci Polym Ed* 19, 725-53.

Yang, B., van Hoek, A. N. and Verkman, A. S. (1997). Very high single channel water permeability of aquaporin-4 in baculovirus-infected insect cells and liposomes reconstituted with purified aquaporin-4. *Biochemistry* 36, 7625-32.

Yu, W., Sato, K., Wakabayashi, M., Nakaishi, T., Ko-Mitamura, E. P., Shima, Y., Urabe, I. and Yomo, T. (2001). Synthesis of functional protein in liposome. *J Biosci Bioeng* 92, 590-3.

Yuana, Y., Oosterkamp, T. H., Bahatyrova, S., Ashcroft, B., Garcia Rodriguez, P., Bertina, R. M. and Osanto, S. (2010). Atomic force microscopy: a novel approach to the detection of nanosized blood microparticles. *J Thromb Haemost* 8, 315-23.

4Summary and Outlook

4.1Summary and Outlook

In this work we rebuilt NPC function *in vitro* using two different approaches. The first part of this work suggests that the Kaps may contribute to the maintenance of RanGTP/RanGDP gradient as described by the Kap-centric control model. Our results support the view that the NPC transport barrier is not composed of FG Nups exclusively. FG-Nups, instead, are highly occupied with transport receptors – Kaps. As such, because of the different binding affinity of Kaps toward RanGTP and RanGDP, the NPC is able to recognize which form to retain within the nucleus. It would be interesting to observe similar effect in living cells.

The second part of this research demonstrates how two membrane nucleoporins can self-assemble into nanopores. This research lays the groundwork for future molecular logistic systems that could rely on the NPC-like transport. Further developments could involve the introduction of additional NPC and NCT components to the system.

To conclude, the work presented in this thesis provides essential insights into the role of Kaps and membrane nucleoporins on NPC function. In particular, I have addressed questions regarding Ran gradient and NPC pre-pore formation. The key findings are that 1) Karyopherins modulate RanGTP/RanGDP gradient at the NPC, 2) the concentration and binding strength of karyopherins within NPC contributes to the NPC selective barrier function and 3) Pom121 and Ndc1 self-assemble into nanopores, indicating that only few NPC components might drive pre-pore formation.